Role of H_2O in Generating Subduction Zone Earthquakes

Akira Hasegawa

Research Center for Prediction of Earthquakes and Volcanic Eruptions,
Graduate School of Science, Tohoku University,
Sendai 980-8578, Japan
e-mail: akira.hasegawa.d8@tohoku.ac.jp

Received January 7, 2016; **Revised** June 13, 2016; **Accepted** July 3, 2016; **Online published** March 22, 2017.

Citation: Hasegawa, A. (2017), Role of H_2O in generating subduction zone earthquakes, *Monogr. Environ. Earth Planets*, *5*, 1–34, doi:10.5047/meep.2017.00501.0001.

Abstract A dense nationwide seismic network and high seismic activity in Japan have provided a large volume of high-quality data, enabling high-resolution imaging of the seismic structures defining the Japanese subduction zones. Here, the role of H_2O in generating earthquakes in subduction zones is discussed based mainly on recent seismic studies in Japan using these high-quality data. Locations of intermediate-depth intraslab earthquakes and seismic velocity and attenuation structures within the subducted slab provide evidence that strongly supports intermediate-depth intraslab earthquakes, although the details leading to the earthquake rupture are still poorly understood. Coseismic rotations of the principal stress axes observed after great megathrust earthquakes demonstrate that the plate interface is very weak, which is probably caused by overpressured fluids. Detailed tomographic imaging of the seismic velocity structure in and around plate boundary zones suggests that interplate coupling is affected by local fluid overpressure. Seismic tomography studies also show the presence of inclined sheet-like seismic low-velocity, high-attenuation zones in the mantle wedge. These may correspond to the upwelling flow portion of subduction-induced secondary convection in the mantle wedge. The upwelling flows reach the arc Moho directly beneath the volcanic areas, suggesting a direct relationship. H_2O originally liberated from the subducted slab is transported by this upwelling flow to the arc crust. The H_2O that reaches the crust is overpressured above hydrostatic values, weakening the surrounding crustal rocks and decreasing the shear strength of faults, thereby inducing shallow inland earthquakes. These observations suggest that H_2O expelled from the subducting slab plays an important role in generating subduction zone earthquakes both within the subduction zone itself and within the magmatic arc occupying its hanging wall.

Keywords: H_2O, Fluid overpressure, Weak fault, Subduction zone, Earthquake generation mechanism, Fluid-related embrittlement, Mantle upwelling flow.

1. Introduction

New oceanic plates are produced at mid-ocean ridges by the upwelling of materials from the mantle directly below. The production of new oceanic plates at mid-ocean ridges does not expand the Earth's surface, as an equal amount of surface material returns downward back into the mantle. This consumption of surface materials occurs at "subduction zones", where oceanic plates sink downward into the mantle. At a subduction zone, two plates collide, with one overriding the other, forcing the heavier one back into the mantle. The heavier oceanic plate subducts beneath the lighter continental plate. This subduction of oceanic plates causes high seismic activity along the margin between the plates. Indeed, most of world's large earthquakes occur in subduction zones with >90% of global seismic moment release occurring there (Pacheco and Sykes, 1992). Plate subduction also causes volcanic activity along the subduction zone, forming belt-like volcanic chains on the upper plate distributed nearly parallel to the trench axis. Viewing the Earth as a system, subduction zones are the sites where oceanic plates are recycled back into the mantle, where material flux back into the deep mantle takes place. Subduction of an oceanic plate in the upper mantle beneath a volcanic arc, and the ultimate fate of the plate as it plunges downward into the lower mantle, play important roles in the recycling of chemical elements into the Earth's interior.

Before subduction, an oceanic plate contains water as pore water and OH-bearing minerals. This is expelled by dewatering and dehydration as the oceanic plate subducts and its temperature and pressure increase, generating aqueous fluids within the slab. Being less dense than the surrounding rocks, the fluids migrate upward to the upper plate interface. A portion migrates further upward along the plate interface, with the remaining portion entering the overlying mantle wedge. The fluids that enter the mantle wedge directly above react chemically with the surrounding rocks and migrate even fur-

doi:10.5047/meep.2017.00501.0001 ISSN: 2186-4853

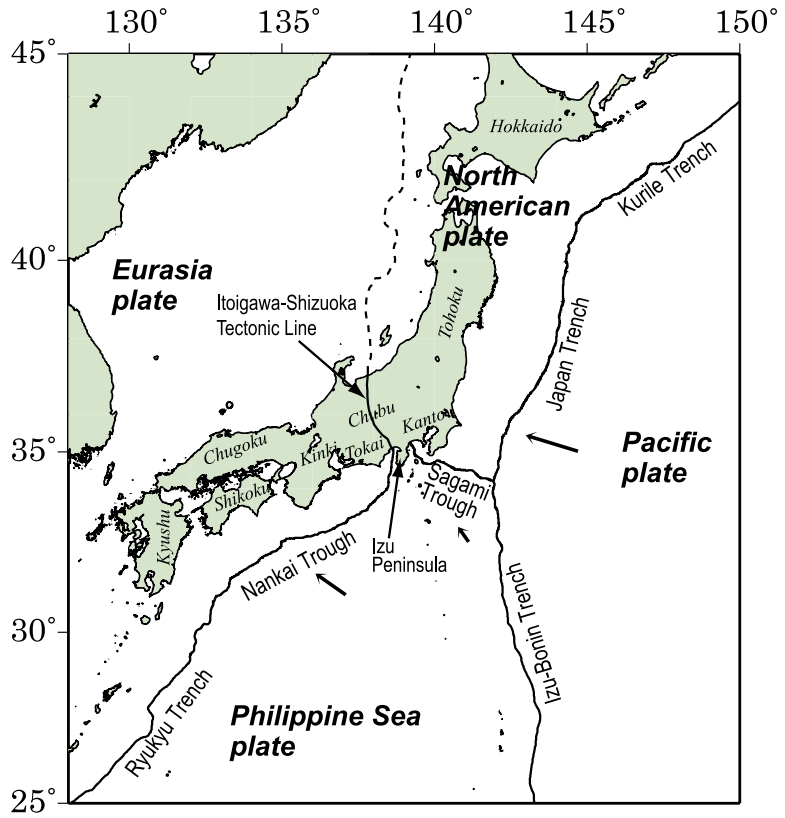

Fig. 1. Tectonic setting around the Japanese Islands.

ther upward within the mantle wedge, finally reaching the arc crust.

The H_2O-rich fluids thus formed play an important role in the processes occurring in the crust and upper mantle. The presence of fluids strongly influences the deformation of crustal rocks. The pore-fluid pressure affects the mechanical processes that control rock deformation and contributes to decrease fault strengths. Fault frictional strength is significantly reduced by fluid overpressure if a Coulomb-type frictional strength criterion is applicable to the frictional regime (effective stress law). Here, fluid overpressure refers to the state in which the fluid pressure prevailing in the pore/crack/fracture space is greater than the hydrostatic fluid pressure. Fluids strongly influence the deformation of mantle rocks as well. The presence of fluids lowers the viscosity coefficient, significantly affecting the flow pattern in the mantle wedge. The H_2O-rich fluids also contribute to the formation of arc volcanoes by lowering the melting point of mantle rocks. Recent studies have shown that the generation of the three main types of earthquakes in subduction zones, i.e., interplate, intraslab, and shallow inland intraplate earthquakes, are all closely related to the H_2O-rich fluids thus formed within the subducted slab, and then transported to the shallow plate interface or the arc crust.

Japan is located in one of the most well-studied subduction zones of the world. NE Japan lies on the North American plate (or the Okhotsk Plate) and SW Japan lies on the Eurasia plate (or Amuria plate) as shown in Fig. 1. These two plates converge along the eastern margin of the Japan Sea in the north, and along the Itoigawa–Shizuoka Tectonic Line in the south. Two oceanic plates subduct beneath the Japanese Islands. In NE Japan, the Pacific plate subducts beneath the North American plate west–northwestward at a rate of 8–9 cm/yr along the Kuril and Japan trenches, and beneath the Philippine Sea plate at a rate of about 6 cm/yr along the Izu–Bonin Trench (DeMets *et al*., 1994). In SW Japan, the Philippine Sea plate subducts beneath the Eurasia plate northwestward at 3–5 cm/yr along the Sagami Trough in the east and along the Nankai Trough in the west (Seno *et al*., 1993, 1996; Wei and Seno, 1998; Heki and Miyazaki, 2001; Miyazaki and Heki, 2001). This plate convergence causes very high seismic activity in the Japanese Islands. Many disastrous earthquakes have occurred repeatedly, causing extensive damage and casualties, such as the 2011 M_w 9.0 Tohoku-Oki earthquake. A dense nationwide seismic network recently constructed covers the whole area of the Japanese Islands (e.g., Okada *et al*., 2004). This spatially dense seismic network and the high seismic activity have provided a large volume of high-quality seismic data, enabling high-resolution imaging of the deep seismic structures of the Japanese subduction zones. Many studies have been carried out in this region using data acquired by the dense seismic network. These studies have revealed the detailed structure of the subducting plates and the associated mantle wedges and overlying crust, and have contributed to the understanding of earthquake generating mechanisms in the subduction zones, especially in the shallow portions.

Here, I review recent seismic studies on the role of H_2O in

doi:10.5047/meep.2017.00501.0001

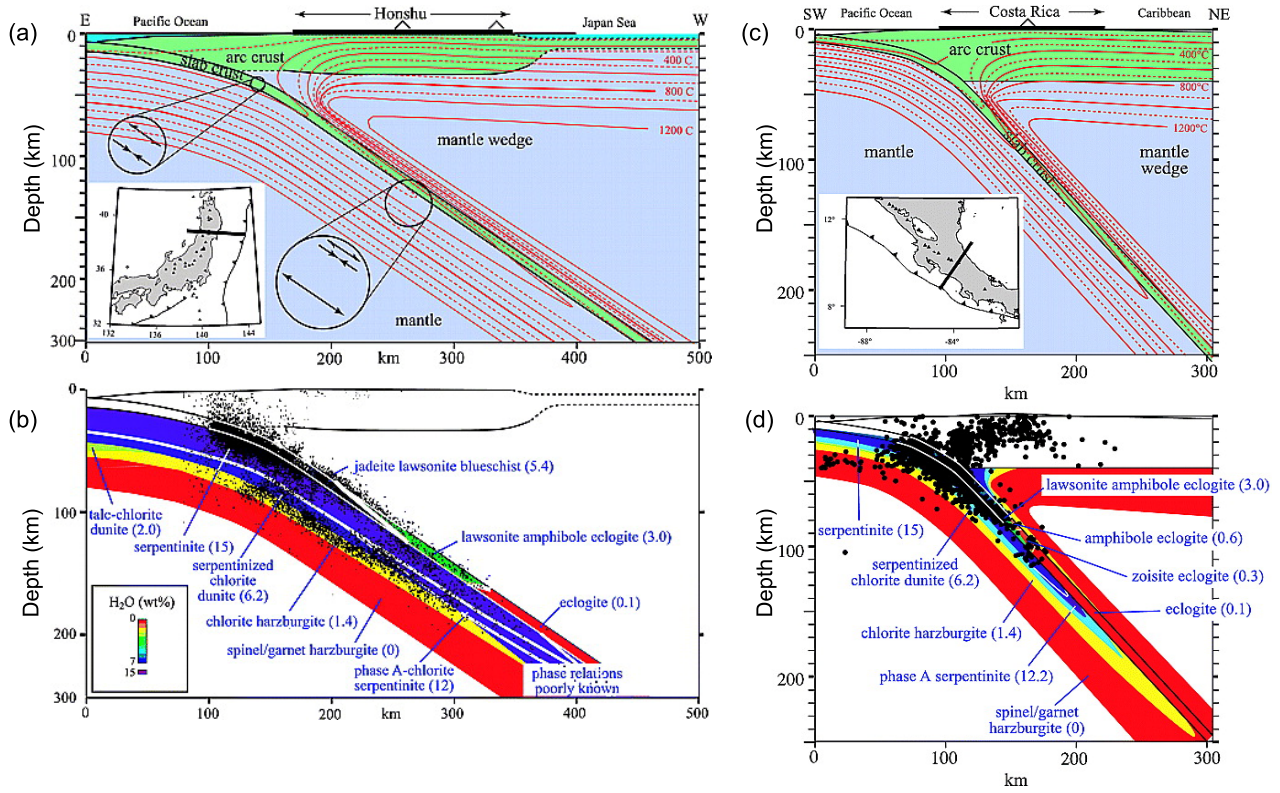

Fig. 2. Across-arc vertical cross-sections showing correlation between intraslab earthquakes and phase transformation in the NE Japan and Costa Rica subduction zones (Hacker *et al*., 2003a). (a) and (c) thermal model. (b) and (d) Metamorphic facies and earthquake foci.

generating subduction zone earthquakes, with an emphasis on the Japanese Islands as a typical example of subduction zones, and inferred mechanisms are discussed.

2. Intermediate-depth Intraslab Earthquakes

At the depths of intraslab earthquakes, the lithostatic pressure is too high and frictional strength too large to allow brittle faulting. Therefore, there must be some special mechanism that weakens shear strength and drives the generation of intraslab earthquakes. Dehydration embrittlement has been proposed as a possible mechanism for reducing the effective normal stress exerted by overpressured fluid and reducing shear strength, allowing intraslab earthquakes to occur (e.g., Griggs and Handin, 1960; Raleigh and Paterson, 1965; Raleigh, 1967; Meade and Jeanloz, 1991; Nishiyama, 1992; Green and Houston, 1995; Kirby, 1995; Kirby *et al*., 1996; Seno and Yamanaka, 1996).

Seismological and petrological studies on subducted slabs, and the materials composing the crust and mantle of subducted slabs, have provided evidence supporting the hypothesis that intermediate-depth intraslab earthquakes are triggered by overpressured fluids but not necessary through the traditional dehydration embrittlement mechanism. Here, intermediate-depth refers to a depth range of 60–300 km. Hacker *et al*. (2003a, b) estimated the locations of the areas within the slabs that contain hydrous minerals in four of the world's typical subduction zones based on the thermal structure of the slabs, and experimentally derived phase diagrams of the crust and mantle materials. As an example, Fig. 2 shows the results for two subduction zones: NE Japan and Costa Rica. As shown in the figure, comparing this information with hypocenter locations revealed that intermediate-depth intraslab events occur within the confined part of the slab retaining the hydrous minerals, where dehydration is expected to occur. Earthquakes mostly do not occur within the other part of the slab, where hydrous minerals are not expected to be found.

Yamasaki and Seno (2003) estimated the dehydration loci of metamorphosed slab crust and serpentinized slab mantle, using phase diagrams of the crust and mantle materials and the thermal structure of the slab, for six of the world's typical subduction zones. Comparing these loci with the hypocenter distribution of intermediate-depth intraslab events revealed that the lower plane seismicity of the double-planed deep seismic zone in the slab occurs at the lower dehydration loci of the serpentinized mantle, whereas the upper plane seismicity is located at the dehydration loci of the metamorphosed oceanic crust (Fig. 3). This strongly supports the hypothesis that intermediate-depth intraslab seismicity is caused by fluid-related embrittlement, and that embrittlement also causes the formation of the double seismic zone within the slab, as previously suggested by Peacock (2001). The earthquakes are concentrated along the dehydration loci of the metamorphosed crust, which forms the upper seismic plane, and the dehydration loci of the serpentine (the lower boundary of the hydrated slab mantle), which forms the lower seismic plane. The formation of the lower seismic plane along the dehydration loci of the serpentine further im-

doi:10.5047/meep.2017.00501.0001

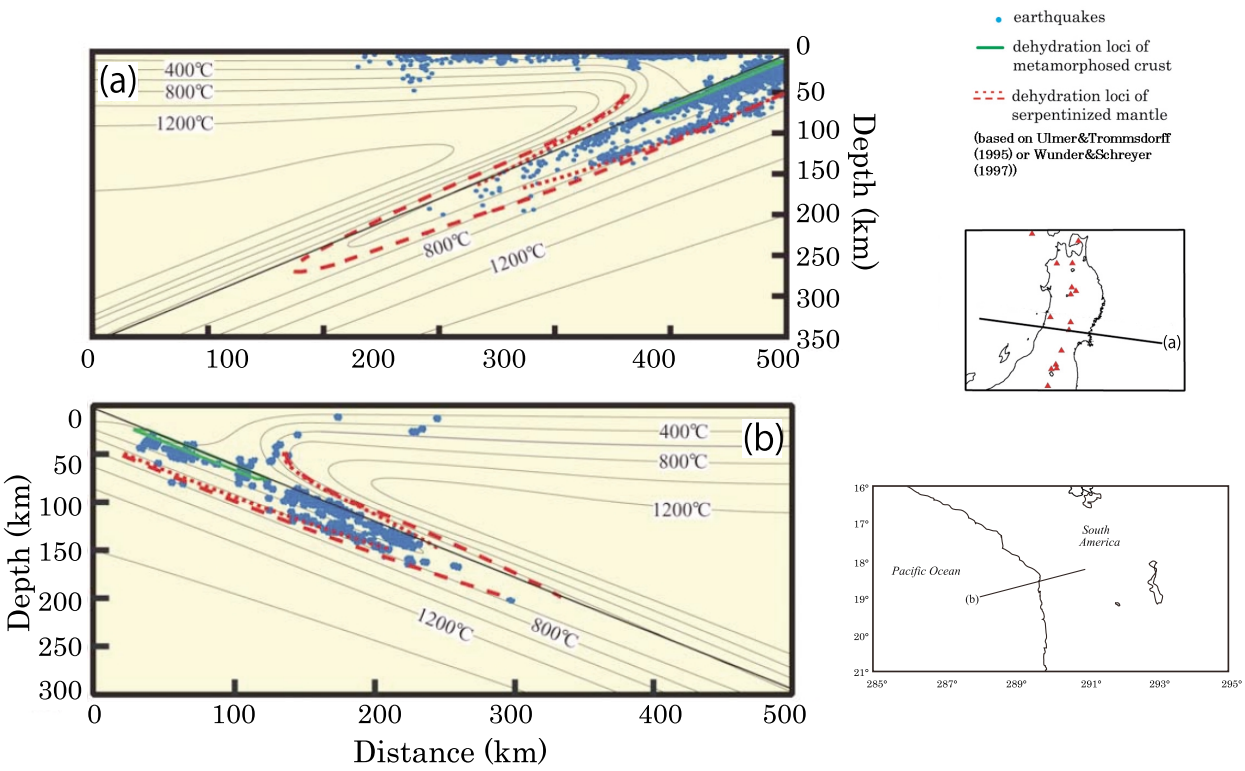

Fig. 3. Across-arc vertical cross-sections of earthquakes and dehydration loci within the subducting slabs beneath (a) Tohoku and (b) N Chile (Yamasaki and Seno, 2003). Dehydration loci of metamorphosed crust and serpentinized mantle are shown by the green lines and red broken or dotted lines, respectively, on vertical cross-sections along the profiles shown in the inset maps. Red broken and dotted lines are based on the phase diagrams by Ulmer and Trommsdorff (1995) and Wunder and Schreyer (1997), respectively. Blue dots are earthquake foci. Thermal structure is shown by isothermal contours.

plies that dehydration reactions are greater when materials reach the facies boundary in the slab mantle.

If even the deep part of the slab mantle is hydrated before its subduction and intermediate-depth intraslab earthquakes are caused by dehydration-derived fluids as discussed above, almost all subduction zones are expected to have double seismic zones within the slabs. Moreover, the separation between the upper and lower seismic planes is expected to decrease with decreasing age of the slab. Brudzinski *et al*. (2007) confirmed this expectation by investigating intermediate-depth intraslab seismicity for 16 subduction zones based on global seismicity data accurately relocated by Engdahl *et al*. (1998) and Engdahl (2006). They demonstrated that such double seismic zones could be observed in all of the 16 subduction zones they investigated, and that the separation of the double seismic zone increases with age, as shown in Fig. 4.

The recent resolution of the hypocenter distribution and seismic velocity structure within the subducted slabs, using data from the dense nationwide seismic network in Japan, has provided further evidence supporting the dehydration-related embrittlement hypothesis for the generation of intermediate-depth intraslab earthquakes. More detailed spatial correlations between concentrated seismicity, the dehydration loci of metamorphosed crust, and changes in seismic velocity within the slab crust, have been detected for the Pacific plate subducted beneath eastern Japan as described below.

Studies on seismic tomography, hypocenter locations, and focal mechanisms have made it possible to identify the complex structure of the oceanic plates subducting beneath Japan. The configuration of the subducting Pacific plate was estimated by precisely relocating earthquake hypocenters and by using focal mechanism information for those earthquakes (Kita *et al*., 2006; Nakajima *et al*., 2009b). Arrival time data of *P*-to-*S* and *S*-to-*P* converted waves at the upper plate interface from intermediate-depth events were also used for the estimation (Matsuzawa *et al*., 1986, 1990; Hasegawa *et al*., 1994; Zhao *et al*., 1997b). Although the configuration of the Philippine Sea plate subducting beneath SW Japan had been estimated mainly on the basis of seismicity data by setting the plate interface to coincide with the upper envelope of intraslab events (e.g., Mizoue *et al*., 1983; Kasahara, 1985; Yamazaki and Ooida, 1985; Ishida, 1992; Noguchi, 1998, 2007; Miyoshi and Ishibashi, 2004; Hori, 2006), it was poorly defined because only limited seismic activity is associated with the subduction of this plate. Moreover, seismic reflection and refraction surveys recently carried out in SW Japan suggest that the location of the plate interface is several kilometers shallower than the upper limit of intraslab seismicity (Kodaira *et al*., 2000, 2002, 2004; Kurashimo *et al*., 2002; Nakanishi *et al*., 2002). These observations imply that the upper envelope of intraslab seismicity does not necessarily correspond to the plate interface. A

doi:10.5047/meep.2017.00501.0001

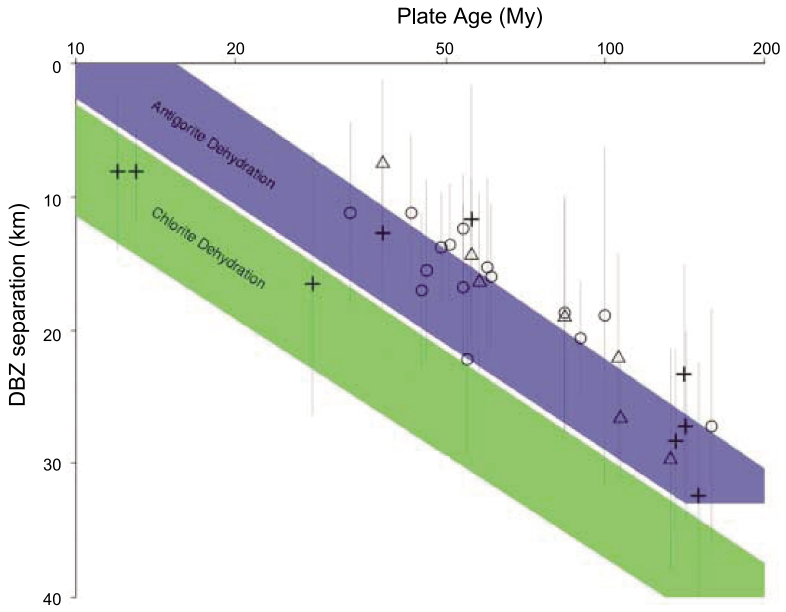

Fig. 4. Separation between the upper and lower planes of the double seismic zone plotted against subducting slab age for 16 subduction zones (Brudzinski *et al*., 2007). The separations are shown by symbols. Different symbols represent stress orientations as triangles for typical down-dip compression, circles for a different pattern, and crosses for unknown. Vertical lines are 1-SD uncertainties from Gaussian fits. Predicted separations of the double seismic zone due to the lower seismic plane resulting from ultimate dehydration of antigorite and chlorite based on Hacker *et al*. (2003b) are shown by blue and green shaded areas, respectively. Antigorite dehydration is more consistent with observed separations than chlorite dehydration.

recent double-difference tomography study by Hirose *et al*. (2008a, b) resolved this problem and clearly imaged the crust portion of the Philippine Sea plate as a layer with low S-wave velocity and high V_p/V_s (P-wave velocity to S-wave velocity ratio), which enabled the location of the Philippine Sea plate to be determined at depths of 20–60 km. The deeper portions (60–200 km) of the plate were determined based on a seismic tomography-derived upper envelope of the high-seismic-velocity slab (Nakajima and Hasegawa, 2007a).

The geometry of the subducting Pacific and Philippine Sea slabs estimated in these ways is shown by contours in Fig. 5. The estimated configuration shows that the Philippine Sea slab subducting under SW Japan undulates down to depths of 60–200 km, and is continuous from Kanto to Kyushu without disruption or splitting, even within areas north of the Izu Peninsula. The contact zone between the Pacific and Philippine Sea slabs, as estimated from seismic tomography and focal mechanism studies (Nakajima *et al*., 2009b; Uchida *et al*., 2009, 2010; Nakajima and Hasegawa, 2010), is present across a broad area beneath the Kanto area, correlating with the location of the Kanto Plain. This broad contact zone beneath the Kanto Plain contributes to an anomalously deep interplate and intraslab earthquake activity due to the low temperatures that result from the subduction of the Philippine Sea slab immediately above the Pacific slab (Hasegawa *et al*., 2009; Nakajima *et al*., 2009b; Uchida *et al*., 2009, 2010; Nakajima and Hasegawa, 2010).

Kita *et al*. (2006) detected a pronounced belt-like concentration of seismicity in the upper plane of the double seismic zone, nearly parallel to the ∼80 km isodepth contour of the upper surface of the Pacific slab beneath Tohoku (Figs. 6(a), (c)) and Hokkaido. This pronounced seismic area, termed an 'upper-plane seismic belt', is located within the oceanic crust at a depth near a metamorphic facies boundary (A in Fig. 6(a)) in the crustal material, suggesting that it is associated with intraslab earthquakes generated by dehydration-related embrittlement. As shown in Fig. 6(b), seismic tomography imaging indicates that low-seismic-velocity slab crust persists down to the depth of this upper-plane seismic belt, but not below (Tsuji *et al*., 2008), suggesting that a phase transformation and eclogite formation occur in the slab crust at this depth.

The depth at which this phase transformation takes place is expected to depend on the temperature within the slab crust. If this is the case, local low-temperature conditions in the Pacific slab immediately below the slab contact zone beneath the Kanto area should cause a delay in phase transformation, resulting in local deepening of the upper-plane seismic belt and of the down-dip end of the low-seismic-velocity oceanic crust. As expected, both the upper-plane seismic belt and the low-velocity oceanic crust deepen beneath the slab contact zone in the Kanto area. Hasegawa *et al*. (2007) showed that the upper-plane seismic belt beneath the Kanto area is oblique to the ∼80 km iso-depth contour, deepening toward the north from a depth of ∼100–140 km along a trend nearly parallel to the down-dip edge of the slab contact zone (Fig. 6(c)). A seismic tomography study by Nakajima *et al*. (2009a) indicated that the low-seismic-velocity region in the slab crust extends to the uppermost depths where the obliquely trending upper-plane seismic belt is observed (Fig. 6(d)). These observations strongly support an interpretation that low-temperature conditions asso-

doi:10.5047/meep.2017.00501.0001

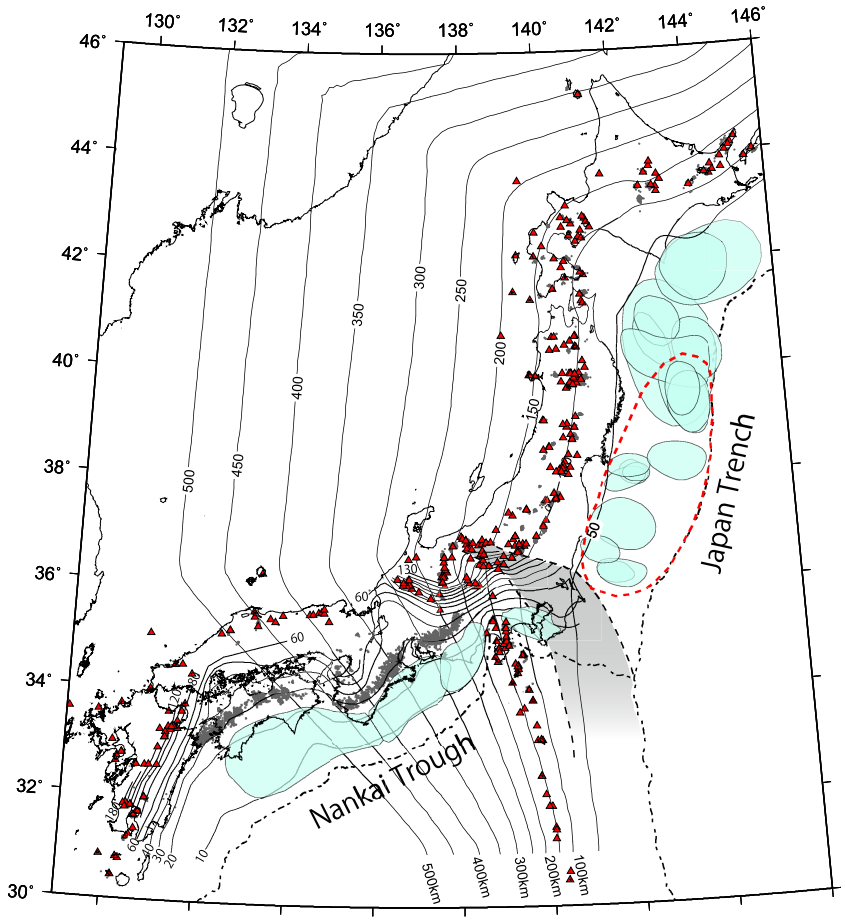

Fig. 5. Map showing isodepth contours of the upper surfaces of the Pacific and Philippine Sea plates subducting beneath the Japanese Islands (Baba *et al*., 2002; Nakajima and Hasegawa, 2007a; Hirose *et al*., 2008a, b; Nakajima *et al*., 2009a, b; Kita *et al*., 2010). The slab-slab contact zone beneath the Kanto area is shaded in gray and enclosed by two broken curves (Nakajima *et al*., 2009b; Uchida *et al*., 2009). The source area of the 1923 Kanto earthquake (Wald and Somerville, 1995) and those of predicted Tokai, Tonankai, and Nankai earthquakes (HERP, MEXT, http://www.jishin.go.jp/main/index.html) are shown as light blue ellipses. Source areas of $M > 7$ interplate earthquakes on the upper interface of the Pacific plate in the past 80 years (Umino *et al*., 1990; Uchida *et al*., 2009) are also shown as light blue ellipses. The source area of the 2011 Tohoku-Oki earthquake is shown by a dashed ellipse. Red triangles denote Quaternary volcanoes. Deep low-frequency tremors/earthquakes are shown as dots.

ciated with the slab-slab contact zone beneath the Kanto area cause a delayed (and so deeper) onset of eclogite-forming phase transformations. A similar local deepening of the upper-plane seismic belt is also seen in the Pacific slab under the Hokkaido corner, which is probably caused by thermal shielding due to the cold subducted forearc crust that caps the slab there, and the resulting delay of eclogite-forming phase transformation in the oceanic crust (Kita *et al*., 2010). These observations also support the fluid-related embrittlement hypothesis that intermediate-depth intraslab earthquakes are caused by highly-reduced effective normal stress by overpressured fluids expelled from the slab due to dehydration-related phase transformations.

The locations of the upper and lower seismic planes of the double seismic zone are likely prescribed by the dehydration loci of the metamorphosed slab crust and serpentinized slab mantle, respectively, as described above (Yamasaki and Seno, 2003; Brudzinski *et al*., 2007). At shallower depths, these two dehydration loci are nearly parallel to each other, but at deeper depths, the dip of the lower dehydration locus becomes less steep and the upper and lower dehydration loci eventually merge (see Fig. 3). The upper and lower seismic planes of the double seismic zone in Tohoku also merge at a depth of about 150 km (Umino and Hasegawa, 1975; Hasegawa *et al*., 1978a, b), suggesting that they just trace the dehydration loci of the slab crust and slab mantle (Seno and Yamanaka, 1996). Serpentinized mantle materials can exist within the area between the upper and lower seismic planes because of lower temperature conditions there. Seismic waveform data recorded by the nationwide dense seismic network in Japan have allowed precision imaging of the internal structure of the subducting slab.

A recent high-resolution seismic attenuation tomography study seems to have detected this serpentinized mantle portion, identifying it as existing in low-Q_p areas. Across-arc vertical cross-sections of ${Q_p}^{-1}$ in Tohoku (Fig. 7; Nakajima *et al*., 2013) clearly show the existence of low-Q_p zones in the area between the upper and lower seismic planes, particularly in the deepest portion of this wedge-shaped interplane area (Figs. 7(b) and 7(e)). As the slab subducts, serpentinized mantle materials in the lowermost portion of the lower seismic plane decompose and release H_2O, causing

doi:10.5047/meep.2017.00501.0001

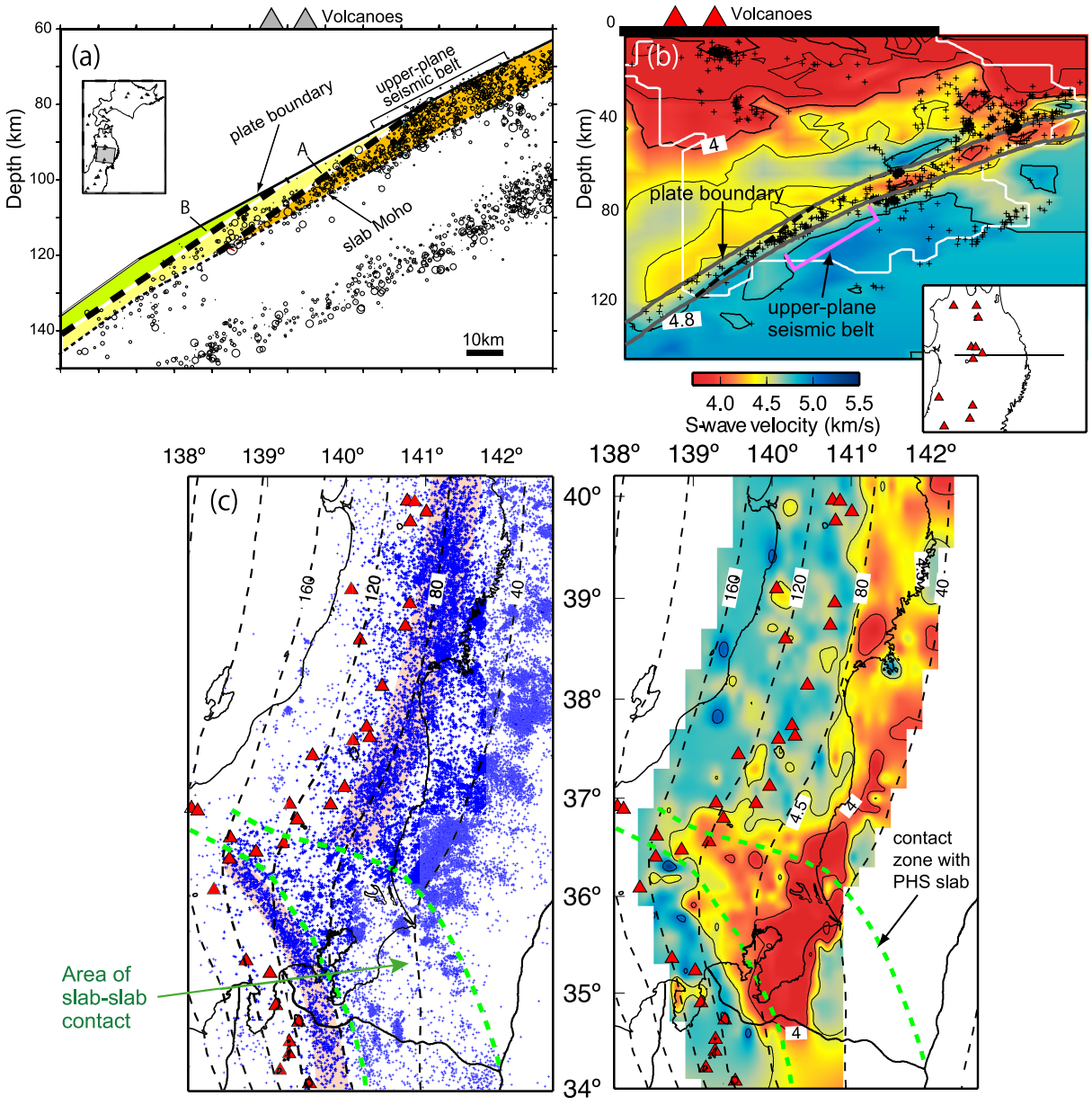

Fig. 6. (a) Across-arc vertical cross-section showing the location of intraslab earthquakes in central Tohoku (Kita *et al*., 2006). Intraslab events are shown by open circles. A and B indicate facies boundaries estimated based on the phase diagram by Hacker *et al*. (2003a) and the thermal structure by Peacock and Wang (1999). A: boundary between jadeite lawsonite blueschist and lawsonite amphibole eclogite facies. B: boundary between lawsonite amphibole eclogite and eclogite facies. (b) Across-arc vertical cross-section showing variations in *S*-wave velocity in central Tohoku (Tsuji *et al*., 2008). *S*-wave velocities are shown by the color scale at the bottom of figure. The upper interface and the Moho of the Pacific plate are shown as solid lines. The facies boundary A shown in (a) is shown here as a broken line. (c) Distribution of earthquake foci within the crust of the Pacific slab. Events at 0–10 km below the upper plate surface are shown as blue dots, and the upper plane seismic belt is pink. (d) *S*-wave velocity distribution in the crust of the Pacific slab on a curved plane 5 km below the upper plate surface (Nakajima *et al*., 2009b). The slab-slab contact zone beneath the Kanto area is delineated by two broken green curves. Black broken curves and red triangles show iso-depth contours of the upper surface of the Pacific slab and the location of active volcanoes, respectively.

lower-plane seismicity. Then H_2O migrates upward passing through the serpentinized layer corresponding to the lower seismic plane and finally hydrates mantle materials immediately above the top of the layer. This process repeats as the slab subducts. Thus, H_2O or the serpentinized mantle materials are expected to accumulate in the wedge-shaped interplane area, especially in its deepest portion, which is actually observed in the slab mantle beneath Tohoku by seismic attenuation tomography (Figs. 7(b) and 7(e)).

As described above, locations of intraslab seismicity and the seismic velocity and attenuation structures within subducting slabs strongly support the fluid-related embrittlement hypothesis for generating intermediate-depth intraslab events. The fluid-related embrittlement posits that the brittle fracture takes place because of the decrease in effective normal stress due to the pore pressure of H_2O released by the dehydration of slab materials. This mechanism should work at shallow depths. In fact, by performing triaxial com-

doi:10.5047/meep.2017.00501.0001

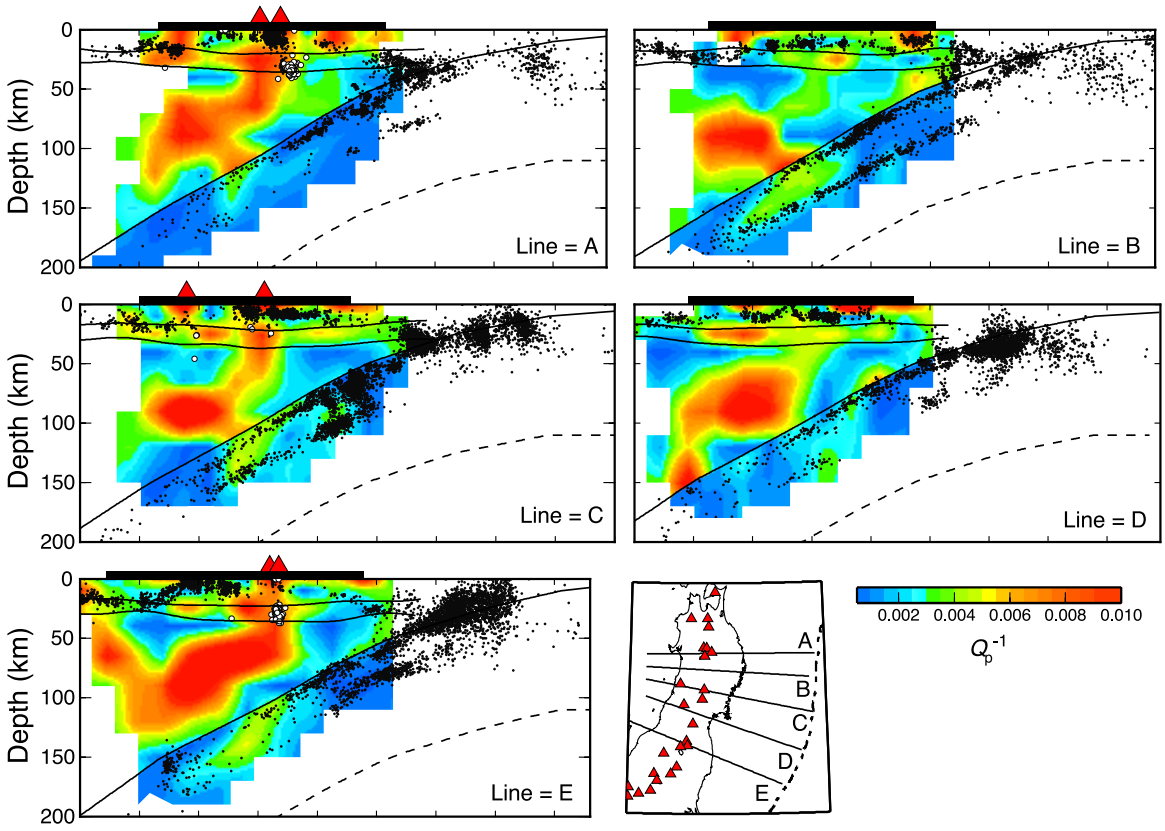

Fig. 7. Across-arc vertical cross-sections of $Q_p{}^{-1}$ in the NE Japan subduction zone (Nakajima *et al.*, 2013). The cross-sections are taken along the five profiles shown in the inset map. Black dots represent ordinary earthquake foci and white circles show deep low-frequency earthquakes. $Q_p{}^{-1}$ is shown by the color scale at the bottom.

pression tests of serpentinite at confining pressures up to 0.5 GPa, Raleigh and Patterson (1965) found that a brittle fracture took place at temperatures higher than 375°C while the plastic deformation occurred below 340°C. However, it is not evident whether the same mechanism is applicable to intermediate-depth events that occur at depths of much higher confining pressures, since the effective stress law does not work efficiently below the brittle-ductile transition depth (e.g., Hirth and Beeler, 2015). Moreover, some of the candidate dehydration reactions which cause the dehydration embrittlement have negative Clapeyron slopes. In that case, the total volume change associated with the dehydration becomes negative, which might work toward suppressing the hydraulic instability.

Some laboratory experiments, however, have shown that hydraulic embrittlement actually takes place even in the case that the confining pressure is higher than the brittle-ductile transition depth and the dehydration reaction has a negative Clapeyron slope (e.g., Dobson *et al.*, 2002; Jung *et al.*, 2004, 2009). On the contrary, other experimental studies argue that the unstable fault behavior does not develop at such a pressure range (e.g., Chernak and Hirth, 2010, 2011; Proctor and Hirth, 2015). As above, the details of the process that actually lead to the earthquake rupture are still being debated and further investigations are needed. Since intermediate-depth events actually occur at the dehydration boundaries within the slab, some sort of hydraulic fracture might take place due to the excess pore fluid pressure locally formed for some reason. Alternatively, intermediate-depth earthquakes are generated both by the fluid-related embrittlement and the thermal shear instability (e.g., Ogawa, 1987; Hobbs and Ord, 1988; Karato *et al.*, 2001; Kelemen and Hirth, 2007): the local excess pore fluid pressure might cause initiation of the earthquake rupture via hydraulic fracture, then triggering the subsequent earthquake ruptures through the thermal shear instability. In any case, it is estimated that H_2O released by the dehydration of slab materials plays an important role in generating intermediate-depth intraslab earthquakes.

3. Interplate Earthquakes

Shallow portions (<∼25–50 km) of the interface between the subducting oceanic plate and the overriding continental plate in subduction zones (megathrust) host the world's largest earthquakes, and the majority of seismic energy on the Earth is released there (e.g., Kanamori, 1978). It is known that seismic coupling coefficients, the ratio of seismic slip to total interplate slip, are not 100% and vary by location on the megathrust. This observation suggests that some interplate slip is accommodated by aseismic slip. The seismic coupling coefficient on the megathrust east of northern Tohoku is estimated to be ∼25%, while that east of southern Tohoku–Kanto is ∼10% or less (e.g., Kanamori, 1977; Kato, 1979; Seno, 1979; Peterson and Seno, 1984; Pacheco *et al.*, 1993). These coupling coefficients indicate that much

doi:10.5047/meep.2017.00501.0001

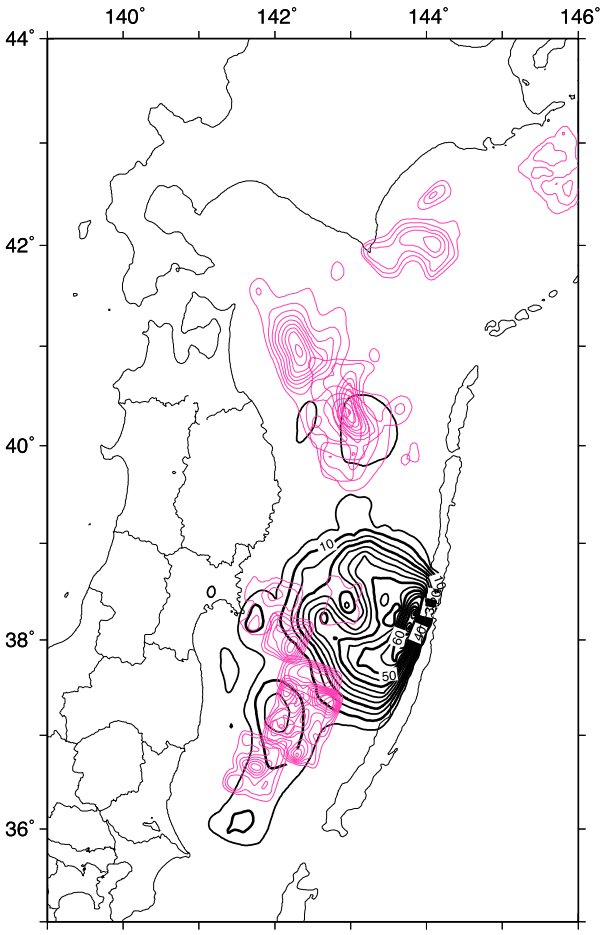

Fig. 8. Slip distribution of large interplate earthquakes along the megathrust in the NE Japan subduction zone. Slip distributions of earthquakes with $M > 7$ over the last ~70 years are shown by pink contours (Murotani, 2003; Yamanaka and Kikuchi, 2003, 2004) and that of the 2011 Tohoku-Oki earthquake is shown by black contours (Iinuma *et al*., 2012).

of the interplate slip is accommodated by aseismic slip in these regions. Detailed analyses of seismic waveforms for large interplate events over the last 70 years in the NE Japan subduction zone have revealed that large slip areas ruptured successively by large earthquakes lie in the same location on a given section of the plate interface and that asperities (locked areas) are persistent features in those areas (e.g., Yamanaka and Kikuchi, 2003, 2004). The estimated slip distributions of large ($M > 7$) interplate events are shown by pink contours in Fig. 8, where the large slip areas of the earthquakes are asperities. Inversions of GPS data on land provide information on the spatial distribution of interplate coupling, showing that these asperities are actually located in areas with strong coupling on the plate boundary (e.g., Ito *et al*., 2000; Nishimura *et al*., 2000; Suwa *et al*., 2006; Hashimoto *et al*., 2009; Loveless and Meade, 2010).

The 2011 M_w 9.0 Tohoku-Oki earthquake, the greatest earthquake in the modern history of Japan, ruptured a broad area of the plate boundary east of Tohoku approximately 500 km long and 200 km wide. The slip distribution of this earthquake, estimated from crustal deformation data on land and at the ocean bottom (e.g., Iinuma *et al*., 2012; Ozawa *et al*., 2012; Romano *et al*., 2012), indicates that this event ruptured several asperities simultaneously as shown in Fig. 8. Moreover, an anomalously large slip exceeding ~50 m occurred in the shallow portion of the plate interface near the trench axis. This was the main cause of the incredible tsunami height along the Sanriku coast of northern Tohoku. Unfortunately, this large asperity patch on the shallow plate interface near the trench axis had not been detected before the earthquake, since the GPS network on land is completely insensitive to the interplate coupling there. This is part of the reason why the Japanese government's long-term earthquake forecasts did not anticipate such a large earthquake to occur in this subduction zone (http://www.jishin.go.jp/main/index.html). Figure 8 further shows that even the non-asperity areas on the plate interface slipped considerably in the Tohoku-Oki earthquake, demonstrating that several asperity patches, as well as non-asperity areas, may all slip simultaneously in the case of such a great earthquake. Actually, analyses of GPS data on land, before the earthquake, suggested that even non-asperity areas on the plate interface are partly coupled (e.g., Ito *et al*., 2000; Nishimura *et al*., 2000; Suwa *et al*., 2006; Hashimoto *et al*., 2009; Loveless and Meade, 2010). Furthermore, slip rates on the asperity patches estimated from the repeated ruptures of recent large interplate earthquakes are significantly smaller than the relative rate of plate motion in this subduction zone (e.g., Yamanaka and Kikuchi, 2003). These observations indicate that such areas on the plate interface eventually slip in a large episodic slow slip event or a large earthquake (Kanamori *et al*., 2006), as actually occurred in the 2011 M_w 9.0 event.

What causes asperities to form on the plate interface? Of course, the question has not yet been resolved, but some observations suggest that H_2O might play a role. Seismic tomography studies show that seismic wave velocities in the mantle wedge right above the asperity patches on the megathrust have normal values, whereas those just above the non-asperity (stably sliding) areas have anomalously low values, indicating that serpentinized mantle exists there (Mishra *et al*., 2003; Yamamoto *et al*., 2006; Zhao *et al*., 2007a, b). These low-velocity areas in the forearc mantle wedge have a high V_p/V_s and probably correspond to hydrated mantle affected by slab-origin H_2O. This suggests that serpentinized mantle wedge materials immediately above the plate interface, formed by the supply of H_2O derived from the slab, contribute to the frictional properties on the megathrust, allowing aseismic slip to occur on the plate interface due to its stable sliding nature (Peacock and Hyndman, 1999).

Pore fluid pressure on the megathrust might make a more direct contribution. Slow slip events that accompany deep non-volcanic, low-frequency tremors/earthquakes occur periodically at intervals of approximately 3 or 6 months at the down-dip extension of the locked area of the Tokai, Tonankai, and Nankai earthquakes on the plate interface in SW Japan (Obara, 2002, 2010; Obara *et al*., 2004). Slow slip events that recur regularly at an interval of approximately 14 months accompanying deep low-frequency

doi:10.5047/meep.2017.00501.0001

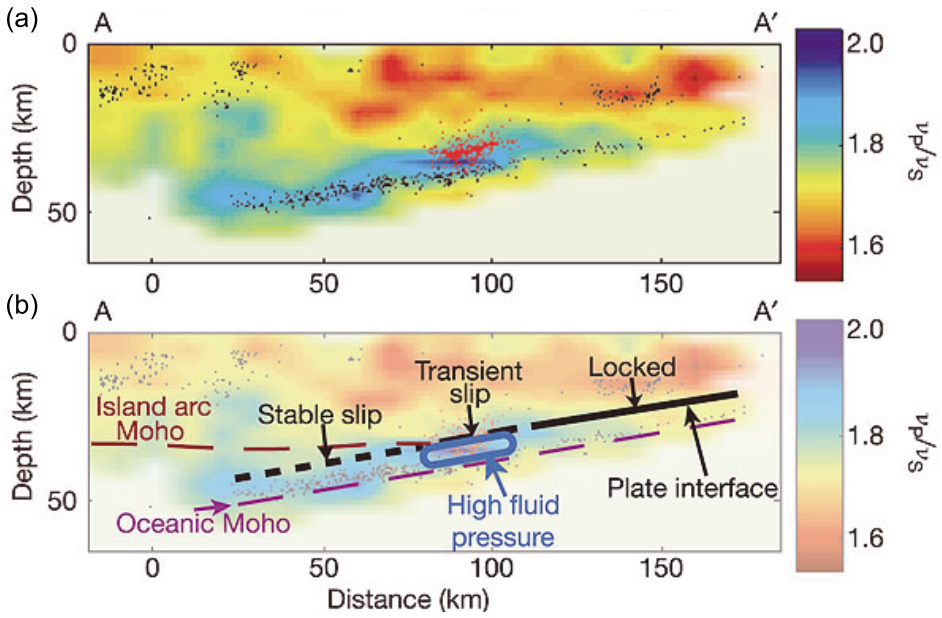

Fig. 9. (a) Across-arc vertical cross-section of V_p/V_s in Shikoku, SW Japan and (b) schematic diagram of the interpretation overlaid on the V_p/V_s structure (Shelly *et al*., 2006). V_p/V_s is shown by the color scale on the right. Faded areas represent regions of poor resolution. Red and gray dots are relocated hypocenters of deep low-frequency earthquakes/tremors and ordinary earthquakes, respectively. Deep low-frequency earthquakes/tremors occur along the plate interface, coincident with the zone of transient slip, while ordinary earthquakes within the slab occur primarily within the lower crust.

tremors/earthquakes were also detected in the Cascadia subduction zone (Dragert *et al*., 2001; Rogers and Dragert, 2003). Later, similar slow slip events and deep low-frequency tremors/earthquakes have been detected in many plate boundary zones around the world, including the San Andreas Fault, Alaska, New Zealand, and Mexico (e.g., Nadeau and Dolenc, 2005; Peterson and Christensen, 2009; Payero *et al*., 2008; Peng and Gomberg, 2010). The low-frequency tremors/earthquakes are interpreted as accelerations and/or decelerations of slow shear slips on the plate interface associated with slow slip events (Shelly *et al*., 2006; Ide *et al*., 2007). They are thought to be caused by overpressured fluids on the plate interface, since they occur at a depth much deeper than the unstable/stable transition depth (e.g., Obara, 2002, 2010; Obara *et al*., 2004). Actually, precise images of seismic velocity structures show that those low-frequency tremors/earthquakes occur in areas with low seismic velocities and anomalously high V_p/V_s values, demonstrating the existence of overpressured fluids there (Kodaira *et al*., 2004; Shelly *et al*., 2006; Audet *et al*., 2009; Kato *et al*., 2010). Figure 9 is an example of such precise seismic velocity structure imaging showing a vertical cross-section of V_p/V_s along a line crossing Shikoku, in SW Japan. The figure clearly shows anomalously high V_p/V_s values in the slab crust immediately below the low-frequency tremors/earthquakes on the plate interface, suggesting a high fluid pressure there.

Information on earthquake-generating stress fields can be obtained from stress tensor inversion of earthquake focal mechanism data. The orientations of the principal stress axes and the stress ratio can be estimated from the inversion, but we cannot estimate the differential stress magnitude. Stress field changes after a large earthquake, if they exist, provide a unique opportunity to estimate the magnitude of the differential stress (e.g., Hardebeck and Hauksson, 2001; Wesson and Boyd, 2007). Because of its extremely large magnitude and the dense broadband seismic network deployed in the Japanese Islands, temporal changes in the stress field after the 2011 great Tohoku-Oki earthquake were able to be clearly determined using stress tensor inversions (Hasegawa *et al*., 2011, 2012a). Figure 10 shows the spatial distribution of focal mechanisms obtained by centroid-moment tensor inversions of broadband seismograms recorded at F-net and Hi-net stations on land (Asano *et al*., 2011). The focal mechanisms are shown on vertical cross-sections along lines normal to the trench axis in the inset map. This figure clearly shows that thrust fault-type earthquakes were predominant before the Tohoku-Oki earthquake, whereas normal fault-type earthquakes increased significantly after the earthquake, suggesting that the Tohoku-Oki earthquake changed the stress field there.

Stress tensor inversion results for earthquakes before and after the Tohoku-Oki earthquake near its fault plane are shown in Fig. 11 (Hasegawa *et al*., 2011). As the figure shows, the maximum compressive stress (σ_1) axis before the earthquake is directed toward the plate convergence, plunging oceanward at an angle of 25–30° for both the north and south parts of the source area (Figs. 11(a) and 11(c)). After the Tohoku-Oki earthquake, however, the plunge angle increased significantly by 30–35° (Figs. 11(b) and 11(d)). The observed angles of rotation of the σ_1 axis due to the earthquake are plotted in Fig. 12 on a $\Delta\theta$-θ diagram (Hardebeck and Hauksson, 2001), where $\Delta\theta$ is the angle of rotation and θ is the angle the σ_1 axis makes with the fault plane. The fig-

doi:10.5047/meep.2017.00501.0001

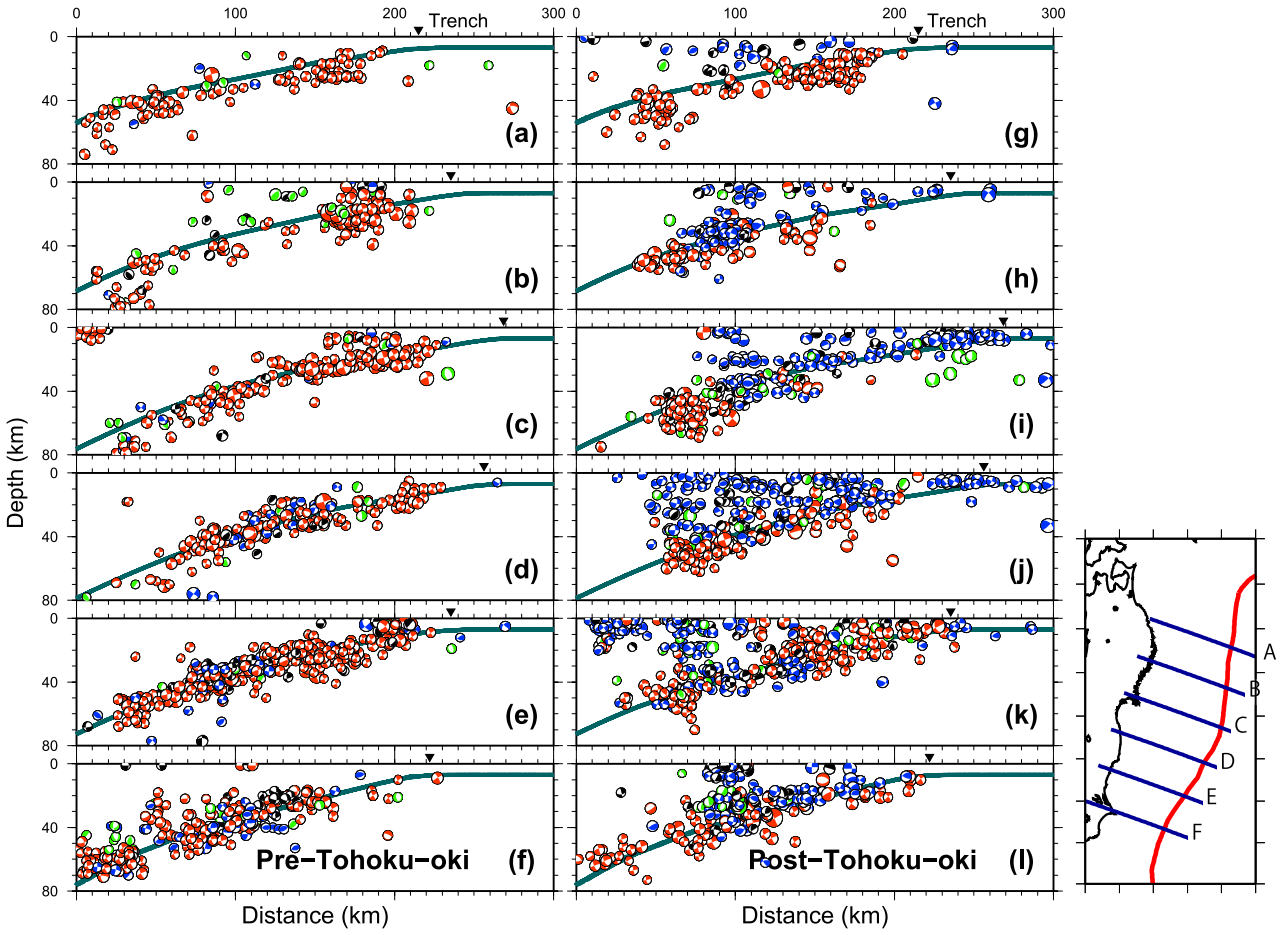

Fig. 10. Trench-perpendicular vertical cross-sections of centroid-moment tensors determined by Asano *et al.* (2011) (a)–(f) before and (g)–(l) after the 2011 Tohoku-Oki earthquake (Hasegawa *et al.*, 2012a). The before (a)–(f) and after (g)–(l) pairs represent cross-sections along lines A to F in the inset map. Blue, green, red, and black 'beach balls' denote normal, strike-slip, thrust, and other types of focal mechanisms, respectively. The heavy blue line shows the plate interface. An inverted triangle marks the position of the trench axis.

ure shows that the ratio of the mainshock stress drop to the background maximum shear stress is estimated to be 0.5–1.0 (Fig. 12). This indicates that the shear stress that caused the M_w 9.0 Tohoku-Oki earthquake was mostly released by the earthquake, or that the stress drop during the earthquake was nearly complete. Adopting the average stress drop of 8 MPa obtained by observed crustal deformation data on land and at the ocean bottom (Iinuma *et al.*, 2012), the magnitude of the shear stress that caused the Tohoku-Oki earthquake is estimated to be 8–16 MPa. This suggests that the plate interface is very weak, probably due to the effect of overpressured fluids. If this is the case, the pore pressure ratio, i.e., the ratio of pore pressure to the lithostatic pressure, on the megathrust is estimated to be 0.96–0.98.

Similar coseismic rotations of the principal stress axes were also reported for two other recent great megathrust earthquakes, the 2004 M_w 9.2 Sumatra-Andaman earthquake and the 2010 M_w 8.8 Maule, Chile, earthquake as shown in Fig. 13 (Hardebeck, 2012). Although the analysis used Global Centroid Moment Tensor (GCMT) solutions (Ekström *et al.*, 2012), so the amount of focal mechanism data used for stress tensor inversions is much smaller than in the case of the 2011 Tohoku-Oki earthquake described above, it showed significant rotations of the σ_1 axis associated with those earthquakes, from shallow plunging σ_1 axes to steeper plunging axes near 45° (Fig. 14). The observed stress rotations imply nearly complete stress drops in these two great megathrust earthquakes, as in the case of the Tohoku-Oki earthquake. More than 80% of the pre-mainshock stress was estimated to have been relieved in the Maule, Chile, earthquake and in the northern part of the Sumatra-Andaman rupture and ∼60% was relieved in the southern part of the Sumatra-Andaman rupture. The GCMT data also showed significant rotations of the principal stress axes and thus a near-complete stress drop in the Tohoku-Oki earthquake (Fig. 14), as already shown by the dense local broadband network (F-net and Hi-net) data (Fig. 12). These observations suggest that megathrusts are weak in general.

Changes in stress fields due to the Tohoku-Oki earthquake were also observed in the upper plate right above its fault plane (Hasegawa *et al.*, 2012a; Hasegawa and Yoshida, 2015). Before the earthquake, the σ_1 axis was oriented in the direction of the plate convergence, specifically, in the direction of an estimated large slip area near the trench axis (Fig. 15(a)). For the area in which the static stress change was larger than 15–25 MPa (Fig. 15(c)), the stress field

doi:10.5047/meep.2017.00501.0001

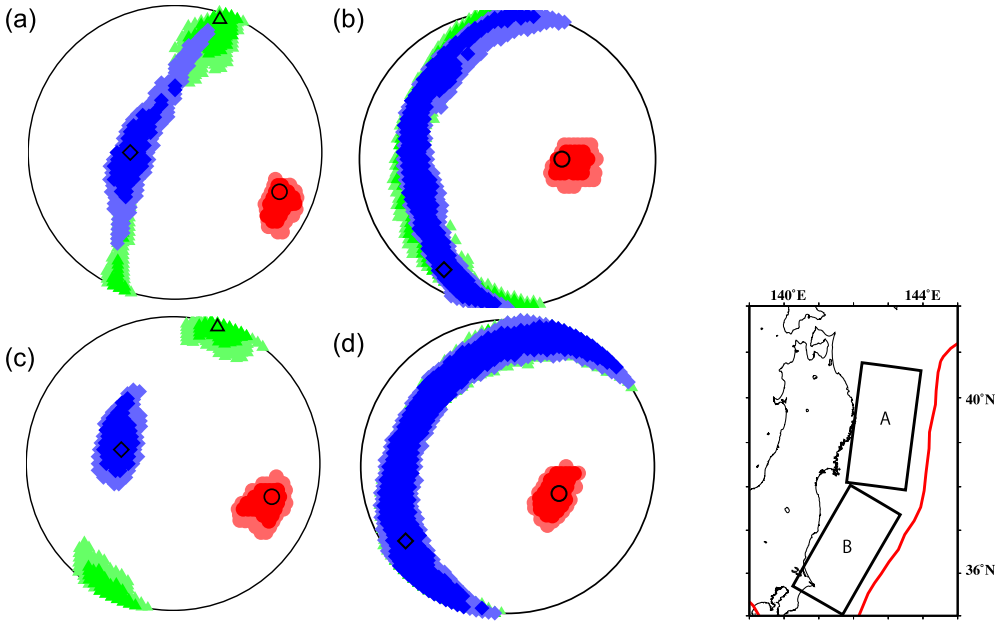

Fig. 11. Orientations of principal stresses σ_1 (maximum compressive stress, red circle), σ_2 (intermediate principal stress, green triangle), and σ_3 (minimum compressive stress, blue square) (a) before and (b) after the 2011 M_w 9.0 Tohoku-Oki earthquake in region A in the inset map (Hasegawa *et al*., 2011). (c) and (d) show the same principal stresses for region B. Principal stress orientations are shown on the lower focal hemisphere, deep and light colors indicating principal stresses falling within 68% and 95% confidence levels, respectively.

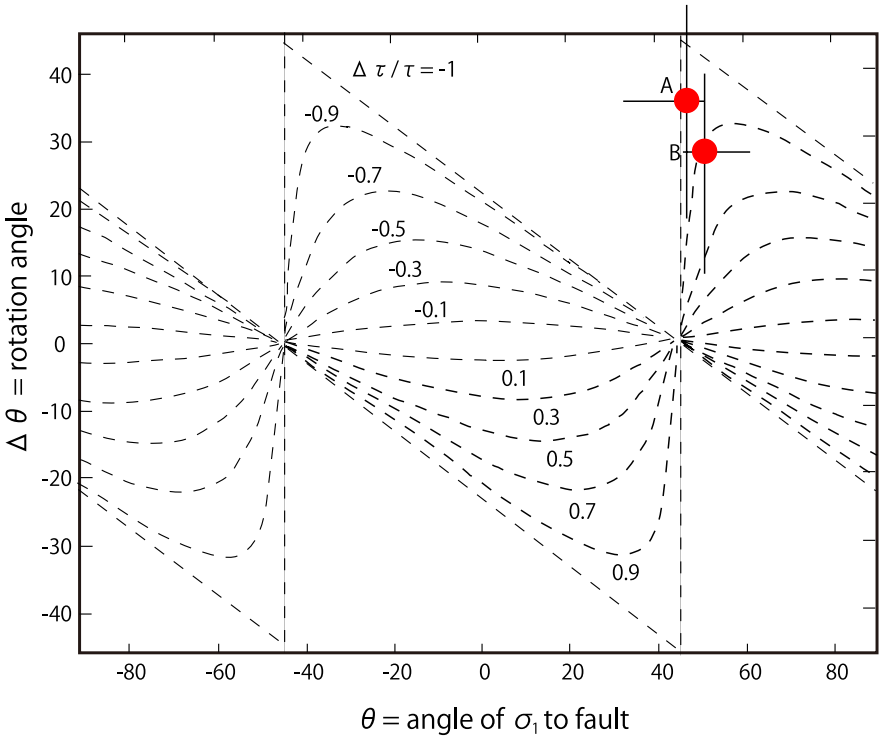

Fig. 12. Stress rotations associated with the mainshock rupture. Rotation of σ_1 axis ($\Delta\theta$) is shown as a function of the angle of the σ_1 axis to the fault plane (θ) for various values of $\Delta\tau/\tau$, the ratio of stress drop to the maximum shear stress before the mainshock. Observed rotation angles associated with the 2011 Tohoku-Oki earthquake for regions A and B are plotted as red circles with their confidence ranges. (After Hasegawa *et al*., 2011)

doi:10.5047/meep.2017.00501.0001

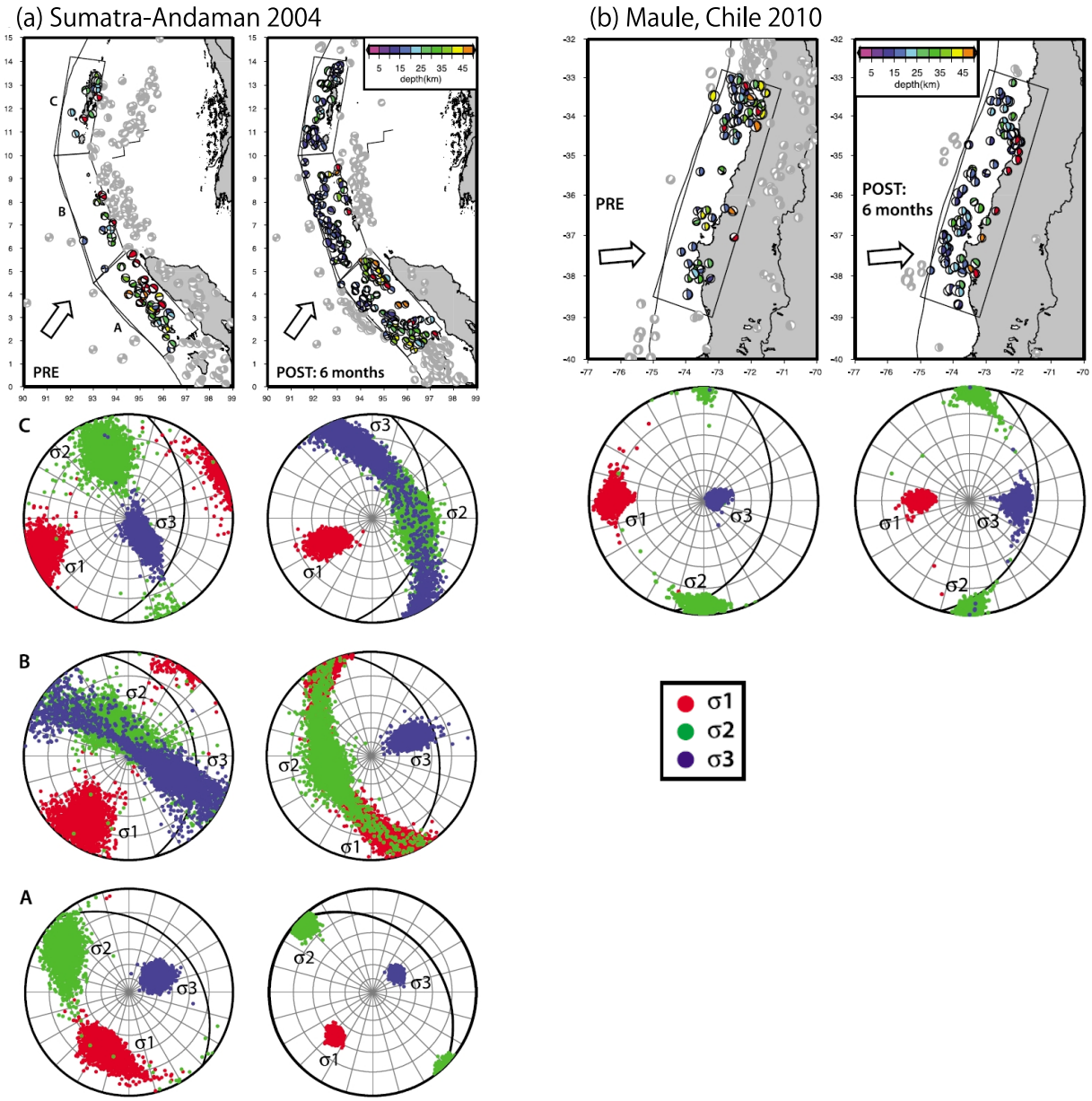

Fig. 13. Maps of moment tensors from the GCMT catalog and principal stress orientations before and after the (a) 2004 M_w 9.2 Sumatra-Andaman and (b) 2008 M_w 8.8 Maule, Chile, earthquakes (Hardebeck, 2012). The left figures in (a) and (b) show those before the mainshocks and the right figures after the mainshocks. Rectangles denote the approximate rupture areas of the mainshocks. The rupture area of the Sumatra-Andaman earthquake is divided into 3 zones A through C. The trench axis is shown by black lines, and the plate convergence direction by white arrows. Estimated orientations of the principal stress axes are shown on the lower focal hemisphere, with an uncertainty distribution obtained from bootstrap resampling. Red:, σ_1. Green: σ_2. Blue: σ_3.

completely reversed and became similar to the static stress change after the Tohoku-Oki earthquake, with the minimum compressive stress (σ_3) axis being oriented in the direction of the large near-trench slip area (Fig. 15(b)). This indicates that the differential stress magnitude in the upper plate prior to the earthquake was less than the static stress change, i.e., less than 15–25 MPa, a very small stress. If we assume that this was caused by overpressured fluids, the pore pressure ratio in the upper plate is estimated to have been larger than ∼0.95–0.97.

Small shear stresses operating in the subduction megathrust have been reported from analyses of different data sources. Lamb (2006) derived a very small shear stress of about 16 MPa on the megathrust in the NE Japan subduction zone based on the force balance between the shear stress at the plate interface and the lithostatic pressure in the fore-arc wedge. Later, Seno (2009) estimated the shear stress on the megathrust off Miyagi Prefecture, the central part of the 2011 Tohoku-Oki rupture area, to be ∼20 MPa, based on the force balance between the shear stress and lithostatic pressure, similarly to Lamb (2006), but having improved the estimation of the lithostatic pressure using seismic profiling

doi:10.5047/meep.2017.00501.0001

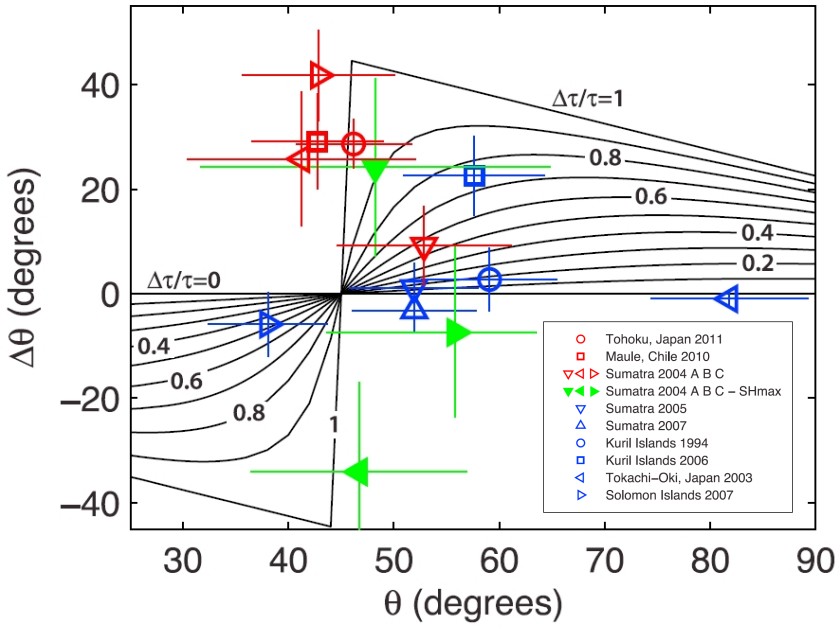

Fig. 14. Stress rotations associated with the mainshock rupture (Hardebeck, 2012). Rotation of σ_1 axis ($\Delta\theta$) is shown as a function of the angle of the σ_1 axis to the fault plane (θ) for various values of $\Delta\tau/\tau$ as in Fig. 12. Observed rotation angles associated with the 2011 Tohoku-Oki, 2008 Maule, 2004 Sumatra-Andaman, 2005 Sumatra, 2007 Sumatra, 1994 Kurile Islands, 2006 Kurile Islands, 2003 Tokachi-Oki and 2007 Solomon Islands earthquakes together with their confidence ranges are shown by different symbols.

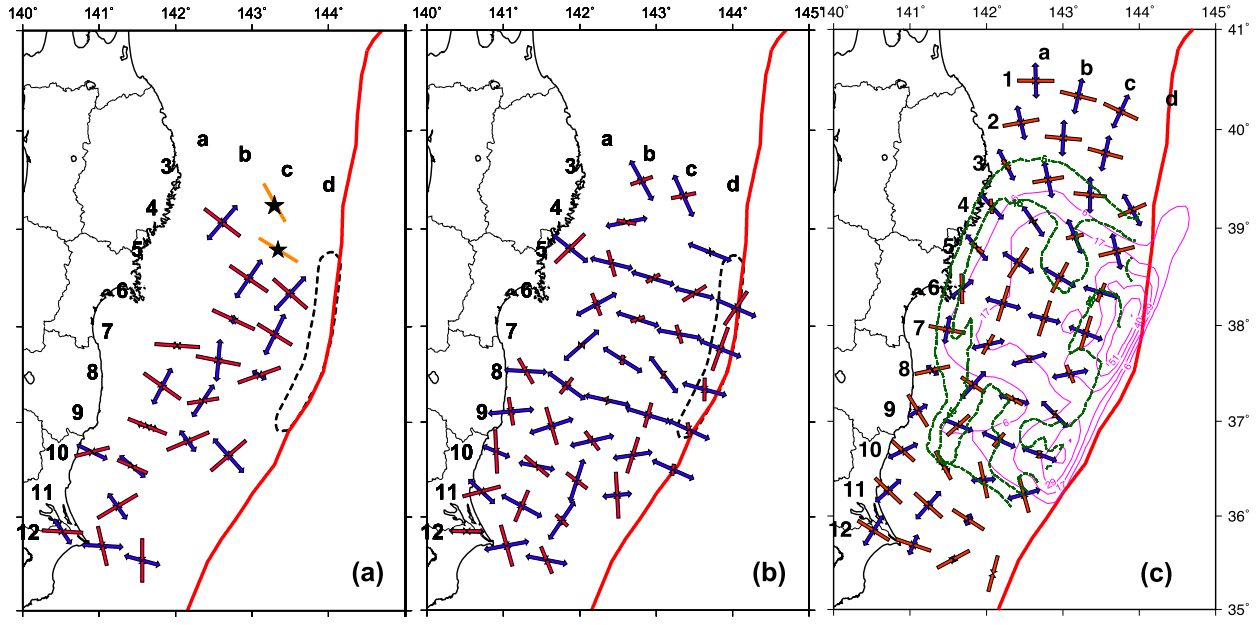

Fig. 15. Orientations of the best-fit σ_1 and σ_3 axes obtained by stress tensor inversions of upper plate events before (a), and after (b), the 2011 Tohoku-Oki earthquake, and (c) predicted orientations of σ_1 and σ_3 axes of the static stress change caused by the Tohoku-Oki earthquake along a plane 10 km above the plate interface (Hasegawa *et al*., 2012a). The σ_1 and σ_3 axes are indicated by red and blue arrows, respectively, at each grid node. The arrow lengths correspond to the plunge of the principal stress axes. Orange bars with stars in (a) show the orientations of the maximum horizontal principal stress axis estimated from borehole breakouts at two sites on ODP Leg 186 (Lin *et al*., 2011). The static stress change in (c) is calculated by the slip models of Lay *et al*. (2011) shown by pink contours. Differential stresses of the static stress change are represented by green contours labeled 5, 15, and 25 MPa.

results. This analysis yielded an extremely high pore pressure ratio of 0.965 at the megathrust. Furukawa and Uyeda (1989) also derived a very small shear stress of around 20 MPa at the megathrust of the NE Japan subduction zone to reasonably explain the observed heat flow data in the area. Very small shear stresses and anomalously high pore fluid pressures (pore pressure ratio more than 0.95) in the shallow portion of the megathrust in the range within 50–60 km of the trench axis were also estimated from slope angle, dip angle of the plate interface and the internal deformation of the

doi:10.5047/meep.2017.00501.0001

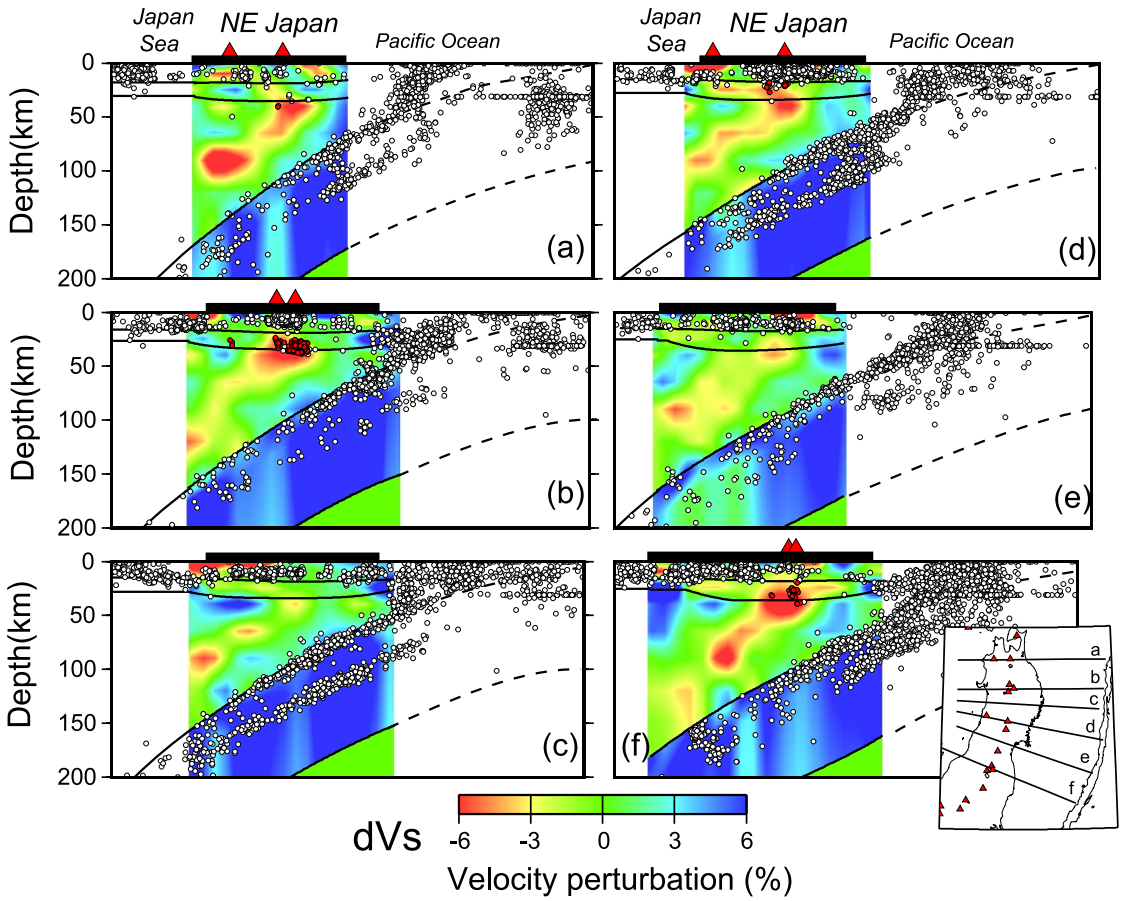

Fig. 16. Across-arc vertical cross-sections of *S*-wave velocity perturbations in the NE Japan subduction zone (Nakajima *et al*., 2001a). Cross-sections are taken along six profiles (a)–(f) shown in the inset map. *S*-wave velocity perturbations are shown by the color scale at the bottom. Red triangles and the solid black bar at the top of each figure denote the location of active volcanoes and the land area, respectively. Open circles indicate earthquake locations, and red circles denote deep low-frequency earthquakes.

fore-arc prism (Kimura *et al*., 2012).

Aqueous fluids in the plate boundary zone which contribute to the generation of interplate events are probably supplied from the sediment layer directly below and from the dehydration decomposition of slab crust and slab mantle materials occurring at greater depths. A recent geochemical study provides clear evidence of fluids flowing through the entire plate interface induced by the 2011 Tohoku-Oki earthquake. Sano *et al*. (2014) detected a bottom seawater ^{3}He anomaly near the trench axis after the earthquake, which suggests that the mainshock rupture provided a fluid pathway connecting the mantle wedge to the trench surface and that aqueous fluids supplied from greater depths also contributed to generating the Tohoku-Oki earthquake.

4. Transportation of Aqueous Fluids from Slab to Arc Crust

Pathways for H_2O from the slab to the arc crust by way of the mantle wedge have been inferred from seismic observations beneath NE Japan (Hasegawa and Nakajima, 2004; Hasegawa *et al*., 2005, 2008). H_2O liberated from the slab during dehydration rises up to the mantle wedge just above, where it reacts with mantle materials to form a layer containing hydrated minerals such as serpentine, chlorite, and amphibole (e.g., Davies and Stevenson, 1992; Iwamori, 1998, 2000). This hydrated layer immediately above the slab is thought to be dragged downward, being entrained with the subducting slab, to depths where further dehydration-related decomposition may occur (Iwamori, 1998, 2000; Schmidt and Poli, 1998; Maruyama and Okamoto, 2007). This hydrated layer formed directly above the slab has been detected as a thin seismic low-velocity layer located immediately above the slab at depths ranging between ∼70 km and ∼130 km, by both receiver function analyses (Kawakatsu and Watada, 2007) and a double-difference tomography study (see Fig. 6(b); Tsuji *et al*., 2008). The depth limit of the hydrated layer for old plate subduction zones, such as that in NE Japan, has been estimated to be 150–200 km by the numerical simulation of a plate subduction model (Iwamori, 1998), which is slightly deeper than the observed depth, demonstrating the need for further investigation.

McKenzie (1969) predicted that entrainment of mantle material with slab subduction results in the migration of mantle material on the back-arc side to fill the enclosed space. Seismic tomography studies have detected this return flow portion of secondary convection associated with slab subduction as a clear inclined sheet-like seismic low-velocity, high-attenuation layer oriented nearly parallel to

doi:10.5047/meep.2017.00501.0001

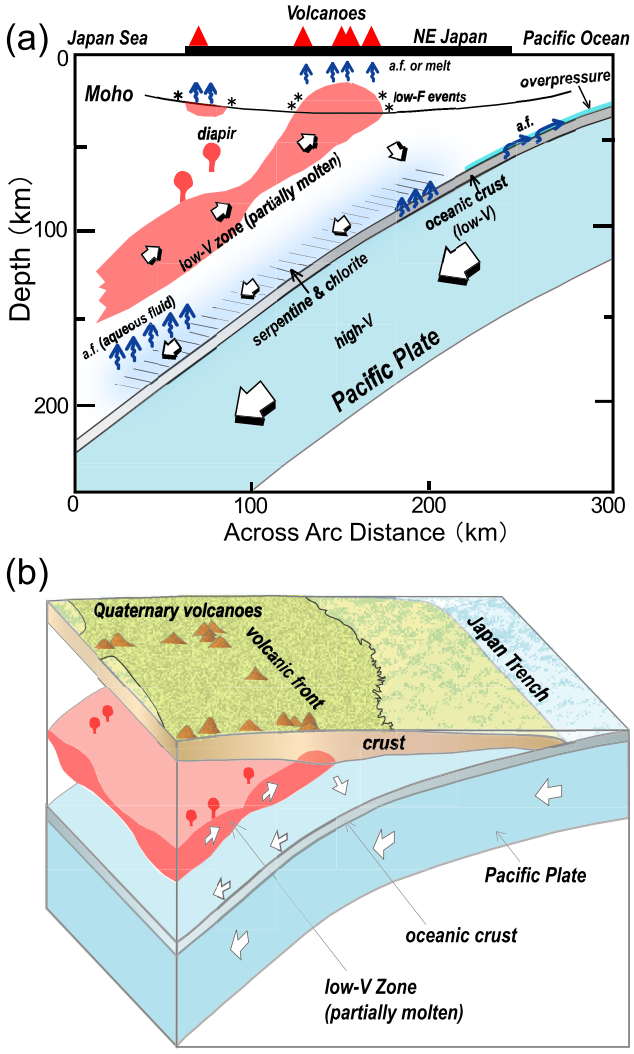

Fig. 17. (a) S-wave velocity perturbations along the inclined low-velocity zone in the mantle wedge of NE Japan, and (b) topography of NE Japan (Hasegawa and Nakajima, 2004). White and red circles denote deep low-frequency microearthquakes and Quaternary volcanoes, respectively. Thick lines denote active faults (Active Fault Research Group, 1991). S-wave velocity perturbations and topography are shown by the color scale at the bottom of each figure.

the subducting slab (Hasegawa *et al*., 1991; Zhao *et al*., 1992, 1994, 2007a; Zhao and Hasegawa, 1993; Nakajima *et al*., 2001a, b, 2013; Tsumura *et al*., 2000). Figure 16 shows across-arc vertical cross-sections of S-wave velocity, demonstrating an inclined low-velocity layer continuously distributed underneath the entire Tohoku area sub-parallel to the subducting slab (Nakajima *et al*., 2001a). Across-arc vertical cross-sections of $Q_p{}^{-1}$ in Fig. 7 also demonstrate the existence of an inclined high-attenuation layer continuously distributed in the mantle wedge beneath all of Tohoku. This inclined, sheet-like, low-velocity, high-attenuation zone is thought to represent the upwelling portion of a secondary convection cell mechanically induced in the mantle wedge by slab subduction (Hasegawa and Nakajima, 2004; Hasegawa *et al*., 2005, 2008), as schematically illustrated in Fig. 17(a).

H_2O liberated at depth from the hydrated layer directly above the slab by dehydration decomposition migrates further upward to meet this immediately overlying upwelling flow zone. The addition of H_2O to hot mantle material within the upwelling flow probably causes partial melting. This mechanism occurs along with decompression melting. In fact, temperatures in the upwelling flow, estimated by comparing the observed seismic wave attenuation structure with the experimental results of olivine-dominated rocks, are higher than the wet solidus of peridotite (Nakajima and Hasegawa, 2003b). Moreover, Nakajima *et al*. (2005) showed that melt-filled pores with melt fraction volumes of 0.1 to several percent exist within this upwelling flow, by comparing the observed fall-off rates of V_p and V_s with a diagram from Takei (2002). H_2O originally released from the slab is, thus, eventually incorporated into melt within the inclined upwelling flow in the mantle wedge. The upwelling flow finally meets the arc Moho, and melt within the upwelling flow accumulates immediately below the Moho along the volcanic front. This melt then rises, penetrating the arc crust and ultimately reaching the surface to form volcanoes. Thus, the volcanic front is formed nearly parallel to the trench axis at locations where inclined sheet-like upwelling flows in the mantle wedge reach the arc Moho (Hasegawa and Nakajima, 2004; Hasegawa *et al*., 2005, 2008, 2013).

Seismic tomography has further revealed that the velocity of this inclined sheet-like low-velocity layer varies along the arc. Very low-velocity areas exist periodically every 80 km or so along the strike of the arc (Hasegawa and Nakajima, 2004), as illustrated in Fig. 18(a), which shows the S-wave velocity distribution along the inclined sheet-like low-velocity layer. Comparing this with the topographic map shown in Fig. 18(b) reveals that the velocity reduction in the low-velocity layer at depths of 30–150 km in the mantle wedge correlates well spatially with the distribution of deep low-frequency earthquakes in the lowermost crust, the distribution of Quaternary volcanoes, and the distribution of topographic highs that run from the backbone range to the back-arc region at the surface.

Figure 17 shows the main transport paths of H_2O from the slab to the arc crust, including the mantle upwelling flow in NE Japan, as estimated from seismic observations. The volcanic front, which runs through the middle of the arc nearly parallel to the trench axis, is formed above the region where the inclined upwelling flow reaches the Moho (Fig. 17(a)). The upwelling flow in the mantle wedge, resolved as an inclined low-velocity and high-attenuation layer, is sheet-like, with its thickness varying locally along the strike of the arc (Fig. 17(b)). In regions characterized by a local thickening of the upwelling flow and by large volume fractions of melt, some of the melt may separate from the inclined upwelling flow before the upwelling flow reaches the arc Moho. This separated melt rises vertically from the point of separation in the form of a plume and accumulates below the Moho. Some of this melt migrates upward and penetrates into the crust contributing to the formation of volcanoes and to crustal uplift in the back-arc region.

The inclined upwelling flow mechanically induced by slab

doi:10.5047/meep.2017.00501.0001

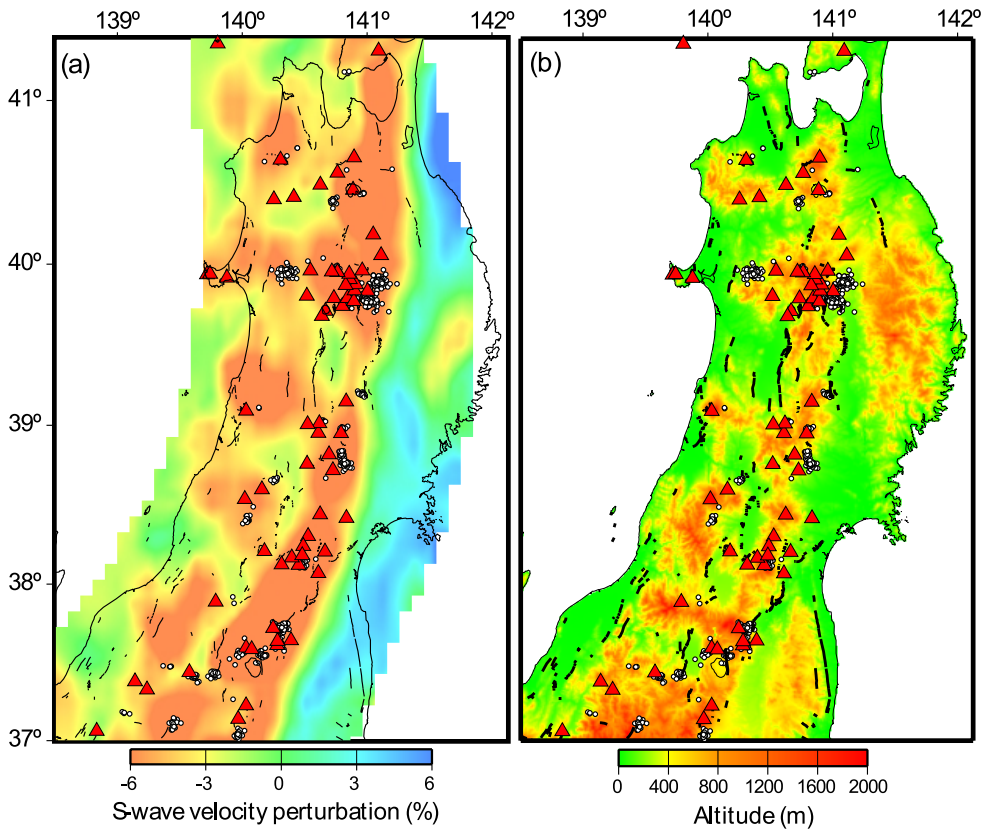

Fig. 18. Schematic illustration of the crust and upper mantle structure of Tohoku showing the inferred H_2O transportation path and upwelling flow with varying thicknesses in the mantle wedge (Hasegawa and Nakajima, 2004; Hasegawa *et al*., 2013). (a) across-arc vertical cross-section and (b) 3D expression.

subduction in the mantle wedge is thought to be common to all subduction zones. Inclined low-velocity zones that probably correspond to upwelling flow have been detected in the mantle wedge of several other subduction zones, including Alaska (Zhao *et al*., 1995), the eastern Aleutians (Abers, 1994), Kamchatka (Gorvatov *et al*., 1999), Hokkaido (Wang and Zhao, 2005), Kyushu (Abdelwahed and Zhao, 2007), and Tonga (Zhao *et al*., 1997a, b), although the images of the low-velocity zones are not as clear as those of Tohoku (Fig. 16). Recent seismic tomography studies, using data from both local and teleseismic events recorded by the dense nationwide seismic network, have clearly shown the existence of inclined low-velocity layers in the mantle wedge beneath the entire Japanese archipelago (Yanada *et al*., 2010; Zhao *et al*., 2012; Huang *et al*., 2013).

Figure 19 shows clear images of this inclined low-velocity layer in the mantle wedge for an area between the southwestern portion of the Kuril Arc and the northern portion of the Izu–Bonin Arc in eastern Japan. Inclined low-velocity layers in the mantle wedge are distinctly visible in all the cross-sections between Hokkaido (sections A and B) and the Izu arc (sections L and M), except in the arc–arc junction areas beneath the Hokkaido corner (section D) and Kanto (section K). Inclined low-velocity layers corresponding to upwelling flow are also distinctly visible in the subduction zone in SW Japan associated with the subduction of the Philippine Sea slab. Figure 20 shows the existence of inclined low-velocity layers in the mantle wedge at depths of 30–200 km, except in the area beneath Chugoku (sections Q through T). The lack of a visible inclined low-velocity layer there is perhaps an artifact of lower spatial resolution in that area beneath the Japan Sea caused by poor ray-path coverage.

The existence of inclined low-velocity layers in the mantle wedge across the entire Japanese archipelago, except at arc–arc junctions associated with volcanic gaps and in the Chugoku region, where the resolution of the seismic tomography is not sufficient, suggests that inclined upwelling flow in the mantle wedge probably occurs in all subduction zones and that volcanoes are formed at locations where these inclined upwelling flows in the mantle wedge reach the arc Moho. These upwelling flows likely contribute to the transportation of H_2O originally released from the subducting slab to the arc crust. Although the upwelling flow probably plays a major role in H_2O transportation passing through the mantle wedge, some amount of H_2O released from the shallower portion of the slab crust may infiltrate the mantle wedge in the forearc area, finally reaching the forearc crust. However, traces of such transport paths of H_2O have not yet been imaged by seismic tomography studies. Katayama *et al*. (2010) inferred that such transport paths of H_2O by way of the forearc mantle wedge are mainly operating in SW Japan because eclogite-forming phase transformation occur there at much shallower depths of 50–60 km in the slab crust because of warmer temperature conditions. This suggests

doi:10.5047/meep.2017.00501.0001

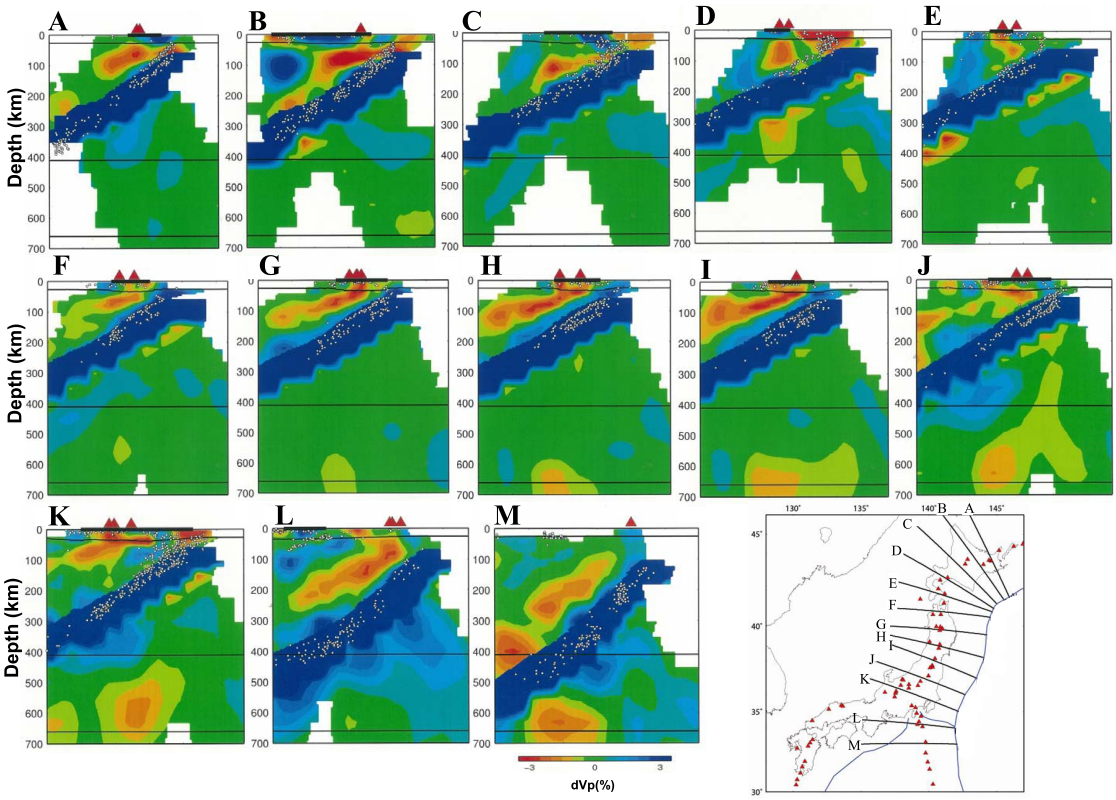

Fig. 19. Across-arc vertical cross-sections of *P*-wave velocity perturbations in E Japan along profiles shown in the inset map (Yanada *et al.*, 2010). *P*-wave velocity perturbations are indicated by the color scale at the bottom. Red triangles and thick horizontal lines at the top of each figure denote active volcanoes and the land area, respectively, and open circles show earthquake foci.

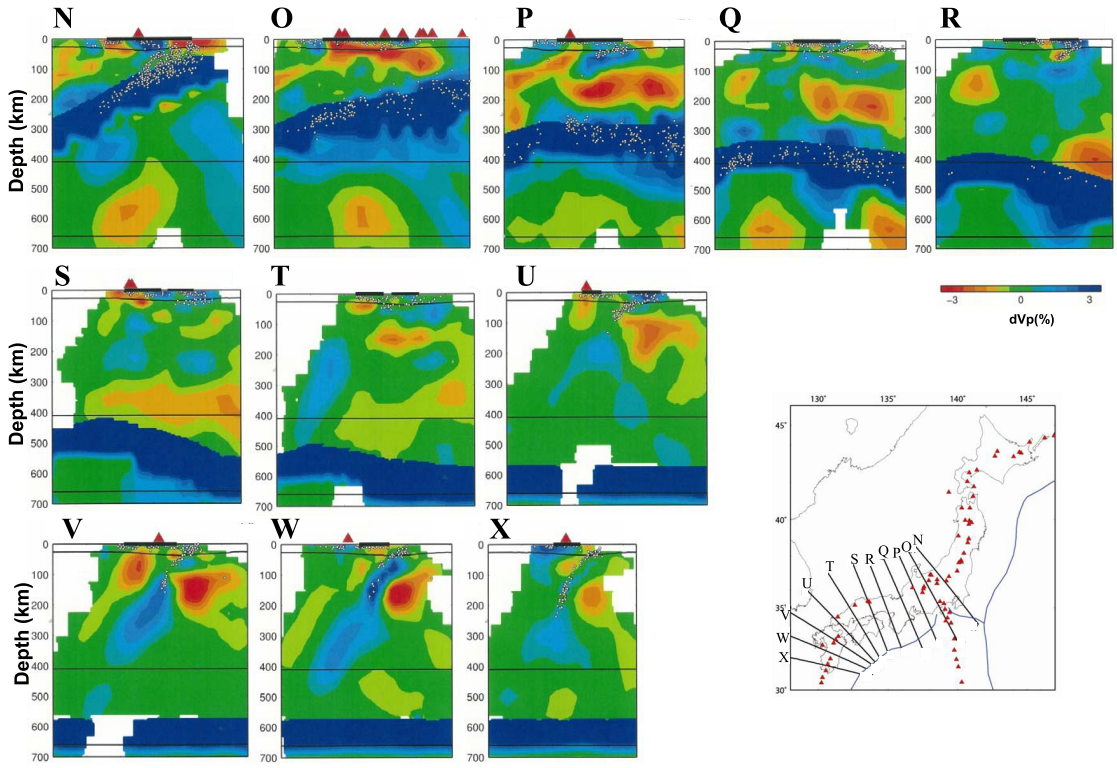

Fig. 20. Across-arc vertical cross-sections of *P*-wave velocity perturbations in W Japan along profiles shown in the inset map (Yanada *et al.*, 2010). Others are the same as in Fig. 19.

doi:10.5047/meep.2017.00501.0001

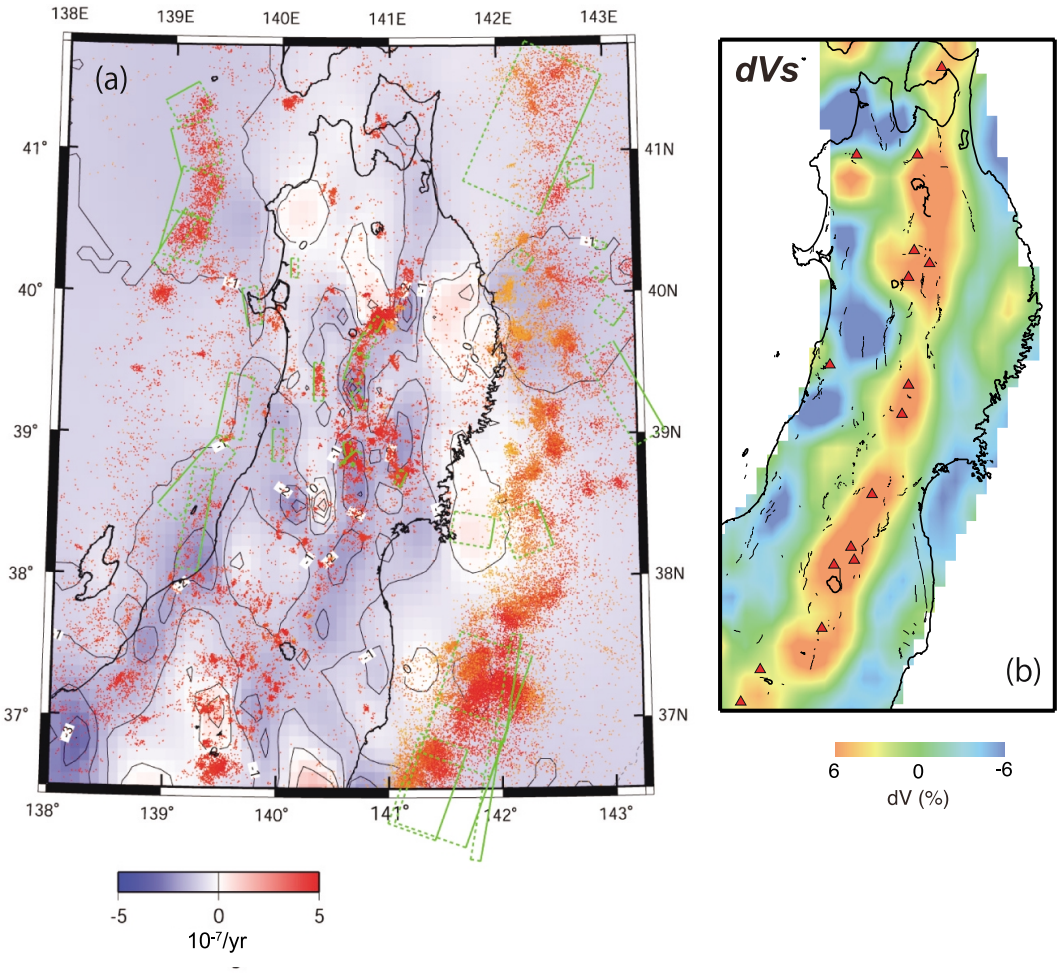

Fig. 21. (a) Horizontal E-W strain rates estimated from nationwide dense GPS network data for the period 1997–2001 (Sato *et al*., 2002; Miura *et al*., 2004). Red dots show shallow microearthquakes that occurred during the same period, and green rectangles denote the fault planes of large earthquakes (Sato *et al*., 1997). (b) Map showing *S*-wave velocity perturbations at a depth of 40 km in the uppermost mantle (Nakajima *et al*., 2001a). The color scale on the bottom shows *S*-wave velocity perturbations. The triangles denote volcanoes.

the presence of a considerable amount of H_2O in the forearc crust of the SW Japan subduction zone.

5. Shallow Inland Earthquakes

The dense nationwide GPS network in Japan has allowed a high-strain-rate zone along the Ou backbone range in Tohoku to be identified (Sato *et al*., 2002; Miura *et al*., 2004; Hasegawa *et al*., 2005). The spatial distribution of the E–W components of horizontal strain rates estimated from GPS network data demonstrates the existence of a high-strain-rate zone passing through the middle of Tohoku in the along-arc direction (Fig. 21(a)). The figure also shows the existence of another high-strain-rate zone along the Japan Sea coast corresponding to the northern extension of the Niigata-Kobe Tectonic Zone in central Japan (Sagiya *et al*., 2000). A concentration of shallow earthquakes is clearly visible in this high-strain-rate zone along Tohoku's backbone range (Fig. 21(a)), suggesting that this seismicity is caused by the presence of contractional crustal deformation. Active reverse faults are distributed along the eastern and western edges of the backbone range (Active Fault Research Group, 1991), on both edges of the high-strain-rate zone.

The evidence points to the locally concentrated contractive arc crust deformation, as indicated by the high-strain-rate zones, as being caused by aqueous fluids originally released from the subducting slab, and being responsible for large shallow inland earthquakes (Hasegawa *et al*., 1991, 2000, 2005). As described in the previous section, the inclined sheet-like upwelling flow in the mantle wedge reaches the bottom of the arc crust along the volcanic front or along the Ou backbone range in the NE Japan arc, as Fig. 17 shows schematically. Actually, the inclined seismic low-velocity zone in the mantle wedge corresponding to this upwelling flow meets the Moho right below the volcanic front within the Ou backbone range as shown in Fig. 21(b). The melt contained in this upwelling flow either underplates the arc crust or penetrates into it, causing a locally elevated geotherm along the backbone range defined by heat flow measurements (Tanaka and Ishikawa, 2002). Some of the melt that penetrates the arc crust may cool and partially solidify, expelling H_2O. Thus, H_2O originally released from the subducted slab reaches the arc's mid-crust along the Ou backbone range.

doi:10.5047/meep.2017.00501.0001

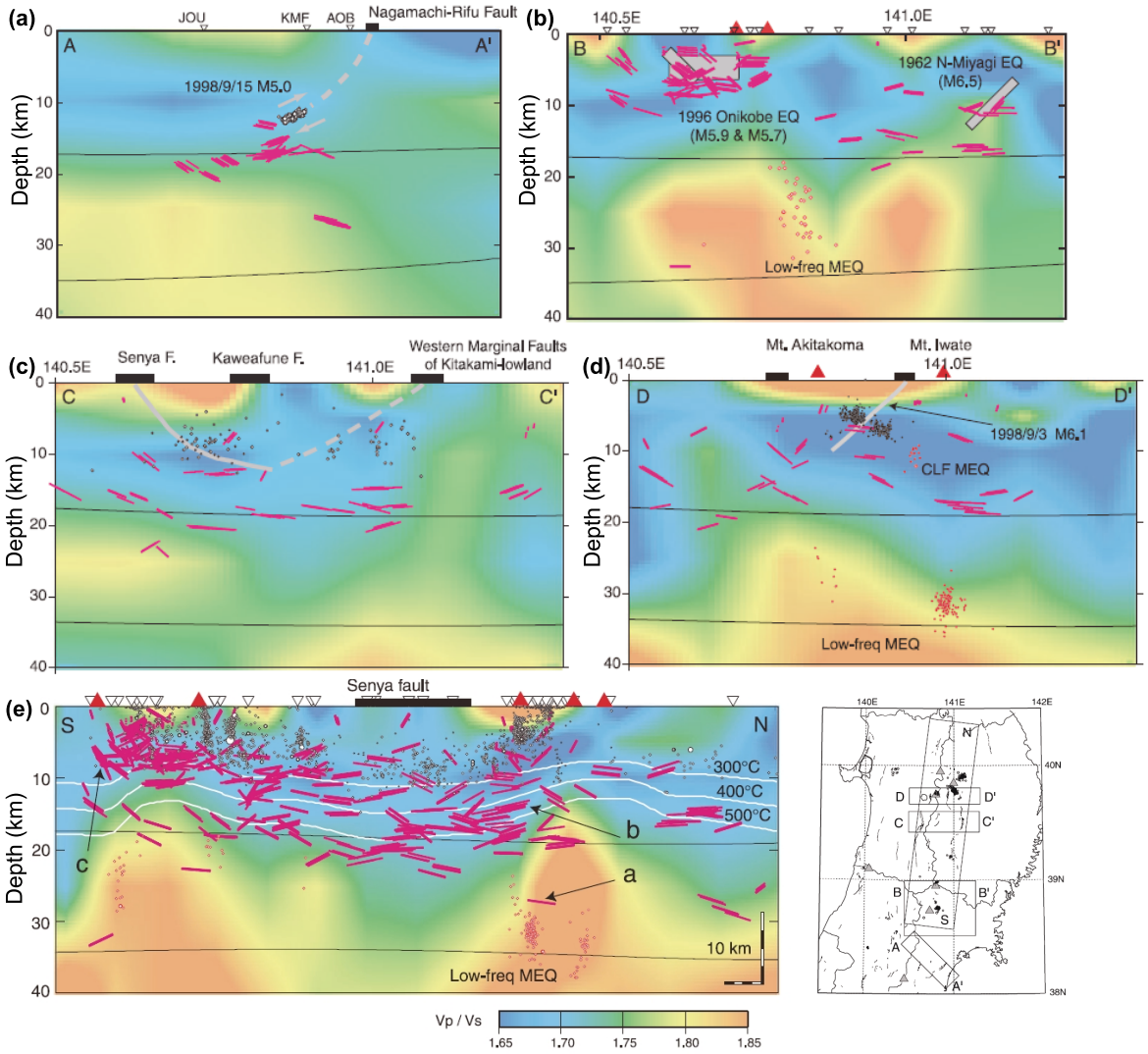

Fig. 22. Vertical cross-sections of V_p/V_s ratio and S-wave reflectors in central Tohoku (Hori *et al*., 2004). V_p/V_s ratio (Nakajima *et al*., 2001b) and S-wave reflectors are shown by the color scale at the bottom and by red lines, respectively, on the vertical cross sections along lines (a) AA′, (b) BB′, (c) CC′, (d) DD′ and (e) NS in the inset map. Red and black dots are deep low-frequency earthquakes and regular earthquakes, respectively. Two thin lines denote the Conrad and Moho discontinuities. White lines in (e) show isothermal contours. Thick lines and red triangles on the top of each figure denote faults and volcanoes, respectively. Aftershocks of 1998 M 5.0 Sendai earthquake (Umino *et al*., 2002b) are shown by open circles in (a). Fault planes of 1996 M 5.9 and M 5.7 Onikobe earthquakes (Umino *et al*., 1998a), 1998 M 6.1 Shizukuishi earthquake (Unimo *et al*., 1998b) and 1962 M 6.5 northern Miyagi earthquake (Kono *et al*., 1993) are shown by gray rectangles or a gray line. Deep portions of the Senya fault and western Marginal faults of Kitakami lowland estimated from a deep seismic reflection survey (Sato *et al*., 2002) are shown by gray and dashed lines, respectively.

The presence of H_2O is expected to weaken the crustal material there, which intensifies local contractional deformation of the arc crust in the present margin-normal compression stress field.

Across-arc and along-arc vertical cross-sections of seismicity, V_p/V_s ratio and S-wave reflectors in central Tohoku are shown in Fig. 22 (Hori *et al*., 2004). The figure clearly shows the existence of anomalously high V_p/V_s zones in the lower crust right beneath volcanoes. The geotherms shown in Fig. 22(e) are locally elevated right below the volcanoes, and so is the bottom of the seismogenic zone, which approximately corresponds to the 350° isothermal contour. Deep low-frequency earthquakes occur on the edge of the high V_p/V_s zones. S-wave reflectors are widely distributed in the mid-crust beneath the backbone range, locally shallowing right above the high V_p/V_s zones beneath volcanoes. Prominent S-wave reflectors are detected not only beneath volcanoes but also beneath earthquake faults.

Figure 23(a) is a schematic illustrating the deformation pattern of the arc crust in Tohoku inferred by these observations. Melt contained in the inclined upwelling flow in the mantle wedge and intruded into the arc crust heats the surrounding crustal rocks beneath the Ou backbone range. This locally elevates the brittle–ductile transition zone there. Some of the melt cools and solidifies, expelling H_2O that can move rapidly at lower crustal levels. It is the H_2O thus expelled from the melt that causes anomalously deep low-frequency earthquakes occurring in the lowermost crust (Hasegawa *et al*., 1991; Hasegawa and Yamamoto, 1994). Many bright sub-horizontal S-wave reflectors have been de-

doi:10.5047/meep.2017.00501.0001

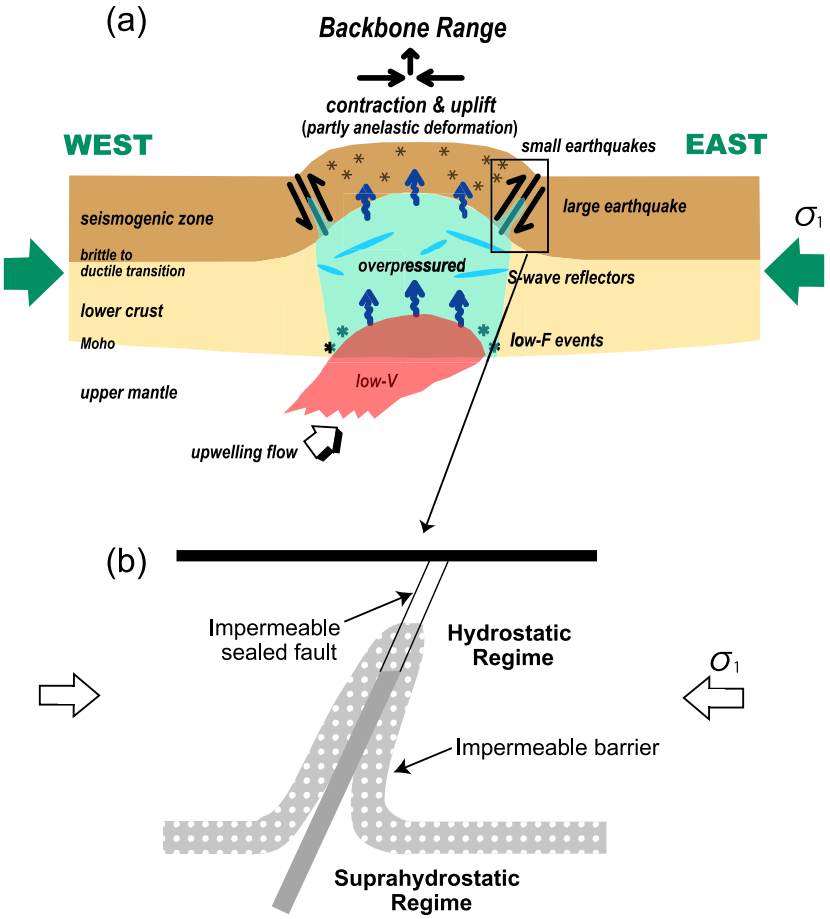

Fig. 23. Schematic illustrations showing (a) a model of the deformation pattern of the arc crust and generation of shallow inland earthquakes, and (b) fluid overpressure formed along a steep reverse fault beneath Tohoku. (After Hasegawa *et al*., 2012b)

tected at mid-crustal levels throughout the backbone range (Hori *et al*., 2004). These *S*-wave reflectors may be accumulations of near-lithostatically overpressured H_2O within thin horizontal sill-like reservoirs in the mid-crust (Matsumoto and Hasegawa, 1996; Umino *et al*., 2002a). Some of the H_2O migrates upward further and reaches the upper crust. Thus, the entire crust along the backbone range is locally weakened compared to the surrounding crust, concentrating contractional deformation and uplift along the backbone range under the current margin-normal compressive stress field. In turn, localized contractional deformation along the backbone range concentrates stress in the upper crust, which may eventually lead to rupture of the entire upper crust, generating a large shallow inland earthquake (Hasegawa *et al*., 2005). This concentrated contractional deformation along the backbone range is also likely to be responsible for the extremely high smaller-magnitude earthquake activity there (Fig. 21(a)).

In central to western Japan, Sagiya *et al*. (2000) detected the existence of a high-strain-rate zone extending from Niigata to Kobe based on an analysis of dense GPS network data. This high-strain-rate zone, termed the Niigata-Kobe Tectonic Zone (NKTZ), was first noticed by Hashimoto (1990) and Hashimoto and Jackson (1993) based on an analysis of triangulation data for the past 100 years. The NKTZ is approximately 100 km wide and extends about 500 km in a NE–SW direction. It undergoes contraction in the WNW–ESE direction at a rate of about 10^{-7}/year, orders of magnitude greater than that of the surrounding areas. Historically, there have been many large earthquakes along this zone, suggesting that the present tectonic deformation pattern has persisted over the last several hundred years (Sagiya *et al*., 2000). Strikingly high strain rates observed along this zone have been interpreted in terms of both interplate deformation (e.g., Shimazaki and Zhao, 2000) and intraplate deformation (e.g., Iio *et al*., 2002, 2004; Hyodo and Hirahara, 2003; Yamasaki and Seno, 2003).

Shimazaki and Zhao (2000) regarded the NKTZ as a collisional plate boundary, and discussed its strikingly high strain rates in terms of interplate deformation. In contrast, Iio *et al*. (2002, 2004) insisted that the NKTZ is not a colliding plate boundary. To explain the observed high strain rates, the latter proposed a model of a weak zone with low viscosity existing in the lower crust immediately beneath the NKTZ. They inferred that this weak zone results from locally elevated H_2O content caused by the upward migration of H_2O from the dehydration of the subducting Philippine Sea slab immediately below. Using numerical simulations employing a viscoelastic finite element model, Hyodo and Hirahara (2003) showed that the observed high strain rates along the NKTZ can be

doi:10.5047/meep.2017.00501.0001

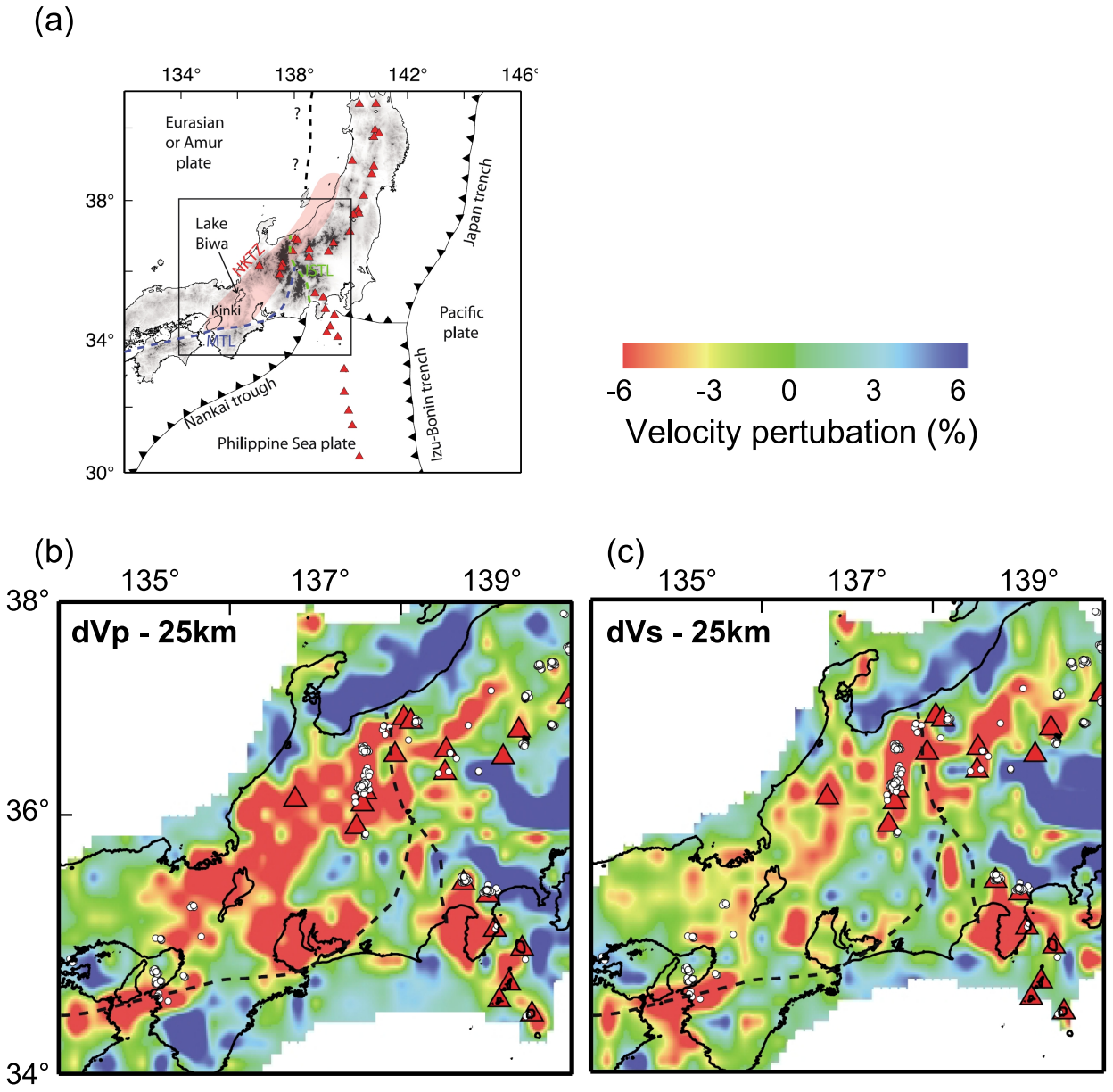

Fig. 24. (a) Map showing the location of the Niigata-Kobe Tectonic Zone (NKTZ) shown by a pink belt. The red triangles represent active volcanoes. The Itoigawa-Shizuoka Tectonic Line (ISTL) and the Median Tectonic Line (MTL) are shown by green and blue broken curves, respectively. (b), (c) *P*- and *S*-wave velocity perturbations, respectively, at a depth of 25 km for the rectangular area in (a). The velocity perturbations are shown by color scale at the bottom. The broken black curves represent the ISTL and MTL. (After Nakajima and Hasegawa, 2007b)

well explained by the presence of an underlying 15-km-thick viscoelastic lower crust with a viscosity as low as that of the uppermost mantle. Yamasaki and Seno (2005) assumed that the observed high strain rates along the NKTZ are due to the loading and unloading of the subducting Philippine Sea slab. They examined the effect of rheological heterogeneities in the lower crust or uppermost mantle on the surface deformation using a two-dimensional finite element method. They showed that the observed high strain rates could be reproduced well by a model with a low-viscosity upper mantle immediately beneath, and in the direction of the trench from the NKTZ. Such a low-viscosity uppermost mantle could be formed by the upward migration of H_2O released from the dehydration of the subducting Philippine Sea and Pacific slabs.

In addition, a seismic tomography study by Nakajima and Hasegawa (2007b) revealed a prominent low-velocity anomaly in the lower crust along the NKTZ in its southwest and central parts, extending to the uppermost mantle along the NE and central parts of the zone (Fig. 24). This prominent low-velocity anomaly suggests the presence of melt or aqueous fluids liberated from the Philippine Sea slab directly below. It also points to the possibility that the crust and upper mantle along the NKTZ are weakened by the accumulation of H_2O. These studies suggest that H_2O, originally derived from the subducting slab, or melt produced by the addition of H_2O that originated in the slab, play an important role in stress accumulation and earthquake generation in the arc

doi:10.5047/meep.2017.00501.0001

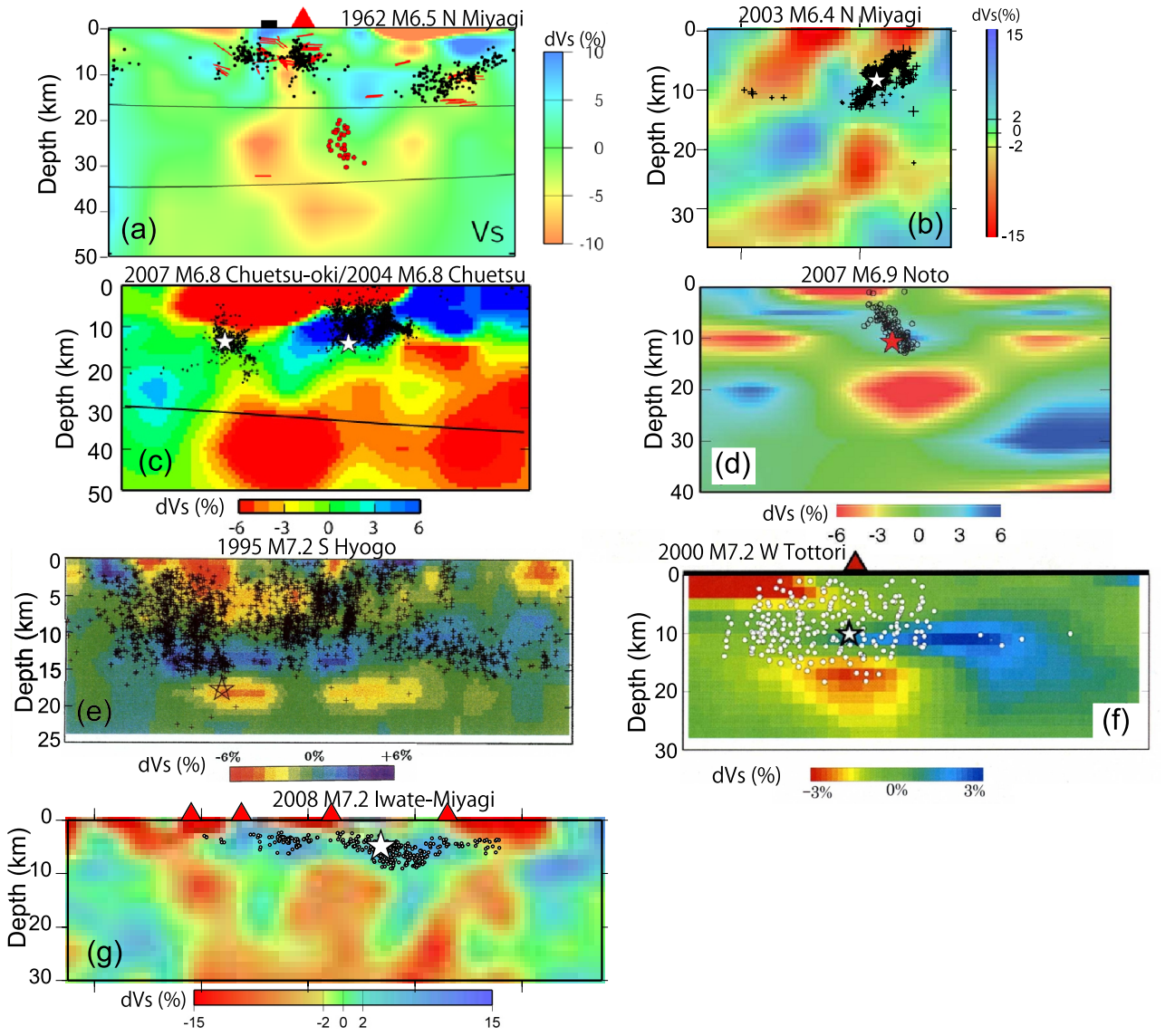

Fig. 25. *S*-wave velocity structure in the source areas of recent large shallow inland earthquakes in Japan (Hasegawa *et al*., 2009). (a) 1962 *M* 6.5 N Miyagi (Nakajima and Hasegawa, 2003a), (b) 2003 *M* 6.4 N Miyagi (Okada *et al*., 2007), (c) 2004 *M* 6.8 Niigata-Chuetsu and 2007 *M* 6.8 Niigata-Chuetsu-Oki (Nakajima and Hasegawa, 2008), (d) 2007 *M* 6.9 Notohanto-Oki, (e) 1995 *M* 7.2 S Hyogo (Kobe) (Zhao *et al*., 1996), (f) 2000 *M* 7.2 W Tottori (Zhao *et al*., 2004), and (g) 2008 *M* 7.2 Iwate-Miyagi Nairiku (Okada *et al*., 2010) earthquakes. Color scale in each figure shows *S*-wave velocity perturbations. (e), (f), and (g) are strike-parallel vertical cross-sections along the mainshock faults, other figures are sections across the mainshock faults. Mainshocks and aftershocks are denoted by stars and circles or crosses, respectively. (Reprinted from *Gondwana Res*., *16*, Hasegawa, A., J. Nakajima, N. Uchida, T. Okada, D. Zhao, T. Matsuzawa, and N. Umino, Plate subduction, and generation of earthquakes and magmas in Japan as inferred from seismic observations: An overview, 370–400, Copyright 2009, with permission from Elsevier.)

crust in central to southwestern Japan. The mechanism by which shallow inland earthquakes are generated is thus similar to that responsible for the high-strain-rate zone along the Ou backbone range in NE Japan.

Seismic tomography using dense temporary seismic observation networks deployed in the source areas of recent large shallow inland crustal earthquakes has provided further evidence of the important role H_2O plays in earthquake generation (Hasegawa *et al*., 2009). Figure 25 shows vertical cross-sections of *S*-wave velocities obtained by temporary observations of aftershocks following seven large, recent, shallow inland earthquakes. We also include the 1962 *M* 6.5 northern Miyagi earthquake, because a dense temporary observation network has been deployed in the area of its source. Prominent *S*-wave low-velocity zones can be readily identified in the lower crust immediately below the fault planes of all the large shallow inland earthquakes. Some of these low-velocity zones extend downward to the uppermost mantle, which suggests that their low velocities are caused by H_2O, or melt, supplied from the uppermost mantle just below. We infer that they are caused by H_2O of slab origin.

Dense magneto-telluric soundings across active fault structures in the northern South Island of New Zealand also provide evidence of H_2O's important role (Wannamaker *et al*., 2009). The across-fault cross-section of electrical resistivity shown in Fig. 26 clearly indicates the presence of

doi:10.5047/meep.2017.00501.0001

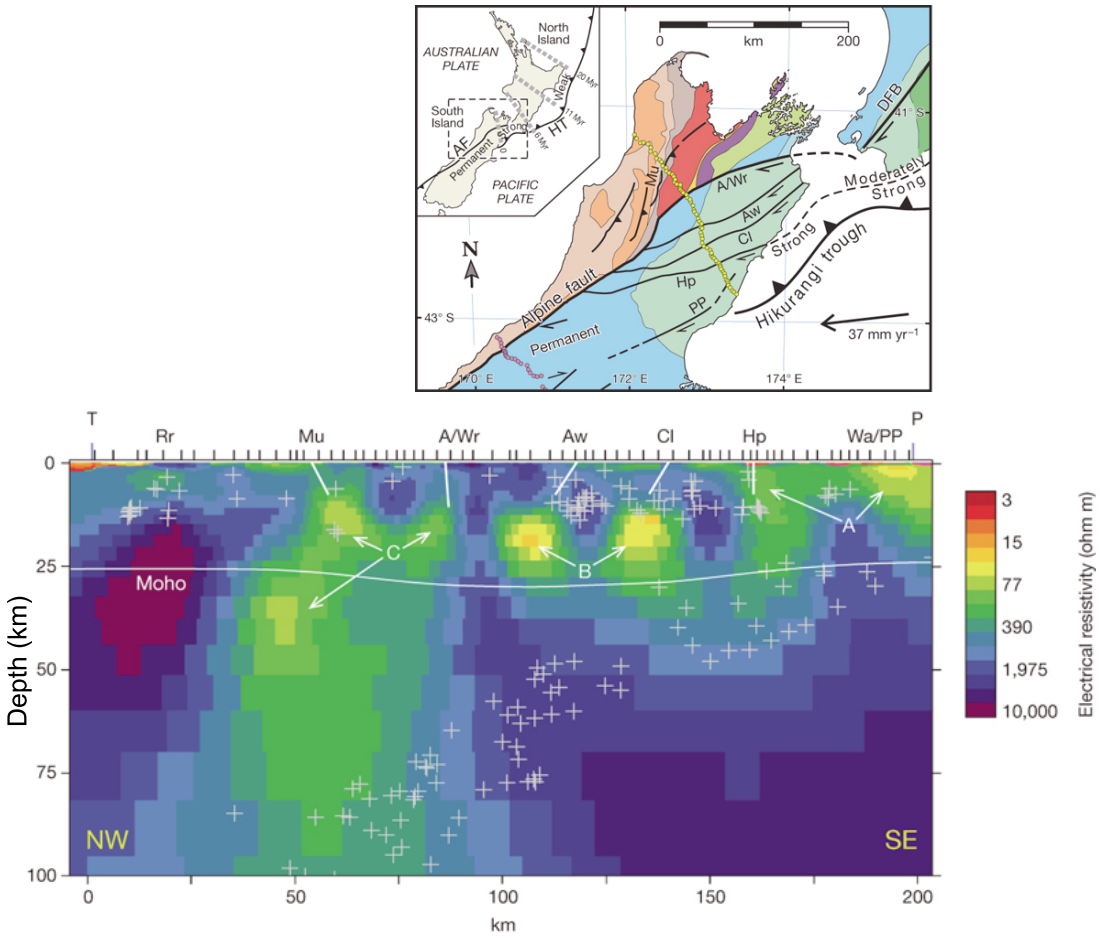

Fig. 26. Electrical resistivity profile across the northern South Island of New Zealand (Wannamaker *et al*., 2009). The Alpine-Wairau (A/Wr) fault separates the Marlborough system of active dextral strike-slip faults to the southeast, from the Buller-Nelson province of active reverse faulting to the northwest. Resistivity is shown by the color scale at the right on a logarithmic scale. Seismicity is shown by plus symbols. The subducting Pacific plate lies to the right of the northwest-dipping deep intraslab seismicity. Nearly horizontal white curved line denotes the arc Moho. Major faults are labelled and shown by white inclined lines. Major conductive zones are labelled A, B and C.

extremely low-resistivity zones in the crust associated with individual faults in the Marlborough strike-slip fault system. In the uppermost mantle northwest of the Alpine-Wairau fault below the crust undergoing active compressional inversion (Ghisetti and Sibson, 2006), there is another broad low-resistivity zone, which can be interpreted as a path for transporting H_2O from the subducting slab to the crust. H_2O thus derived from the slab rises and finally penetrates into the fault zones in the upper crust where historic great earthquakes have occurred on high-angle reverse faults that are unfavorably oriented for failure (Wannamaker *et al*., 2009). Similar low resistivity zones distributed in the lower crust below faults have also been found in many areas around the world, including the North Anatolian fault, the San Andreas fault and the 2000 Western Tottori earthquake fault (e.g., Mitsuhata *et al*., 2001; Ogawa and Honkura, 2004; Tank *et al*., 2005; Yamaguchi *et al*., 2007; Becken *et al*., 2008).

Seismic tomography seems to show further evidence of aqueous fluids that have migrated upward and infiltrated from the highly overpressured lower crust into the seismogenic fault zone in the upper crust. Figure 27(a) shows across-fault vertical cross-sections of *P*-wave velocity perturbations in the source area of the 2004 *M* 6.7 Niigata-Chuetsu earthquake, which were derived by applying the double-difference tomography of Zhang and Thurber (2003) to travel-time data of many aftershocks obtained from a dense temporary seismic observation network deployed after the mainshock (Okada *et al*., 2006). *P*-wave low-velocity zones distributed along the fault planes of the mainshock and large aftershocks are clearly visible, suggesting the presence of overpressured fluids that have infiltrated fault zones in the upper crust as shown schematically in Fig. 27(b) (Sibson, 2007).

Many large, shallow, inland thrust fault-type earthquakes that occur along active faults in NE Japan are reactivations of pre-existing normal faults that had formed at the time the Japan Sea opened (e.g., Sato, 1994). Sibson (2009) noticed that these seismogenic faults have steep dips and are unfavorably oriented for frictional reactivation under the current stress field that has nearly horizontal maximum compressive stress. He inferred that overpressured conditions along the faults are required to re-activate these pre-existing faults, and estimated that pore pressure ratios must be greater than 0.8. Based on these observations, the overpressured condi-

doi:10.5047/meep.2017.00501.0001

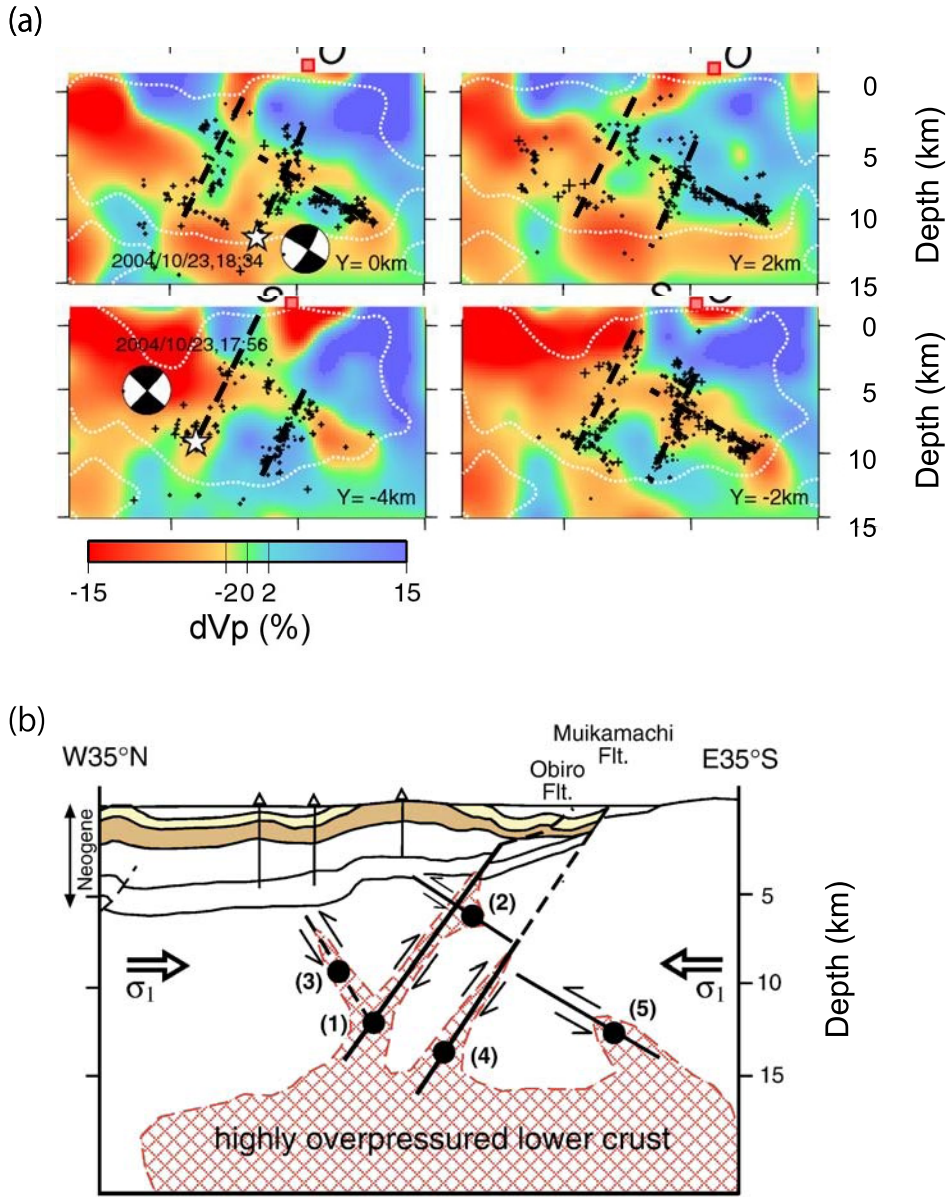

Fig. 27. (a) Across-fault vertical cross-sections of P-wave velocity in the focal area of the 2004 M 6.8 Niigata-Chuetsu earthquake (Okada *et al*., 2006). P-wave velocity perturbations are shown by the color scale at the bottom. White stars denote the main shock and the largest aftershock. Black dots represent other aftershocks. Thick broken lines indicate the fault planes of the main shock and the largest aftershock. (b) Schematic illustration showing over-pressuring localized along the fault planes of the mainshock and its large aftershocks (Sibson, 2007). (Reprinted from *Earth Planet. Sci. Lett*., *257*, Sibson, R. H., An episode of fault-valve behaviour during compressional inversion?—The 2004 M_J6.8 Mid-Niigata Prefecture, Japan, earthquake sequence, 188–199, Copyright 2007, with permission from Elsevier.)

tion of a seismogenic fault zone is schematically shown in Fig. 23(b), which is modified from Fig. 6 of the fault valve model by Sibson (1990, 1992).

Following the 2011 Tohoku-Oki earthquake, stress fields seem to have changed in some inland areas of NE Japan, where the principal stresses came to be oriented in approximately the same direction as the static stress change associated with the Tohoku-Oki earthquake (Yoshida *et al*., 2012). Changes in the stress field following large earthquakes have also been detected in the source areas of the 2008 M 7.2 Iwate-Miyagi Nairiku earthquake and after the 2011 M 7.0 Fukushima-Hamadori earthquake that occurred inland (Yoshida *et al*., 2014, 2015b, 2016). The principal stress orientations also became approximately the same as those of the static stress change associated with each mainshock. Figures 28(a)–(c) show the post-earthquake stress field in the source area of the 2008 M 7.2 Iwate-Miyagi Nairiku earthquake obtained by stress tensor inversions of many aftershock focal mechanism data (Yoshida *et al*., 2014). The observed orientations of the σ_1 axis have a spatially heterogeneous distribution, being approximately similar to those of the static stress change by the mainshock rupture as shown in Figs. 28(d)–(f). Orientations of the σ_1 axis after the mainshock, estimated by assuming a differential stress magnitude of 10 MPa prior to the mainshock (Figs. 28(g)–(i)), well explain the observed stress

doi:10.5047/meep.2017.00501.0001

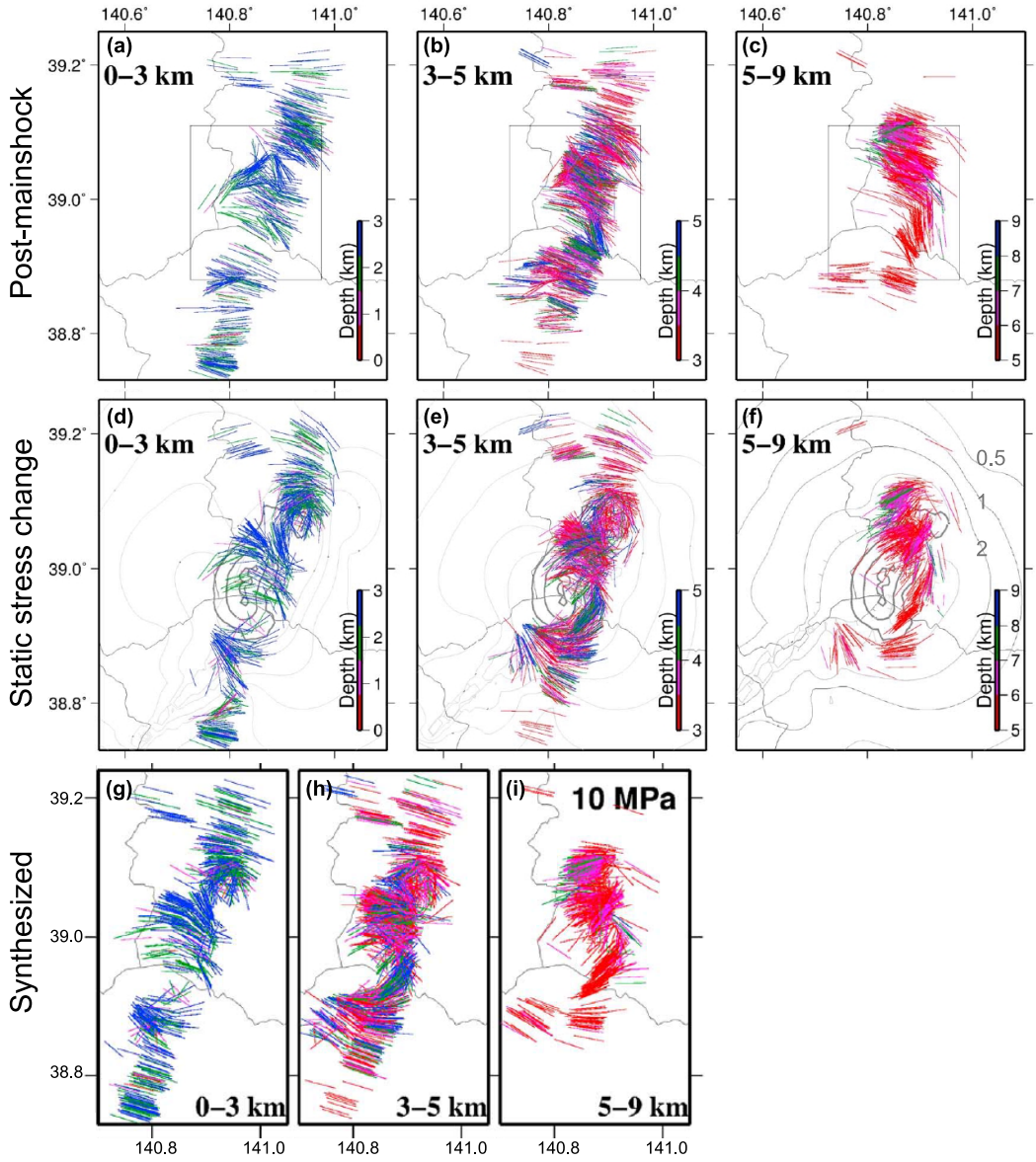

Fig. 28. Stress field in the source area of the 2008 M 7.2 Iwate-Miyagi Nairiku reverse fault rupture and static stress change by the mainshock (Yoshida *et al*., 2014). (a), (b) and (c) Orientations of σ_1 axes after the mainshock obtained by stress tensor inversions. (d), (e) and (f) Orientations of the σ_1 axes of the static stress change by the mainshock rupture based on the slip model of Iinuma *et al*. (2009). These are plotted at the same locations where the stress tensor inversions were performed. Slip distributions are shown by thick contours. Differential stresses (MPa) of the static stress change are shown by thin contours of 0.5, 1, 2, 5, and 10 MPa. (g), (h) and (i) Estimated σ_1 axis orientations after the main shock, given by the sum of stress tensors before the mainshock and the static stress change. Assumed differential stress before the mainshock is 10 MPa. Orientations of the σ_1 axis are plotted separately into three depth ranges, 0–3 km, 3–5 km, and 5–8 km, so that they do not overlap. They are colored by depth. Length of bar corresponds to the plunge of the σ_1 axes.

field (Figs. 28(a)–(c)), which indicates that the shear stress working prior to the mainshock was very small. The estimated shear stress magnitude is ∼5–15 MPa (Yoshida *et al*., 2014). Figure 29 shows the post-earthquake stress field and static stress change for the 2011 M 7.0 Fukushima-Hamadori earthquake. In this case again, the observed post-earthquake stress field and the static stress change associated with the mainshock have nearly the same spatial pattern of the σ_3-axis orientations. If this is the case, the magnitude of the differential stress prior to the mainshock in this area was also extremely low with an estimated value of ∼2–30 MPa (Yoshida *et al*., 2015b).

A recent study on stress fields in NE Japan, using an extensive set of focal mechanism data, revealed that there is a tendency for highland regions to be characterized by a strike-slip stress regime while the lowlands have a reverse fault stress regime (Fig. 30; Yoshida *et al*., 2015a). This suggests that the gravity effect of topography is reflected in the present stress field, so that the differential stress magnitudes inland in NE Japan are as small as ∼16–26 MPa. Since earthquakes are actually occurring under such small stress magnitudes, the faults in the inland area must be weak. The weak faults are probably due to overpressured fluids there. If the weakness of the fault is attributed to the presence of overpressured

doi:10.5047/meep.2017.00501.0001

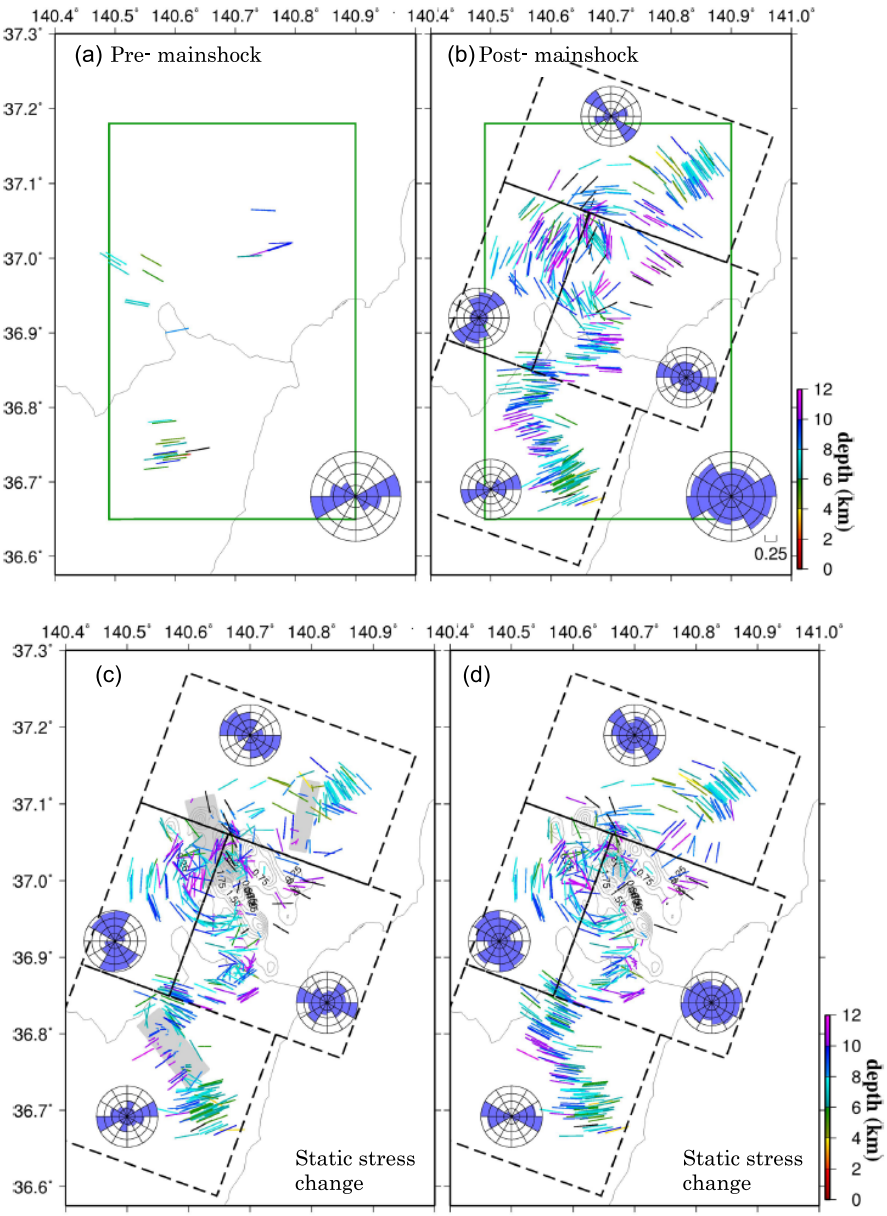

Fig. 29. Stress field in the source area of 2011 M 7.0 Fukushima-Hamadori normal fault rupture and static stress change by the mainshock (Yoshida *et al*., 2015b). (a) and (b) Estimated stress fields before and after the mainshock, respectively. (c) and (d) Static stress changes by the mainshock with and without three other $M_w > 5.5$ earthquakes, respectively. Orientations of σ_3-axes obtained by stress tensor inversions for (a) before, and (b) after, the mainshock are shown by bars. Panels (c) and (d) show orientations of σ_3-axes of the static stress changes at the same locations, calculated by the coseismic slip model of the mainshock (Hikima, 2012) with and without the fault models of the other three $M_w > 5.5$ earthquakes. Orientations of σ_3-axes are colored by depth. Length of the bars corresponds to the plunge of the σ_3-axes. Rose diagrams denote frequency distributions of σ_3-axis azimuths. Mainshock slip distribution is shown by thin contours in (c) and (d), and fault models for the three $M_w > 5.5$ earthquakes are shown by grey rectangles in (c).

fluids, a pore pressure ratio is estimated to be ~0.86–0.92. Stress fields possibly affected by high topography are also visible in several high-altitude areas of the world, such as Central Asia and Tibet (England and McKenzie, 1982; England and Houseman, 1989; England and Molnar, 1997a, b; Flesch *et al*., 2001), western North America (Flesch *et al*., 2000, 2007) and the Andes (Wdowinski *et al*., 1989; Lamb 2000; Ghosh *et al*., 2009), suggesting that similar low differential stresses also prevail there.

All of these observations suggest that H_2O, originally expelled from the subducting slab and transported to the arc crust, plays an important role in generating shallow inland earthquakes in subduction zones.

6. Summary

Precise determinations of the hypocenters of intraslab earthquakes and the seismic velocity and attenuation structures in the slab crust have provided evidence that the dehydration-derived H_2O triggers intermediate-depth intraslab earthquakes. Intermediate-depth events tend to be

doi:10.5047/meep.2017.00501.0001

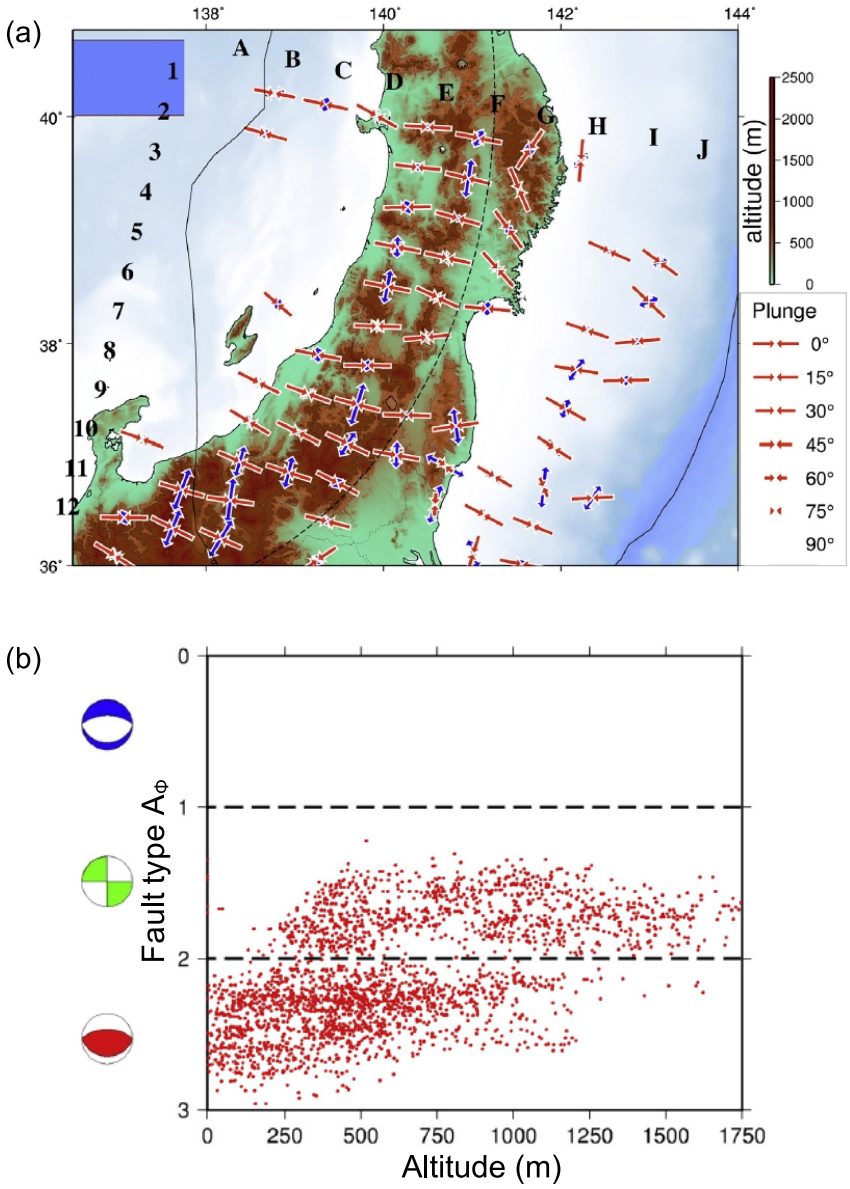

Fig. 30. Estimated stress field and fault type distribution in NE Japan (Yoshida *et al.*, 2015b). (a) Orientations of σ_1 and σ_3 axes projected onto a gridded horizontal plane. σ_1 and σ_3 axes are shown by red and blue arrows, respectively. Length of arrows corresponds to the plunge of the σ_1 or σ_3 axes. Altitude is shown by the color scale on the right. (b) Relative magnitude of the three principal stress axes, A_ϕ (Simpson, 1997) plotted against altitude in the arc–backarc region. $A_\phi = (n + 0.5) + (-1)^n(R - 0.5)$ where $R = (\sigma_2 - \sigma_3)/(\sigma_1 - \sigma_3)$, $n = 0$ (normal fault), 1 (strike-slip fault), or 2 (thrust fault). The correlation coefficient between altitude and A_ϕ is 0.67. (Reprinted from *Tectonophysics*, Yoshida, K., A. Hasegawa, and T. Okada, Spatial variation of stress orientations in NE Japan revealed by dense seismic observations, doi:10.1016/j.tecto.2015.02.013, Copyright 2015, with permission from Elsevier.)

concentrated at the dehydration loci of the metamorphosed slab crust and the serpentinized slab mantle. Earthquakes in the oceanic crust of the Pacific slab below NE Japan form a concentrated belt-like seismic zone oriented parallel to the isodepth contours of the upper plate interface and located near the dehydration loci of the metamorphosed slab crust. This seismic belt deepens locally in the Kanto area of central Japan, where the dehydration loci are also expected to deepen because of contact with the cold overlying Philippine Sea slab. The down-dip limit of the seismic low-velocity slab crust reaches the depth of this seismic belt, consistent with the expectation that the dehydration-related phase transformation causes higher seismic velocity below that depth. The down-dip limit of the low-velocity slab oceanic crust is also locally depressed in the Kanto area, again as expected.

Recent studies demonstrate that interplate earthquakes are generated by dynamic slip at asperities that have strong frictional coupling dominated by stick-slip behavior on the plate interface. Asperities are embedded in regions of weak frictional coupling dominated by stable sliding, and aseismic slip in the surrounding stably sliding areas causes incremental stress accumulation at the asperities, eventually leading to dynamic slip and generating interplate earthquakes. The size of an earthquake is determined not only by the size of the

doi:10.5047/meep.2017.00501.0001

asperity but also by the interaction between asperity and non-asperity areas. The 2011 great Tohoku-Oki earthquake actually attained its moment magnitude of 9.0 by the simultaneous ruptures of several asperities that had previously caused $M > 7$ earthquakes and some non-asperity areas. H_2O of slab origin is considered to contribute to determining the frictional properties on the megathrust and, thus, the formation of asperities. Deep low-frequency tremors/earthquakes, accompanied by episodic slow slip events in some cases, have been detected by both seismic and GPS observations in areas surrounding locked zones on the plate interface. Seismic tomography studies have revealed seismic low-velocity and anomalously high V_p/V_s zones in the vicinity of the low-frequency tremors/earthquakes, suggesting that H_2O plays an important role in generating these low-frequency events. A near-complete stress drop was observed in the 2011 Tohoku-Oki earthquake, which indicates that the plate interface is very weak. This weakness is probably caused by overpressured fluid with an extremely high pore pressure ratio of ∼0.96–0.98. Nearly complete stress drops have also been estimated in two other recent great megathrust earthquakes, the 2004 M_w 9.2 Sumatra-Andaman and M_w 8.8 Maule, Chile, quakes, suggesting that megathrusts are weak in general.

The transport of H_2O from the slab to the arc crust via the mantle wedge beneath NE Japan has been estimated based on seismic observations. Both the ascending and descending portions of secondary convection flow in the mantle wedge have been resolved as inclined seismic low-velocity zones. The ascending flow contains melt-filled pores with volume fractions of 0.1 to several percent, which are formed both by the addition of H_2O of slab origin and by decompression melting. This inclined upwelling flow in the mantle wedge reaches the arc Moho immediately below the volcanic front, demonstrating that the formation of the volcanic front is caused by this upwelling flow. Such inclined upwelling flow was detected by the presence of prominent seismic low-velocity zones in the mantle wedge beneath active volcano chains in the whole of the Japanese archipelago from Hokkaido to Kyushu, indicating that the volcano chains in the entire area are formed by this upwelling mantle flow.

H_2O of slab origin, thus transported to the arc crust, appears not only to cause arc magmatism but also enables local contractional deformation of the arc crust, which eventually leads to shallow inland earthquakes. Recent GPS observations reveal the existence of a high-strain-rate zone that extends from Niigata to Kobe in central to SW Japan, and along the Ou backbone range in NE Japan. Many large shallow inland earthquakes have occurred along these high-strain-rate zones. Prominent seismic low-velocity zones have been detected in the lower crust and/or upper mantle immediately beneath these high-strain-rate zones, suggesting the presence of H_2O, which perhaps weakens the arc crust there, causing local contractional deformation.

All these observations suggest that earthquakes in subduction zones occur in the presence of fluid in overpressured conditions, produced by H_2O supplied directly from the sediments on top of the slab and/or the dehydration decomposition of hydrated minerals in the slab and the migration of H_2O thus derived from the slab. Earthquakes occur along faults whose strength has been sufficiently lowered by overpressured fluids. Thus, the faults are considered to be very weak when earthquakes rupture, with strengths roughly estimated to be several to a few tens of MPa.

If earthquakes really take place under such small shear stresses and if the weak faults are caused by fluid overpressure, then such considerations are very important in developing the research strategy of earthquake forecasting. How large the pore fluid pressure is, and so how weak the fault is, becomes necessary information, particularly for long-term forecasts, although to develop and establish a method for assessing pore fluid pressure at depths along faults is extremely difficult. Further studies are needed to resolve the question as to whether or not the faults are indeed so weak.

Acknowledgments. I would like to thank many colleagues and coworkers, including A. Takagi, N. Umino, T. Matsuzawa, S. Miura, D. Zhao, R. Hino, T. Okada, J. Nakajima, N. Uchida, S. Horiuchi, A. Yamamoto, K. Obara, S. Matsumoto, N. Tsumura, Y. Ito, T. Igarashi, Y. Asano, S. Kita, F. Hirose, K. Ariyoshi, A. Ito, A. Hasemi, M. Kosuga, Y. Ohta, T. Iinuma, Y. Suwa, Y. Tsuji, T. Yanada, K. Yoshida, T. Sato, S. Hori, T. Kono, S. Hirahara, T. Nakayama, I. S. Sacks, A. T. Linde, M. Wyss, S. Kirby, C. H. Thurber, H. Zhang, Y. Takei, H. Sato, I. Wada, T. Yoshida and Y. Sano for their kind collaborations and fruitful discussions. I wish to thank the editor Hiroo Kanamori, R. H. Sibson and an anonymous reviewer for constructive comments that helped to improve this article. I am also grateful to K. Oshida and M. Tagawa for their help during the preparation of this review.

References

Abdelwahed, M. F., and D. Zhao (2007), Deep structure of the Japan subduction zone, *Phys. Earth Planet. Inter.*, *162*, 32–52.

Abers, G. A. (1994), Three-dimensional inversion of regional *P* and *S* arrival times in the East Aleutians and source of subduction zone gravity highs, *J. Geophys. Res.*, *99*, 4395–4412.

Active Fault Research Group (1991), *Active Faults in Japan*, Rev. Ed. University of Tokyo Press, Tokyo, 437 pp. (in Japanese).

Asano, Y., T. Saito, Y. Ito, K. Shiomi, H. Hirose, T. Matsumoto, S. Aoi, S. Hori, and S. Sekiguchi (2011), Spatial distribution and focal mechanisms of aftershocks of the 2011 off the Pacific coast of Tohoku Earthquake, *Earth Planets Space*, *63*, 669–673, doi:10.5047/eps.2011.06.016.

Audet, P., M. G. Bostock, N. I. Christensen, and S. M. Peacock (2009), Seismic evidence for overpressured subducted oceanic crust and megathrust fault sealing, *Nature*, *457*, 76–78, doi:10.1038/nature07650.

Baba, T., Y. Tanioka, P. R. Cummins, and K. Uhira (2002), The slip distribution of the 1946 Nankai earthquake estimated from tsunami inversion using a new plate model, *Phys. Earth Planet. Inter.*, *132*, 59–73.

Becken, M., O. Ritter, S. K. Park, P. A. Bedrosian, U. Weckmann, and M. Weber (2008), A deep crustal fluid channel into the San Andreas Fault system near Parkfield, California, *Geophys. J. Int.*, *173*, 718–732.

Brudzinski, M. R., C. H. Thurber, B. R. Hacker, and E. R. Engdahl (2007), Global prevalence of double Benioff zones, *Science*, *316*, 1472–1474.

Chernak, L. C., and G. Hirth (2010), Deformation of antigorite serpentinite at high temperature and pressure, *Earth Planet. Sci. Lett.*, *296*, 23–33.

Chernak, L. C., and G. Hirth (2011), Syndeformational antigorite dehydration produces stable fault slip, *Geology*, *39*, 847–850, doi:10.1130/G31919.1.

Davies, J. H., and D. J. Stevenson (1992), Physical model of source region of subduction zone volcanic, *J. Geophys. Res.*, *97*, 2037–2070.

DeMets, C., R. G. Gordon, D. F. Argus, and S. Stein (1994), Effect of recent revisions to the geomagnetic reversal time scale on estimates of current plate motions, *Geophys. Res. Lett.*, *21*, 2192–2194.

Dobson, D. P., P. G. Meredith, and S. A. Boon, (2002), Simulation of subduction zone seismicity by dehydration of serpentine, *Science*, *298*, 1407–1410.

Dragert, H., K. Wang, and T. S. James (2001), A silent slip event on the

deeper Cascadia subduction interface, *Science*, *292*, 1525–1528.
Ekström, G., M. Nettles, and A. M. Dziewonski (2012), The Global CMT Project 2004–2010: Centroid-moment tensors for 13,017 earthquakes, *Phys. Earth Planet. Inter.*, *200–201*, 1–9, doi:10.1016/j.pepi.2012.04.002.
Engdahl, E. R. (2006), Application of an improved algorithm to high precision relocation of ISC test events, *Phys. Earth Planet. Inter.*, *158*, 14–18.
Engdahl, E. R., R. van der Hilst, and R. Buland (1998), Global teleseismic earthquake relocation with improved travel times and procedures for depth determination, *Bull. Seismol. Soc. Am.*, *88*(3), 722–743.
England, P. C., and G. A. Houseman (1989), Extension during continental convergence, with application to the Tibetan Plateau, *J. Geophys. Res.*, *94*, 17561–17579.
England, P. C., and D. P. McKenzie (1982), A thin viscous sheet model for continental deformation, *Geophys. J. Int.*, *70*, 295–321.
England, P. C., and P. Molnar (1997a), The field of crustal velocity in Asia calculated from Quaternary rates of slip on faults, *Geophys. J. Int.*, 130551–130582.
England, P. C., and P. Molnar (1997b), Active deformation of Asia: from kinematics to dynamics, *Science*, *278*, 647–649.
Flesch, L. M., W. E. Holt, A. J. Haines, and B. Shen-Tu (2000), Dynamics of the Pacific-North American Plate boundary in the Western United States, *Science*, *287*, 834–836.
Flesch, L. M., A. J. Haines, and W. E. Holt (2001), Dynamics of the India-Eurasia collision zone, *J. Geophys. Res.*, *106*(B8), 16435–16460.
Flesch, L. M., W. E. Holt, A. J. Haines, L. Wen, and B. Shen-Tu (2007), The dynamics of western North America: Stress magnitudes and the relative role of gravitational potential energy, plate interaction at the boundary and basal tractions, *Geophys. J. Int.*, *169*, 866–896.
Furukawa, Y., and S. Uyeda (1989), Thermal state under the Tohoku arc with consideration of crustal heat generation, *Tectonophysics*, *164*, 175–187.
Ghisetti, F. C., and R. H. Sibson (2006), Accommodation of compressional inversion in north-western South Island (New Zealand): Old faults versus new?, *J. Struct. Geol.*, *28*, 1994–2010.
Ghosh, A., W. E. Holt, and L. M. Flesch (2009), Contribution of gravitational potential energy differences to the global stress field, *Geophys. J. Int.*, *179*(2), 787–812.
Gorbatov, A., J. Dominguez, G. Suarez, V. Kostoglodov, D. Zhao, and E. Gordeev (1999), Tomographic imaging of the *P*-wave velocity structure beneath the Kamchatka peninsula, *Geophys. J. Int.*, *137*, 269–279.
Green, H. W., and H. Houston (1995), The mechanics of deep earthquakes, *Ann. Rev. Earth Planet. Sci.*, 169–213.
Griggs, D. T., and J. Handin (1960), Observations on fracture and a hypothesis of earthquakes, in *Rock Deformation*, edited by D. T. Griggs, and J. Handin, *Geol. Soc. Am. Memoir*, *79*, 347–373.
Hacker, B. R., G. A. Abers, and S. M. Peacock (2003a), Subduction Factory 1. Theoretical mineralogy, densities, seismic wave speeds, and H_2O contents, *J. Geophys. Res.*, *108*(B1), 2029, doi:10.1029/ 2001JB001127.
Hacker, B. R., S. M. Peacock, G. A. Abers, and S. D. Holloway (2003b), Subduction Factory 2. Are intermediate-depth earthquakes in subducting slabs linked to metamorphic dehydration reactions?, *J. Geophys. Res.*, *108*, doi:10.1029/2001JB001129.
Hardebeck, J. (2012), Coseisimic and postseismic stress rotations due to great subduction zone earthquakes, *Geophys. Res. Lett.*, *39*, L21313, doi:10.1029/2012GL053438.
Hardebeck, J., and E. Hauksson (2001), Crustal stress field in southern California and its implications for fault mechanics, *J. Geophys. Res.*, *106*(B10), 21859–21882.
Hasegawa, A., and J. Nakajima (2004), Geophysical constraints on slab subduction and arc magmatism, in *The State of the Planet: Frontiers and Challenges in Geophysics*, edited by R. S. J. Sparks, and C. J. Hawkesworth, pp. 81–94, AGU Geophysical Monograph, *150*, IUGG volume 19.
Hasegawa, A., and A. Yamamoto (1994), Deep, low-frequency microearthquakes in or around seismic low-velocity zones beneath active volcanoes in northeastern Japan, *Tectonophysics*, *233*, 233–252.
Hasegawa, A., and K. Yoshida (2015), Preceding seismic activity and slow slip events in the source area of the 2011 M_w 9.0 Tohoku-Oki earthquake: A review, *Geosci. Lett.*, 2–6, doi:10.1186/s40562-015-0025-0.
Hasegawa, A., N. Umino, and A. Takagi (1978a), Double-planed structure of the deep seismic zone in the northeastern Japan arc, *Tectonophysics*, *47*, 43–58.
Hasegawa, A., N. Umino, and A. Takagi (1978b), Double-planed deep seismic zone and upper-mantle structure in the northeastern Japan arc, *Geophys. J. Int.*, *54*, 281–296.
Hasegawa, A., D. Zhao, S. Hori, A. Yamamoto, and S. Horiuchi (1991), Deep structure of the northeastern Japan arc and its relationship to seismic and volcanic activity, *Nature*, *352*, 683–689.
Hasegawa, A., S. Horiuchi, and N. Umino (1994), Seismic structure of the northeastern Japan convergent margin: A synthesis, *J. Geophys. Res.*, *99*, 22295–22311.
Hasegawa, A., A. Yamamoto, N. Umino, S. Miura, S. Horiuchi, D. Zhao, and T. Sato (2000), Seismic activity and deformation process of the crust within the overriding plate in the northeastern Japan subduction zone, *Tectonophysics*, *319*, 225–239.
Hasegawa, A., J. Nakajima, N. Umino, and S. Miura (2005), Deep structure of the northeastern Japan arc and its implications for crustal deformation and shallow seismic activity, *Tectonophysics*, *403*, 59–75.
Hasegawa, A., J. Nakajima, S. Kita, T. Okada, T. Matsuzawa, and S. Kirby (2007), Anomalous deepening of a belt of intraslab earthquakes in the Pacific slab crust under Kanto, central Japan: Possible anomalous thermal shielding, dehydration reactions, and seismicity caused by shallower cold slab material, *Geophys. Res. Lett.*, *34*, L09305, doi:10.1029/2007GL029616.
Hasegawa, A., J. Nakajima, S. Kita, Y. Tsuji, K. Nii, T. Okada, T. Matsuzawa, and D. Zhao (2008), Transportation of H_2O in the NE Japan Subduction Zone as Inferred from Seismic Observations: Supply of H_2O from the Slab to the Arc Crust, *J. Geography*, *117*(1), 59–75 (in Japanese with English abstract).
Hasegawa, A., J. Nakajima, N. Uchida, T. Okada, D. Zhao, T. Matsuzawa, and N. Umino (2009), Plate subduction, and generation of earthquakes and magmas in Japan as inferred from seismic observations: An overview, *Gondwana Res.*, *16*, 370–400, doi:10.1016/j.gr.2009.03.007.
Hasegawa, A., K. Yoshida, and T. Okada (2011), Nearly complete stress drop in the 2011 M_w 9.0 off the Pacific coast of Tohoku Earthquake, *Earth Planets Space*, *63*, 703–707, doi:10.5047/eps.2011.06.007.
Hasegawa, A., K. Yoshida, Y. Asano, T. Okada, T. Iinuma, and Y. Ito (2012a), Change in stress field after the 2011 great Tohoku-oki earthquake, *Earth Planet. Sci. Lett.*, *355–356*, 231–243, doi:10.1016/j.epsl.2012.08.042.
Hasegawa, A., J. Nakajima, N. Uchida, T. Yanada, T. Okada, D. Zhao, T. Matsuzawa, and N. Umino (2012b), Mechanism generating earthquakes in subduction zones: Vital role of geofluids in earthquake generation, *J. Geogr.*, *121*, 128–160 (in Japanese with English abstract).
Hasegawa, A., J. Nakajima, T. Yanada, N. Uchida, T. Okada, D. Zhao, T. Matsuzawa, and N. Umino (2013), Complex slab structure and arc magmatism beneath the Japanese Islands, *J. Asian Earth Sci.*, *78*, 277–290.
Hashimoto, M. (1990), Horizontal strain rates in the Japanese Islands during interseismic period deduced from geodetic surveys (part 1): Honshu, Shikoku and Kyushu, *J. Seismol. Soc. Japan*, *43*, 13–26 (in Japanese with English abstract).
Hashimoto, M., and D. D. Jackson (1993), Plate tectonics and crustal deformation around the Japanese islands, *J. Geophys. Res.*, *98*, 16149–16166.
Hashimoto, C., A. Noda, T. Sagiya, and M. Matsu'ura (2009), Interplate seismogenic zones along the Kuril–Japan trench inferred from GPS data inversion, *Nature Geosci.*, *2*, 141–144, doi:10.1038/ngeo421.
Heki, K., and S. Miyazaki (2001), Plate convergence and long-term crustal deformation in Central Japan, *Geophys. Res. Lett.*, *28*, 2313–2316.
Hikima, K. (2012), Rupture process of the April 11, 2011 Fukushima Hamadori earthquake (M_j 7.0)—Two fault planes inferred from strong motion and relocated aftershocks, *J. Seismol. Soc. Japan*, *64*, 243–256 (in Japanese with English abstract).
Hirose, F., J. Nakajima, and A. Hasegawa (2008a), Three-dimensional velocity structure and configuration of the PHS slab beneath Kanto district, central Japan, estimated by double-difference tomography, *J. Seismol. Soc. Japan*, *60*, 123–138 (in Japanese with English abstract).
Hirose, F., J. Nakajima, and A. Hasegawa (2008b), Three-dimensional seismic velocity structure and configuration of the Philippine Sea slab in southwestern Japan estimated by double-difference tomography, *J. Geophys. Res.*, *13*, B09315, doi:10.1029/2007JB005274.
Hirth, G., and N. M. Beeler (2015), The role of fluid pressure on frictional behavior at the base of the seismogenic zone, *Geology*, *43*, 223–225.
Hobbs, B. E., and A. Ord (1988), Plastic instabilities: implications for the origin of intermediate and deep focus earthquakes, *J. Geophys. Res.*, *93*, 10521–10540.

doi:10.5047/meep.2017.00501.0001

Hori, S. (2006), Seismic activity associated with the subducting motion of the Philippine Sea plate beneath the Kanto district, Japan, *Tectonophysics*, *417*, 85–100.

Hori, S., N. Umino, T. Kono, and A. Hasegawa (2004), Distinct *S*-wave reflectors (bright spots) extensively distributed in the crust and upper mantle beneath the northeastern Japan arc, *J. Seism. Soc. Japan*, *56*, 435–446 (in Japanese with English abstract).

Huang, Z., D. Zhao, A. Hasegawa, N. Umino, J. Park, and I. Kang (2013), Aseismic deep subduction of the Philippine Sea plate and slab window, *J. Asian Earth Sci.*, *75*, 82–94.

Hyodo, M., and K. Hirahara (2003), A viscoelastic model of interseismic strain concentration in Niigata-Kobe Tectonic Zone of central Japan, *Earth Planets Space*, *55*, 667–675.

Ide, S., D. R. Shelly, and G. C. Beroza (2007), Mechanism of deep low frequency earthquakes: Further evidence that deep non-volcanic tremor is generated by shear slip on the plate interface, *Geophys. Res. Lett.*, *34*, L03308, doi:10.1029/2006GL028890.

Iinuma, T. *et al.* (2009), Aseismic slow slip on an inland active fault triggered by a nearby shallow event, the 2008 Iwate-Miyagi Nairiku earthquake (M_w 6.8), *Geophys. Res. Lett.*, *36*, L20308, doi:10.1029/2009GL040063.

Iinuma, T., R. Hino, M. Kido, D. Inazu, Y. Osada, Y. Ito, M. Ohzono, H. Tsushima, S. Suzuki, H. Fujimoto, and S. Miura (2012), Coseismic slip distribution of the 2011 off the Pacific Coast of Tohoku Earthquake (M9.0) refined by means of seafloor geodetic data, *J. Geophys. Res.*, *117*, doi:10.1029/2012JB009186.

Iio, Y., T. Sagiya, Y. Kobayashi, and I. Shiozaki (2002), Water weakened lower crust and its role in the concentrated deformation in the Japanese Islands, *Earth Planet. Sci. Lett.*, *203*, 245–253.

Iio, Y., T. Sagiya, and Y. Kobayashi (2004), Origin of the concentrated deformation zone in the Japanese Islands and stress accumulation process of intraplate earthquakes, *Earth Planets Space*, *56*, 831–842.

Ishida, M. (1992), Geometry and relative motion of the Philippine Sea plate and Pacific plate beneath the Kanto-Tokai district, Japan, *J. Geophys. Res.*, *97*, 453–489.

Ito, T., S. Yoshioka, and S. Miyazaki (2000), Interplate coupling in northeast Japan deduced from inversion analysis of GPS data, *Earth Planet. Sci. Lett.*, *176*, 117–130, doi:10.1016/S0012-821X(99)00316-7.

Iwamori, H. (1998), Transportation of H_2O and melting in subduction zones, *Earth Planet. Sci. Lett.*, *160*, 65–80.

Iwamori, H. (2000), Bending of volcanic chain near the triple junction by thermal effect, and deep subduction of H_2O, *Earth Planet. Sci. Lett.*, *181*, 41–46.

Jung, H., H. W. Green, and F. Dobrzhinetskaya (2004), Intermediate-depth earthquake faulting by dehydration embrittlement with negative volume change, *Nature*, *428*, 545–549.

Jung, H., Y. Fei, P. Silver, and H. W. Green, (2009), Frictional sliding in serpentine at very high pressure, *Earth Planet. Sci. Lett.*, *277*, 273–279, http://dx.doi.org/10.1016/j.epsl.2008.10.019.

Kanamori, H. (1977), Seismic and aseismic slip along subduction zones and their tectonic implications, AGU Geophys. Monograph, 163–174.

Kanamori, H. (1978), Quantification of earthquakes, *Nature*, *271*, 411–414.

Kanamori, H., M. Miyazawa, and J. Mori (2006), Investigation of the earthquake sequence off Miyagi prefecture with historical seismograms, *Earth Planets Space*, *58*, 1533–1541.

Karato, S., M. R. Ridel, and D. A. Yuen (2001), Rheological structure and deformation of subducted slabs in the mantle transition zone: implications for mantle circulation and deep earthquakes, *Phys. Earth Planet. Inter.*, *127*, 83–108.

Kasahara, K. (1985), Patterns of crustal activity associated with the convergence of three plates beneath the Kanto–Tokai area, central Japan, *Rep. National Res. Inst. Earth Sci. Disas. Prev.*, *35*, 33–137 (in Japanese with English abstract).

Katayama, I., K. Hirauchi, and J. Nakajima (2010), Variability of subduction processes beneath Japan, *J. Geogr.*, *119*, 205–223 (in Japanese with English abstract).

Kato, A., T. Iidaka, I. Ikuta, Y. Yoshida, K. Katsumata, T. Iwasaki, S. Sakai, C. Thurber, N. Tsumura, K. Yamaoka, T. Watanabe, T. Kunitomo, F. Yamazaki, M. Okubo, M. Suzuki, and N. Hirata (2010), Variations of fluid pressure within the subducting oceanic crust and slow earthquakes, *Geophys. Res. Lett.*, *37*, L14310, doi:10.1029/2010GL043723.

Kato, T. (1979), Crustal movements in the Tohoku district, Japan, during the period 1900–1975, and their tectonic implications, *Tectonophysics*, *60*, 141–167.

Kawakatsu, H., and S. Watada (2007), Seismic evidence for deep water transportation in the mantle, *Science*, *316*, 1468–1471.

Kelemen, P. B. and G. Hirth (2007), A periodic shear-heating mechanism for intermediate-depth earthquakes in the mantle, *Nature*, *446*, 787–790, doi:10.1038/nature05717.

Kimura, G., S. Hina, Y. Hamada, J. Kameda, T. Tsuji, M. Kinoshita, and A. Yamaguchi (2012), Runaway slip to the trench due to rupture of highly pressurized megathrust beneath the middle trench slope: The tsunamigenesis of the 2011 Tohoku earthquake off the east coast of northern Japan, *Earth Planet. Sci. Lett.*, *339–340*, 32–45.

Kirby, S. H. (1995), Intraslab earthquakes and phase changes in subducting lithosphere. U.S. Ntl. Rep. Int. Union Geod. Geopys., 1991–1994, *Rev. Geophys.*, *33*, 287–297.

Kirby, S. H., E. R. Engdahl, and R. Denlinger (1996), Intermediate-Depth Intraslab Earthquakes and Arc Volcanism as Physical Expressions of Crustal and Uppermost Mantle Metamorphism in Subducting Slabs, in *Subduction: Top to Bottom*, edited by G. E. Bebout *et al.*, pp. 347–355, Geophys. Monograph Ser., *96*, AGU, Washington, D.C.

Kita, S., T. Okada, J. Nakajima, T. Matsuzawa, and A. Hasegawa (2006), Existence of a seismic belt in the upper plane of the double seismic zone extending in the along-arc direction at depths of 70–100 km beneath NE Japan, *Geophys. Res. Lett.*, *33*, doi:10.1029/2006GL028239.

Kita, S., T. Okada, A. Hasegawa, J. Nakajima, and T. Matsuzawa (2010), Anomalous deepening of a seismic belt in the upper-plane of the double seismic zone in the Pacific slab beneath the Hokkaido corner: Possible evidence for thermal shielding caused by subducted forearc crust materials, *Earth Planet. Sci. Lett.*, *290*, 415–426.

Kodaira, S., N. Takahashi, J. Park, K. Mochizuki, M. Shinohara, and S. Kimura (2000), Western Nankai Trough seismogenic zone: Results from a wide-angle ocean bottom seismic survey, *J. Geophys. Res.*, *105*, 5887–5905.

Kodaira, S., E. Kurashimo, J. Park, N. Takahashi, A. Nakanishi, S. Miura, T. Iwasaki, N. Hirata, K. Ito, and Y. Kaneda (2002), Structural factors controlling the rupture process of a megathrust earthquake at the Nankai trough seismogenic zone, *Geophys. J. Int.*, *149*, 815–835.

Kodaira, S., T. Iidaka, A. Kato, J. Park, T. Iwasaki, and Y. Kaneda (2004), High pore fluid pressure may cause silent slip in the Nankai Trough, *Science*, *304*, 1295–1298.

Kono, T., K. Nida, S. Matsumoto, S. Horiuchi, T. Okada, K. Kaihara, A. Hasegawa, S. Hori, N. Umino, and M. Suzuki (1993), Microearthquake activity in the focal area of the 1962 Northern Miyagi earthquake (*M* 6.5), *J. Seismol. Soc. Japan*, *46*, 85–93 (in Japanese with English abstract).

Kurashimo, E., M. Tokunaga, N. Hirata, T. Iwasaki, S. Kodaira, Y. Kaneda, K. Ito, R. Nishida, S. Kimura, and T. Ikawa (2002), Geometry of the subducting Philippine Sea plate and the crustal and upper mantle structure beneath eastern Shikoku island revealed by seismic refraction/wide-angle reflection profiling, *J. Seismol. Soc. Japan*, *54*, 489–505 (in Japanese with English abstract).

Lamb, S. (2000), Active deformation in the Bolivian Andes, South America, *J. Geophys. Res.*, *105*, 25627–25653.

Lamb, S. (2006), Shear stresses on megathrusts: Implications for mountain building behind subduction zones, *J. Geophys. Res.*, *111*, B07401, doi:10.1029/2005JB003916.

Lay, T., C. J. Ammon, H. Kanamori, L. Xue, and M. J. Kim (2011), Possible large near-trench slip during the 2011 M_w 9.0 off the Pacific coast of Tohoku Earthquake, *Earth Planets Space*, *63*, 687–692, doi:10.5047/eps.2011.05.033.

Lin, W., S. Saito, Y. Sanada, Y. Yamamoto, Y. Hashimoto, and T. Kanamatsu (2011), Principal horizontal stress orientations prior to the 2011 M_w 9.0 Tohoku-Oki, Japan, earthquake in its source area, *Geophys. Res. Lett.*, *38*, L00G10, doi:10.1029/2011GL049097.

Loveless, J. P., and B. J. Meade (2010), Geodetic imaging of plate motions, slip rates, and partitioning of deformation in Japan, *J. Geophys. Res.*, *115*(B02410), doi:10.1029/2008JB006248.

Maruyama, S., and S. Okamoto (2007), Water transportation from the subducting slab into the mantle transition zone, *Gondwana Res.*, *11*, 145–165.

Matsumoto, S., and A. Hasegawa (1996), Distinct *S*-wave reflector in the mid-crust beneath Nikko-Shirane volcano in the northeastern Japan arc, *J. Geophys. Res.*, *101*, 3067–3083.

Matsuzawa, T., N. Umino, A. Hasegawa, and A. Takagi (1986), Upper mantle velocity structure estimated from *PS*-converted wave beneath the

northeastern Japan arc, *Geophys. J. Int.*, *86*, 767–787.
Matsuzawa, T., T. Kono, A. Hasegawa, and A. Takagi (1990), Subducting plate boundary beneath the northeastern Japan arc estimated from SP converted waves, *Tectonophysics*, *181*, 123–133.
McKenzie, D. P. (1969), Speculations on the consequences and causes of plate motions, *Geophys. J. Int.*, *18*, 1–32.
Meade, C., and R. Jeanloz (1991), Deep-focus earthquakes and recycling of water into the Earth's mantle, *Science*, *252*, 68–72.
Mishra, O. P., D. Zhao, N. Umino, and A. Hasegawa (2003), Tomography of northeast Japan forearc and its implications for interplate seismic coupling, *Geophys. Res. Lett.*, *30*, doi:10.1029/2003GL017736.
Mitsuhata, Y., Y. Ogawa, M. Mishina, T. Kono, T. Yokokura, and T. Uchida (2001), Electromagnetic heterogeneity of the seismogenic region of 1962 *M* 6.5 Northern Miyagi Earthquake, northeastern Japan, *Geophys. Res. Lett.*, *28*(23), 4371–4374.
Miura, M., T. Sato, A. Hasegawa, Y. Suwa, K. Tachibana, and S. Yui (2004), Strain concentration zone along the volcanic front derived by GPS observations in NE Japan arc, *Earth Planets Space*, *56*, 1347–355.
Miyazaki, S., and K. Heki (2001), Crustal velocity field of Southwest Japan: subduction and arcarc collision, *J. Geophys. Res.*, *106*, 4305–4326.
Miyoshi, T., and K. Ishibashi (2004), Geometry of the seismic Philippine Sea slab beneath the region from Ise Bay to western Shikoku, southwest Japan, *J. Seismol. Soc. Japan 57*, 139–152 (in Japanese with English abstract).
Mizoue, M., M. Nakamura, N. Seto, Y. Ishiketa, and T. Yokota (1983), Three-layered distribution of microearthquakes in relation to focal mechanism variation in the Kii Peninsula, southwestern Honshu, Japan, *Bull. Earthq. Res. Inst. Univ. Tokyo*, *58*, 287–310.
Murotani, S. (2003), Rupture processes of large Fukushima-Oki earthquakes in 1938, MSc Thesis, Univ. of Tokyo.
Nadeau, R. M., and D. Dolenc (2005), Nonvolcanic tremors deep beneath the San Andreas Fault, *Science*, *307*, 389.
Nakajima, J., and A. Hasegawa (2003a), Tomographic imaging of seismic velocity structure in and around the Onikobe volcanic area, northeastern Japan: Implications for fluid distribution, *J. Volcanol. Geotherm. Res.*, *127*, 1–18.
Nakajima, J., and A. Hasegawa (2003b), Estimation of thermal structure in the mantle wedge of northeastern Japan from seismic attenuation data, *Geophys. Res. Lett.*, *30*(14), 1760, doi:10.1029/2003GL017185.
Nakajima, J., and A. Hasegawa (2007a), Subduction of the Philippine Sea plate beneath southwestern Japan: Slab geometry and its relationship to arc magmatism, *J. Geophys. Res.*, *112*, B08306, doi:10.1029/2006JB004770.
Nakajima, J., and A. Hasegawa (2007b), Deep crustal structure along the Niigata-Kobe Tectonic Zone, Japan: Its origin and segmentation, *Earth Planets Space*, *59*, e5–e8.
Nakajima, J., and A. Hasegawa (2008), Existence of low-velocity zones under the source areas of the 2004 Niigara-Chuetsu and 2007 Niigarta-Chuetsu-Oki earthquakes inferred from travel-time tomography, *Earth Planets Space*, *60*, 1127–1130.
Nakajima, J., and A. Hasegawa (2010), Cause of *M* 7 earthquakes beneath the Tokyo metropolitan area, Japan: Possible evidence for a vertical tear at the easternmost portion of the Philippine Sea slab, *J. Geophys. Res.*, *115*, doi:10.1029/2009JB006863.
Nakajima, J., T. Matsuzawa, A. Hasegawa, and D. Zhao (2001a), Three-dimensional structure of V_p, V_s, and V_p/V_s beneath northeastern Japan: Implications for arc magmatism and fluids, *J. Geophys. Res.*, *106*, 843–857.
Nakajima, J., T. Matsuzawa, A. Hasegawa, and D. Zhao (2001b), Seismic imaging of arc magma and fluids under the central part of northeastern Japan, *Tectonophysics*, *341*, 1–17.
Nakajima, J., Y. Takei, and A. Hasegawa (2005), Quantitative analysis of the inclined low-velocity zone in the mantle wedge of northeastern Japan: A systematic change of melt-filled pore shapes with depth and its implications for melt migration, *Earth Planet. Sci. Lett.*, *234*, 59–70.
Nakajima, J., Y. Tsuji, and A. Hasegawa (2009a), Seismic evidence for thermally-controlled dehydration reaction in subducting oceanic crust, *Geophys. Res. Lett.*, *36*, L03303, doi:10.1029/2008GL036865.
Nakajima, J., F. Hirose, and A. Hasegawa (2009b), Seismotectonics beneath the Tokyo metropolitan area: Effect of slab-slab contact and overlap on seismicity, *J. Geophys. Res.*, *114*, B08309, doi:10.1029/2008JB006101.
Nakajima, J., S. Hada, E. Hayami, N. Uchida, A. Hasegawa, S. Yoshioka, T. Matsuzawa, and N. Umino (2013), Seismic attenuation beneath northeastern Japan: Constraints on mantle dynamics and arc magmatism, *J. Geophys. Res.*, *118*, 5838–5855.
Nakanishi, A., N. Takahashi, J. Park, S. Miura, S. Kodaira, Y. Kaneda, N. Hirata, T. Iwasaki, and M. Nakamura (2002), Crustal structure across the coseismic rupture zone of the 1944 Tonankai earthquake, the central Nankai Trough seismogenic zone, *J. Geophys. Res.*, *107*, 2007. doi:10.1029/2001JB000424.
Nishimura, T., S. Miura, K. Tachibana, K. Hashimoto, T. Sato, S. Hori, E. Murakami, T. Kono, K. Nida, M. Mishina, T. Hirasawa, and S. Miyazaki (2000), Distribution of seismic coupling on the subducting plate boundary in northeastern Japan inferred from GPS observations, *Tectonophysics*, *323*, 217–238.
Nishiyama, T. (1992), Mantle hydrology in a subduction zone: A key to episodic geologic events, double Wadati-Benioff zones and magma genesis, *Mathematical Seismology, VII, Report of Institute of Statistical Mathematics, Tokyo*, *34*, 31–67, 1992.
Noguchi, S. (1998), Seismicity, focal mechanisms and location of volcanic front associated with the subducting Philippine Sea and Pacific plates beneath the Kanto district, Japan, *Bull. Earthq. Res. Inst. Tokyo Univ.*, *73*, 73–103.
Noguchi, S. (2007), Spatial distribution of seismicity in the subducting Philippine Sea slab and Pacific slab beneath the Kanto district, Japan, and their convergence model, *Earth Monthly*, *57*, 42–53 (in Japanese).
Obara, K. (2002), Nonvolcanic deep tremor associated with subduction in southwest Japan, *Science*, *296*, 1679–1681, doi:10.1126/science.1070378.
Obara, K. (2010), Phenomenology of deep slow earthquake family in southwest Japan: Spatiotemporal characteristics and segmentation, *J. Geophys. Res.*, doi:10.1029/2008JB006048.
Obara, K., H. Hirose, F. Yamamizu, and K. Kasahara (2004), Episodic slow slip events accompanied by non-volcanic tremors in southwest Japan subduction zone, *Geophys. Res. Lett.*, *31*, L23602, doi:10.1029/2004GL020848.
Ogawa, M. (1987), Shear instability in a viscoelastic material as the cause of deep focus earthquakes, *J. Geophys. Res.*, *92*, 13801–13810.
Ogawa, Y., and Y. Honkura (2004), Mid-crustal electrical conductors and their correlations to seismicity and deformation at Itoigawa-Shizuoka Tectonic Line, Central Japan, *Earth Planets Space*, *56*, 1285–1292.
Okada, T., T. Yaginuma, N. Umino, T. Matsuzawa, A. Hasegawa, H. Zhang, and C. H. Thurber (2006), Detailed imaging of the fault planes of the 2004 Niigata-Chuetsu, central Japan, earthquake sequence by double-difference tomography, *Earth Planet. Sci. Lett.*, *244*, 32–43.
Okada, T., A. Hasegawa, J. Suganomata, N. Umino, and H. Zhang, and C. Thurber (2007), Imaging the heterogeneous source area of the 2003 *M* 6.4 northern Miyagi earthquake, NE Japan, by double-difference tomography, *Tectonophysics*, *430*, 67–81.
Okada, T., N. Umino, and A. Hasegawa (2010), Deep structure of the Ou mountain range strain concentration zone and the focal area of the 2008 Iwate-Miyagi Nairiku earthquake, NE Japan—Seismogenesis related with magma and crustal fluid, *Earth Planets Space*, *62*, 347–352.
Okada, Y., K. Kasahara, S. Hori, K. Obara, S. Sekiguchi, H. Fujiwara, and A. Yamamoto (2004), Recent progress of seismic observation networks in Japan—Hi-net, F-net, K-NET and KiK-net, *Earth Planets Space*, *56*, 15–18.
Ozawa, S., T. Nishimura, H. Munekane, H. Suito, T. Kobayashi, M. Tobita, and T. Imakiire (2012), Preceding, coseismic, and postseismic slips of the 2011 Tohoku earthquake, Japan, *J. Geophys. Res.*, *117*(B7), B07404, doi:10.1029/2011JB009120.
Pacheco, J. F., and L. R. Sykes (1992), Seismic moment catalog of large shallow earthquakes, 1900 to 1989, *Bull. Seismol. Soc. Am.*, *82*, 1306–1349.
Pacheco, J. F., L. R. Sykes, and C. H. Scholz (1993), Nature of seismic coupling along simple plate boundaries of the subduction type, *J. Geophys. Res.*, *98*, 14133–14159.
Payero, J. S., V. Kostoglodov, N. Shapiro, T. Mikumo, A. Iglesias, X. Perez-Campos, and R. W. Clayton (2008), Nonvolcanic tremor observed in the Mexican subduction zone, *Geophys. Res. Lett.*, *35*, L07305.
Peacock, S. M. (2001), Are the lower planes of double seismic zones caused by serpentine dehydration in subducting oceanic mantle?, *Geology*, *29*, 299–302.
Peacock, S. M., and R. D. Hyndman (1999), Hydrous minerals in the mantle wedge and the maximum depth of subduction thrust earthquakes, *Geophys. Res. Lett.*, *26*, 2517–2520.

doi:10.5047/meep.2017.00501.0001

Peacock, S. M., and K. Wang (1999), Seismic consequences of warm versus cool subduction metamorphism: examples from southwest and northeast Japan, *Science*, *286*, 937–939.

Peng, Z., and J. Gomberg (2010), An integrated perspective of the continuum between earthquakes and slow-slip phenomena, *Nature Geosci*., *3*, 599–607, doi:10.1038/ngeo940.

Peterson, C. L., and D. H. Christensen (2009), Possible relationship between nonvolcanic tremor and the 1998–2001 slow-slip event, south central Alaska, *J. Geophys. Res*., *114*, B06302.

Peterson, E. T., and T. Seno (1984), Factors affecting seismic moment release rates in subduction zones, *J. Geophys. Res*., *89*, 10233–10248.

Proctor, B., and G. Hirth (2015), Role of pore fluid pressure on transient strength changes and fabric development during serpentine dehydration at mantle conditions: Implications for subduction-zone seismicity, *Earth Planet. Sci. Lett*., *421*, 1–12.

Raleigh, C. B. (1967), Tectonic implications of serpentinite weakening, *Geophys. J. Int*., *14*, 113–118.

Raleigh, C. B., and M. S. Paterson (1965), Experimental deformation of serpentinite and its tectonic implications, *J. Geophys. Res*., *70*, 3965–3985.

Rogers, G., and H. Dragert (2003), Episodic tremor and slip on the Cascadia subduction zone: the chatter of silent slip, *Science*, *300*, 1942–1943.

Romano, F., A. Piatanesi, S. Lorito, N. D'Agostino, K. Hirata, S. Atzori, Y. Yamazaki, and M. Cocco (2012), Clues from joint inversion of tsunami and geodetic data of the 2011 Tohoku Earthquake, *NPG Scientific Rep*., *2*, 385 doi:10.1038/srep00385.

Sagiya, T., S. Miyazaki, and T. Tada (2000), Continuous GPS array and present-day crustal deformation of Japan, *Pure Appl. Geophys*., *157*, 2303–2322.

Sano, Y., T. Hara, N. Takahata, S. Kawagucci, M. Honda, Y. Nishio, W. Tanikawa, A. Hasegawa, and K. Hattori (2014), Helium anomalies suggest a fluid pathway from mantle to trench during the 2011 Tohoku-Oki earthquake, *Nature Comm*., *5*, doi:10.1038/ncomms4084.

Sato, H. (1994), The relationship between late Cenozoic tectonic events and stress field and basin development in northeast Japan, *J. Geophys. Res*., *99*, 22261–22274.

Sato, H., N. Hirata, T. Iwasaki, M. Matsubara, and T. Ikawa (2002), Deep seismic reflection profiling across the Ou Backbone range, northern Honshu Island, Japan, *Tectonophysics*, *355*, 41–52.

Sato, R., K. Abe, Y. Okada, K. Shimazaki, and Y. Suzuki (1997), *Handbook of Earthquake Fault Parameters in Japan*, Kajima Institute Publishing Co., pp. 1–390.

Sato, T., S. Miura, K. Tachibana, Y. Satake, and A. Hasegawa (2002), Crustal deformation around Ou Backbone range, northeastern Japan observed by a dense GPS network, *J. Seismol. Soc. Japan*, *55*, 181–191 (in Japanese with English abstract).

Schmidt, M. W., and S. Poli (1998), Experimentally based water budgets for dehydrating slabs and consequences for arc magma generation, *Earth Planet. Sci. Lett*., *163*, 361–379.

Seno, T. (1979), Intraplate seismicity in Tohoku and Hokkaido and large interplate earthquakes: A possibility of a large interplate earthquake off the southern Sanriku coast, northern Japan, *J. Phys. Earth*, *27*, 21–51.

Seno, T. (2009), Determination of the pore fluid pressure ratio at seismogenic megathrusts in subduction zones: Implications for strength of asperities and Andean-type mountain building, *J. Geophys. Res*., *114*, B05405, doi:10.1029/2008JB005889.

Seno, T., and Y. Yamanaka (1996), Double seismic zones, compressional deep trench-outer rise events and superplumes, in *Subduction: Top to Bottom*, edited by G. E. Bebout, *et al*., pp. 347–355, Geophys. Monograph Ser., vol. 96, AGU, Washington, D.C.

Seno, T., S. Stein, and A. E. Gripp (1993), A model for the motion of the Philippine Sea plate consistent with NUVEL-1 and geological data, *J. Geophys. Res*., *98*, 17941–17948.

Seno, T., T. Sakurai, and S. Stein (1996), Can the Okhotsk plate be discriminated from the North American plate?, *J. Geophys. Res*., *101*, 11305–11315.

Shelly, D. R., G. C. Beroza, S. Ide, and S. Nakamura (2006), Low-frequency earthquakes in Shikoku, Japan, and their relationship to episodic tremor and slip, *Nature*, *442*, 188–191, doi:10.1038/nature04931.

Shimazaki, K., and Y. Zhao (2000), Dislocation model for strain accumulation in a plate collision zone, *Earth Planets Space*, *52*, 1091–1094.

Sibson, R. H. (1990), Rupture nucleation on unfavorably oriented faults, *Bull. Seismol. Soc. Am*., *80*, 1580–1604.

Sibson, R. H. (1992), Implications of fault-valve behaviour for rupture nucleation and recurrence, *Tectonophysics*, *211*, 283–293.

Sibson, R. H. (2007), An episode of fault-valve behaviour during compressional inversion?—The 2004 M_J6.8 Mid-Niigata Prefecture, Japan, earthquake sequence, *Earth Planet. Sci. Lett*., *257*, 188–199.

Sibson, R. H. (2009), Rupturing in overpressured crust during compressional inversion—the case from NE Honshu, Japan, *Tectonophysics*, *473*, 404–416.

Simpson, R. W. (1997), Quantifying Anderson's fault types, *J. Geophys. Res*., *102*, 17,909–17,919.

Suwa, Y., S. Miura, A. Hasegawa, T. Sato, and K. Tachibana (2006), Interplate coupling beneath NE Japan inferred from three-dimensional displacement field, *J. Geophys. Res*., *111*, doi:101029/2004JB003203.

Takei, Y. (2002), Effect of pore geometry on V_p/V_s: from equilibrium geometry to crack, *J. Geophys. Res*., *107*(B2), doi:10.1029/2001JB000522.

Tanaka, A., and Y. Ishikawa (2002), Temperature distribution and focal depth in the crust of the northeastern Japan, *Earth Planets Space*, *54*, 1109–1113.

Tank, S. B., Y. Honkura, Y. Ogawa, M. Matsushima, N. Oshiman, M. K. Tunçer, M. K. Tunçer, C. Çelik, E. Tolak, and A. M. Işıkara (2005), Magnetotelluric imaging of the fault rupture area of the 1999 Izmit (Turkey) earthquake, *Phys. Earth Planet. Inter.*, *150*(1), 213–222.

Tsuji, Y., J. Nakajima, and A. Hasegawa (2008), Tomographic evidence for hydrated oceanic crust of the Pacific slab beneath northeastern Japan: Implications for water transportation in subduction zones, *Geophys. Res. Lett*., *35*, L14308, doi:10.1029/2008GL034461.

Tsumura, N., S. Matsumoto, S. Horiuchi, and A. Hasegawa (2000), Three-dimensional attenuation structure beneath the northeastern Japan arc estimated from spectra of small earthquakes, *Tectonophysics*, *319*, 241–260.

Uchida, N., A. Hasegawa, J. Nakajima, and T. Matsuzawa (2009), What controls interplate coupling?: Evidence for abrupt change in coupling across a border between two overlying plates in the NE Japan subduction zone, *Earth Planet. Sci. Lett*., *283*, 111–121, doi:10.1016/j.epsl.2009.04.003.

Uchida, N., T. Matsuzawa, J. Nakajima, and A. Hasegawa (2010), Subduction of a wedge-shaped Philippine Sea plate beneath Kanto, central Japan, estimated from converted waves and small repeating earthquakes, *J. Geophys. Res*., *115*, doi:10.1029/2009JB006962.

Ulmer, P., and V. Trommsdorff (1995), Serpentine stability to mantle depths and subduction-related magmatism, *Science*, *268*, 858–861.

Umino, N., and A. Hasegawa (1975), On the two-layered structure of deep seismic plane in northeastern Japan arc, *J. Seismol. Soc. Japan*, *28*, 125–139 (in Japanese with English abstract).

Umino, N., A. Hasegawa, and A. Takagi (1990), The relationship between seismicity patterns and fracture zones beneath northeastern Japan, *Tohoku Geophys. J*., *33*, 149–162.

Umino, N., T. Matsuzawa, S. Hori, A. Nakamura, A. Yamamoto, A. Hasegawa, and T. Yoshida (1998a), 1996 Onikobe earthquakes and their relation to crustal structure, *J. Seismol. Soc. Japan*, *51*, 253–264 (in Japanese with English abstract).

Umino, N., T. Okada, A. Nakamura, J. Nakajima, T. Sato, S. Hori, T. Kono, K. Nida, S. Ueki, T. Matsuzawa, A. Hasegawa, and H. Hamaguchi (1998b), Aftershock distribution for the *M* 6.1 earthquake of 3 September 1998 in Shizukuishi, Iwate Prefecture, northeastern Japan, *Active Fault Res*., *17*, 1–8 (in Japanese with English abstract).

Umino, N., H. Ujikawa, S. Hori, and A. Hasegawa (2002a), Distinct *S*-wave reflectors (bright spots) detected beneath the Nagamachi-Rifu fault, NE Japan, *Earth Planets Space*, *54*, 1021–1026.

Umino, N., T. Okada, and A. Hasegawa (2002b), Foreshock and aftershock sequence of the 1998 M5.0 Sendai, northeastern Japan, earthquake and its implications for earthquake nucleation, *Bull. Seismol. Soc. Am*., *92*, 2465–2477.

Wald, D. J., and P. G. Somerville (1995), Variable-slip rupture model of the great 1923 Kanto, Japan Earthquake: Geodetic and body-waveform analysis, *Bull. Seismol. Soc. Am*., *85*, 159–177.

Wang, Z., and D. Zhao (2005), Seismic imaging of the entire arc of Tohoku and Hokkaido in Japan using *P*-wave, *S*-wave and sP depth-phase data, *Phys. Earth Planet. Inter*., *152*, 144–162.

Wannamaker, P. E., G. T. Caldwell, G. R. Jiracek, V. Maris, G. J. Hill, Y. Ogawa, H. M. Bibby, S. L. Bennie, and W. Heise (2009), Fluid and deformation regime of an advancing subduction system at Marlborough, New Zealand, *Nature*, *460*, 733–736, doi:10.1038/nature08204.

Wdowinski, S., R. O'Connell, and P. England (1989), A continuum model

doi:10.5047/meep.2017.00501.0001

of continental deformation above subduction zones: Application to the Andes and Aegean, *J. Geophys. Res.*, *94*, 10331–10346.

Wei, D., and T. Seno (1998), Determination of the Amurian plate motion, in *Mantle Dynamics and Plate Interactions in East Asia*, Geodynam. Series, *27*, 337–346.

Wesson, R. L., and O. S. Boyd (2007), Stress before and after the 2002 Denali fault earthquake, *Geophys. Res. Lett.*, *34*, L07303, http://dx.doi.org/10.1029/2007GL029189.

Wunder, B., and W. Schreyer (1997), Antigorite: High-pressure stability in the system MgO-SiO_2-H_2O (MSH), *Lithos*, *41*, 213–227.

Yamaguchi, S., H. Murakami, H. Iwamoto, K. Takemoto, K. Kitada, I. Shiozaki, N. Oshiman, and S. Katoh (2007),Two-dimensional resistivity structure of the fault associated with the 2000 Western Tottori earthquake, *Earth Planets Space*, *59*, 1211–1217.

Yamamoto, Y., R. Hino, M. Nishino, T. Yamada, T. Kanazawa, T. Hashimoto, and G. Aoki (2006), Three-dimensional seismic velocity structure around the focal area of the 1978 Miyagi-Oki earthquake, *Geophys. Res. Lett.*, *33*, L10308, doi:10.1029/2005GL025619.

Yamanaka, Y., and M. Kikuchi (2003), Source process of the recurrent Tokachi-oki earthquake on September 26, 2003, inferred from teleseismic body waves, *Earth Planets Space*, *55*, e21–e24.

Yamanaka, Y., and M. Kikuchi (2004), Asperity map along the subduction zones in northeastern Japan inferred from regional seismic data, *J. Geophys. Res.*, *109*, B07307, doi:10.1029/2003JB002683.

Yamasaki, T., and T. Seno (2003), Double seismic zone and dehydration embrittlement of the subducting slab, *J. Geophys. Res.*, *108*, doi:10.1029/2002JB001918.

Yamasaki, T., and T. Seno (2005), High strain zone in central Honshu resulting from the viscosity heterogeneities in the crust and mantle, *Earth Planet. Sci. Lett.*, *232*, 13–27.

Yamazaki, F., and T. Ooida (1985), Configuration of subducted Philippine Sea plate beneath the Chubu district, central Japan, *J. Seismol. Soc. Japan*, *38*, 193–201 (in Japanese with English abstract).

Yanada, T., D. Zhao, and A. Hasegawa (2010), Teleseismic tomography of the mantle structure under the Japan Islands. *Progr. Abst. Seism. Soc. Japan, 2010 Fall Meeting*, 175.

Yoshida, K., A. Hasegawa, T. Okada, T. Iinuma, Y. Ito, and Y. Asano (2012), Stress before and after the 2011 Great Tohoku-oki earthquake, and induced earthquakes in inland areas of eastern Japan, *Geophys. Res. Lett.*, *39*, doi:10.1029/2011GL049729.

Yoshida, K., A. Hasegawa, T. Okada, and T. Iinuma (2014), Changes in the stress field after the 2008 *M* 7.2 Iwate-Miyagi Nairiku earthquake in northeastern Japan, *J. Geophys. Res.*, *119*, 9016–9030.

Yoshida, K., A. Hasegawa, and T. Okada (2015a), Spatial variation of stress orientations in NE Japan revealed by dense seismic observations, *Tectonophysics*, doi:10.1016/j.tecto.2015.02.013.

Yoshida, K., A. Hasegawa, and T. Okada (2015b), Spatially heterogeneous stress field in the source area of the 2011 M_w 6.6 Fukushima-Hamadori earthquake, NE Japan, probably caused by static stress change, *Geophys. J. Int.*, *201*, 1060–1069.

Yoshida, K., A. Hasegawa, and T. Okada (2016), Heterogeneous stress field in the source area of the 2003 *M* 6.4 Northern Miyagi Prefecture, NE Japan, earthquake, *Geophys. J. Int.*, doi:10.1093/gji/ggw160.

Zhang, H., and C. H. Thurber (2003), Double-difference tomography: The method and its application to the Hayward Fault, California, *Bull. Seismol. Soc. Am.*, *93*, 1875–1889.

Zhao, D., and A. Hasegawa (1993), *P*-wave tomographic imaging of the crust and upper mantle beneath the Japan Islands, *J. Geophys. Res.*, *98*, 4333–4353.

Zhao, D., A. Hasegawa, and S. Horiuchi (1992), Tomographic imaging of P and S wave velocity structure beneath northeastern Japan, *J. Geophys. Res.*, *97*, 19909–19928.

Zhao, D., A. Hasegawa, and H. Kanamori (1994), Deep structure of Japan subduction zones as derived from local, regional, and teleseismic events, *J. Geophys. Res.*, *99*, 22313–22329.

Zhao, D., D. Christensen, and H. Pulpan (1995), Tomographic imaging of the Alaska subduction zone, *J. Geophys. Res.*, *100*, 6487–6504.

Zhao, D., H. Kanamori, and H. Negishi (1996), Tomography of the source area of the 1995 Kobe earthquake: Evidence for fluids at the hypocenter?, *Science*, *274*, 1891–1894.

Zhao, D., Y. Xu, D. A. Wiens, L. Dorman, J. Hildebrand, and S. Webb (1997a), Depth extent of the Lau back-arc spreading center and its relation to subduction processes, *Science*, *278*, 254–257.

Zhao, D., T. Matsuzawa, and A. Hasegawa (1997b), Morphology of the subducting slab boundary and its relationship to the interplate seismic coupling, *Phys. Earth Planet. Inter.*, *102*, 89–104.

Zhao, D., H. Tani, and O. P. Mishra (2004), Crustal heterogeneity of the 2000 western Tottori earthquake region: Effect of fluids from slab dehydration, *Phys. Earth Planet. Inter.*, *145*, 161–177.

Zhao, D., Z. Wang, N. Umino, and A. Hasegawa (2007a), Tomographic imaging outside a seismic network: Application to the northeast Japan arc, *Bull. Seismol. Soc. Am.*, *97*, 1121–1132.

Zhao, D., S. Maruyama, and S. Omori (2007b), Mantle dynamics of western Pacific to East Asia: New insight from seismic tomography and mineral physics, *Gondwana Res.*, *11*, 120–131.

Zhao, D., T. Yanada, A. Hasegawa, N. Umino, and W. Wei (2012), Imaging the subducting slabs and mantle upwelling under the Japan Islands, *Geophys. J. Int.*, *190*, 816–828.

doi:10.5047/meep.2017.00501.0001